Hysteresis Modelling of High Temperature Superconductors

Mårten Sjöström

Thesis No. 2372 (2001)

Laboratory of Nonlinear Systems
Communication Systems Department
Swiss Federal Institute of Technology Lausanne

HYSTERESIS MODELLING OF HIGH TEMPERATURE SUPERCONDUCTORS

THESIS N^{O} 2372 (2001)

PRESENTED AT THE COMMUNICATION SYSTEMS DEPARTMENT

SWISS FEDERAL INSTITUTE OF TECHNOLOGY LAUSANNE
(ECOLE POLYTECHNIQUE FEDERALE LAUSANNE)

FOR OBTAINING THE DEGREE OF ¡¡DOCTEUR ÈS SCIENCES TECHNIQUES¿¿ (PhD)

BY

Mårten SJÖSTRÖM

Licentiate of Engineering, Royal Institute of Technology (KTH), Stockholm, Sweden
of Swedish nationality and originating from Sundsvall, Sweden

accepted on proposition by the jury:

Prof. Martin Hasler, thesis supervisor
Dr. Bertrand Dutoit
Prof. Alain Germond
Prof. Isaak D. Mayergoyz
Dr. Yfeng Yang

Lausanne, EPFL
2001

To Julynette

To my parents,
my brother and my sister

Abstract

The present dissertation considers the capabilities, limitations and possible extensions of modelling the hysteresis that is exhibited by type-II superconductors, especially those with high critical temperature.

Superconductors of type-II, including high temperature superconductors, are partially penetrated by magnetic flux. The tubes, through which the flux passes the superconductor, are 'pinned' to certain locations due to impurities in the crystal structure of the material, and they must be forced by an external magnetic field or a transport current in order to move. Thus, the pinning of flux tubes constitutes a memory that gives rise to a hysteresis with corresponding losses. The critical state model is a well-known, macroscopic model that describes well this partial flux penetration. Furthermore, the flux tubes can start to flow due to the Lorenz-force when a large transport current flows in the superconductor. This produces an additional resistive voltage.

The concept of hysteresis and its main properties are discussed, and a number of various models describing this phenomenon are presented. An emphasis is made on the classical Preisach model of hysteresis, which is a weighted superposition of relay operators. A hysteretic system produces higher harmonics, just as most nonlinear systems. An investigation reveals under what conditions the Preisach model generates only odd harmonics, and also when all odd harmonics are present, as well as how this knowledge can be utilised.

A parameterised Preisach model is proposed, which always applies when the critical state model is an acceptable approximation of the superconductor hysteresis. Its capabilities and limitations as a hysteresis model for superconductors are investigated. It is demonstrated how the parameters can be estimated from different electric measurements on high temperature superconductors and that the output and the losses can quickly and accurately be computed for an arbitrary signal, once the parameter identification is made. Moreover, the structure of the parameterised model is such that an inverse model can easily be obtained. It is also shown that the hysteresis saturation, which occurs when the flux flow starts, can be modelled by introducing limiting functions in the model.

A generalised equivalent circuit has been proposed that takes into account both the hysteretic and resistive behaviour, the latter being due to flux flow. This extended model describes the global electric behaviour of a superconducting device, which can be applied either when the superconductor is part of a larger system or when it stands alone. A few examples of its application are given.

Resumé (version française)

La dissertation actuelle envisage les possibilités, les limitations et les extensions éventuelles de modélisation de l'hystérèse observée dans un supraconducteur de type II, plus particulièrement ceux à haute température critique.

Les supraconducteurs de type II, y compris ceux à haute température critique, sont partiellement pénétrés par le flux magnétique. Les tubes, par lesquels le flux verse le supraconducteur, sont 'épinglé' (anglais 'pinned') à certaines endroits des défauts de la structure cristalline du matériau; ils se déplacent forcés par un champ magnétique externe ou un courant de transport. Donc, ce 'pinning' de tubes de flux est une mémoire qui produit une hystérèse avec les pertes correspondantes. Le modèle d'état critique est un modèle macroscopique connu qui décrit bien cette pénétration partielle du flux. D'ailleurs, le mouvement des tubes de flux peut être initié par la force Lorenz lorsqu'un courant de transport suffisamment grand passe dans le supraconducteur. Ceci génère une tension résistive additionnelle.

Le concept d'hystérèse ainsi que ses propriétés principales sont discutés, et quelques modèles différents décrivant ce phénomène sont présentés. Une attention particulière est donnée au modèle classique hystérétique de Preisach, qui est une superposition pondérée des opérateurs de relais. Un système hystérétique crée des harmoniques, comme presque tous les systèmes nonlinéaires. Une investigation révèle dans quelles conditions le modèle de Preisach ne génère que les harmonies impaires, et également dans quelles conditions toutes ces harmoniques impaires sont présentes, ainsi que l'utilisation de cette information.

Un modèle de Preisach paramétrique est proposé. Celui s'applique toujours lorsque le modèle d'état critique est une approximation acceptable de l'hystérèse d'un supraconducteur. Ses possibilités et limitations comme modèle hystérétique pour les supraconducteurs sont investigués. Il est démontré comment les paramètres peuvent être estimés à partir des différentes mesures électriques de quelques échantillons supraconducteurs à haute température critique, ainsi que comment la sortie et les pertes peuvent être calculés rapidement et précisément lorsque l'identification des paramètres a été faite. De plus, la structure du modèle paramétrique est telle qu'un modèle inverse peut facilement être obtenu. Il est aussi montré que la saturation de l'hystérèse, qui est présente lorsque le mouvement du flux commence, peut être modélisée avec l'introduction de fonctions limites dans le modèle.

Un circuit équivalent généralisé a été proposé qui rend compte les comportements hystérétique et résistif, ce dernier provenant du mouvement du flux. Ce modèle étendu décrit le comportement électrique global d'un appareil supraconducteur, qui peut être appliqué soit tel quel soit quand le supraconducteur est intégré dans un système.

Acknowledgements

The years of research leading to a dissertation as the present involve many encounters with numerous specialist in different fields, researchers, students, administrative personnel and so forth, who all have had an impact on the evolution of the project. It is impossible to mention all and everyone here, so even if you are not personally mentioned here, I still remember the influence you have had on this work and my time at the Swiss Federal Institute of Technology Lausanne (EPFL). Even so, I would like to take the opportunity to show my gratitude to certain persons for their assistance and support through these years.

First of all, I would like to thank Prof. Martin Hasler who has provided me with the opportunity to come to the Laboratory of Nonlinear Systems[1] and perform the research on hysteresis and superconductivity. Also many thanks to Dr. Bertrand Dutoit for his guidance in my research and the many discussions on superconductivity and its modelling.

I would like to direct special thanks to Prof. Isaak Mayergoyz for offering me to visit his laboratory and for always being prepared to answer questions about the Preisach model and its relationship to superconductivity. Dr. Claudio Serpico earns also many thanks for helping during this visit and for interesting discussions on hysteresis. Further appreciation is directed to Dr. Yifeng Yang for explaining me measurement methods and the hysteretic behaviour of superconductors. I would also like to thank Prof. Martin Brokate for initiating me to the inversion of Preisach models.

The weekly discussions held in the 'super-group' have been very encouraging and I am most grateful to Dr. Dejan Djukic, Mr. Francesco Grilli, Dr. Nadia Nibbio, Mr. Svetlomir Stavrev and everyone else who has contributed to those dialogues. Many others of my former and present colleagues in the laboratory have also contributed in different ways to the termination of this work. They have made me feel welcome in group, listened and discussed my ideas, corrected my French and English, assisted me in contacts with Swiss authorities and much more. Special thanks to Dr. Oscar De Feo and Mr. Thomas Schimming, who have been a great help in solving problems associated with computers and software. In particular, Mrs. Christiane Good deserves many thanks for all the practical arrangements related to the work. Several visitors have also contributed with interesting discussions and exchanges of ideas.

I have encountered many people through different national and European projects, and I am most thankful for what I have learnt from them, even if parts of it is not explicitly included in this work. I would like to thank Mr. Diego Politano, Dr. Jakob Rhyner and Dr. Gilbert Schnyder for what I have learnt through them about superconducting applications and power systems. Dr. Bernhard Bachmann and Dr. Hans-Jürg Wiesmann also deserve my thanks for instructing me in the modelling of three-phase power systems and superconducting devices. Thanks also to Mr. Harry Züger for his explanations of superconducting transformers. My special gratitude is directed to Dr. Rachid Cherkaoui, who elucidated the realm of power system stability and gave very useful feedback in general.

[1] Chair of Circuits and Systems before 1st of January 2000.

There is a whole lot of people who have made my time at EPFL worthwhile, but who have no direct link with the present work. Nonetheless, I would like to thank all my new and old friends in choirs and singing groups, from different sports, mountain and church activities, as well as former colleagues from CERN with whom I discussed general aspects of physics and other sciences.

Last but definitely not least, the people who are the closest to me: many special thanks are directed to my parents Bengt and Margot, my brother Jan and my sister Maria with family, my new family in-law and of course to my lovely wife Julynette, who has patiently been supporting me.

Contents

Chapter 1

Introduction

One of the first applications that came to mind for a *superconductor* was to construct a loss-less electric transmission system. The cost due to energy losses in cables would be brought to a minimum because the superconductor has no resistance when cooled below a certain critical temperature, see Fig. 1.1. But nothing is as easy as it appears: the magnetic field induced by the current must also be below a critical value for the material to stay in the superconducting state, which restricted the practicality of the loss-less transmission. A second type of superconductors with better magnetic field properties was later discovered. Then again, another stumbling block appeared. The superconductor is not loss-less for alternating currents, even if it is for direct currents. This is due to a memory effect of the magnetic flux, which commonly goes under the name *hysteresis*. The usage of these superconductors was possible in some applications, even though some losses had to be accepted. The attention to superconducting applications was revived when new, ceramic, *high temperature* superconducting materials were discovered in 1986. Their critical temperatures are up to 130 K (-140°C), instead of 30 K (-240°C) for their low temperature counterparts, so cooling could be made more efficient and much less costly. The electromagnetic behaviour of these new materials is very similar to the second type of low temperature superconductors, but in addition to the hysteretic losses, they have a tendency of producing losses also for direct currents. In order to know how a superconducting device functions under various circumstances, whether it be isolated or in combination with other more conventional elements, a *model*, i.e. some kind of mathematical description of the reality, is a useful tool to predict results.

It is the scope of this thesis to investigate the possibilities and limitations of modelling superconductors with special application to high temperature superconductors, where mainly the hysteresis but also the resistive modelling is considered. This chapter gives a first introduction to the physics and electromagnetic properties that must be explained by such a model. It also brings out questions and problems about the concept of hysteresis and how it can be described, as well as special features related to the hysteresis modelling of superconductors. Finally, the

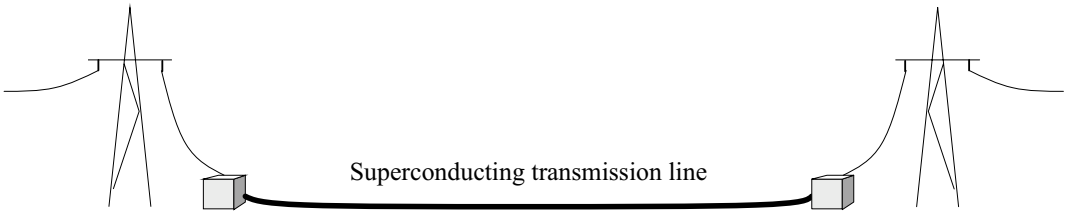

Figure 1.1: The dream of a loss-less transmission started with the discovery of superconductivity, but cooling and hysteretic losses are major stumbling blocks.

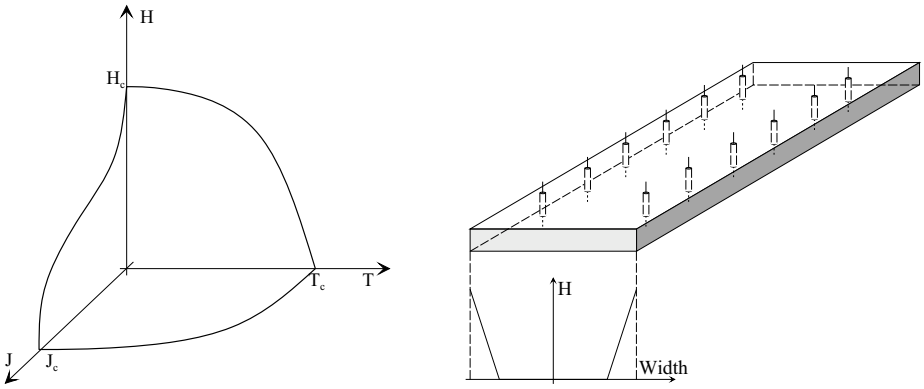

(a) (b)

Figure 1.2: (a) The superconductivity is limited by the critical values of temperature and magnetic field, but also current density for practical applications. (b) Type-II superconductors has a mixed state where magnetic flux passes through microscopic domains of material in normal state. Macroscopically, this is observed as a partial penetration of flux, see the diagram.

aim of the thesis is pronounced and an outline is given.

1.1 Superconductivity

Superconductivity may seem a very complicated matter when examining the physics at a microscopic level. And indeed, even physicists specialised in the subject have not yet fully understood how the superconductivity functions in materials with high critical temperature. So, can then any engineer carry out calculus for applications without being a specialist? Well, it is the hope that this thesis will clarify one approach to deal with superconductivity with a higher level modelling. However, a physical background is desirable for a better understanding.

Superconductivity was discovered by Kammerlingh Onnes in 1911 when he studied the resistivity of metals at low temperatures. He noted that some materials entered a state of *perfect conductivity* (or zero resistivity, $R = 0$) at a critical temperature [Kam11a, Kam11b, Kam11c]. Several years later, Meissner and Ochsenfeld observed that all magnetic flux is expelled from the interior of superconductors, which cannot be fully explained by perfect conductivity [MO33]. This magnetic expulsion ($B = 0$) or *perfect diamagnetism* is a second basic feature of superconductivity. The superconducting state of these material appears only below some critical values of temperature, T_c, and magnetic field, H_c, above which the material enters a normal state again. Moreover, a third critical value limits the usage of superconductivity in practical applications: the critical current density J_c determines where the direct current losses start to be significant, see Fig. 1.2(a).

There exist two types of superconductors, type-I and type-II, which have very different magnetic properties. Whereas the former (mainly pure metals) complies fully to the perfect diamagnetism, the latter (mainly alloys) has a partial magnetic penetration, macroscopically seen, which is called the *mixed state* [Abr57]. In fact, the material in superconducting state has then microscopic domains of normal state, through which a *quantum flux* $\Phi_0 = h/(2e)$ passes, see Fig. 1.2(b). Imperfections in the crystal grid of the material constitute energy barriers, which must be overcome in order to move the flux tubes. Therefore, the flux inside remains still until it is forced to move, and when the tubes move, there is energy dissipating. The *pinned flux* so remains, even if external forces like magnetic field or transport current are removed. This

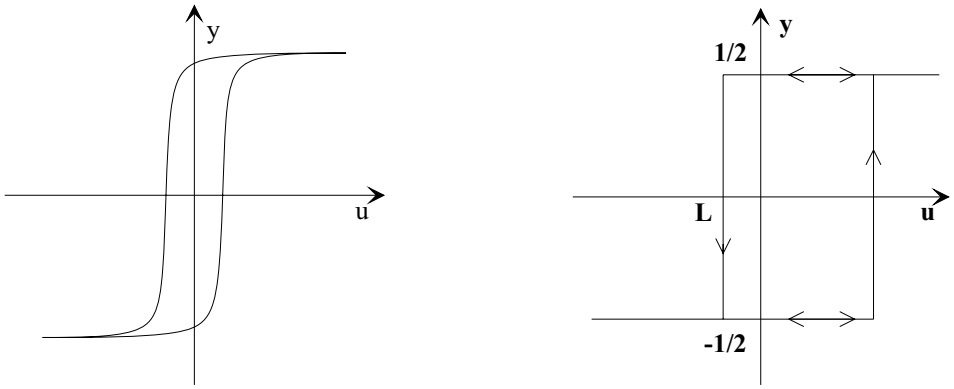

(a) (b)

Figure 1.3: (a) Typical hysteresis loop, e.g. for magnetisation in iron. (b) The relay operator is the simplest hysteresis operator in the Preisach model.

constitutes a memory, which implies a hysteresis with corresponding losses. An explanation named the *critical state model* describes this flux penetration and takes the hysteretic behaviour into account for subcritical currents, temperatures and fields [Bea62]. A large enough transport current may induce a force (Lorenz-force) on each flux tube that is greater than the pinning force, and so produce a *flux flow*. A slower flux motion may also have its origin in thermal activation of the crystal grid, which is more common in high temperature superconductors. At flux motion, the critical state model cannot be applied, so another solution must be found. Moreover, the flux motion induces a voltage in the same direction as the current, so an external viewer observes a resistivity.

The characterisation of various superconducting specimens can be made by a range of measurements. This is not trivial because the voltage drop over the specimen in electric measurements is in principle zero when running a current through it. Alternating current lock-in measurements can be utilised to determine losses, and direct current measurements may be applied to obtain the critical current and other characteristics. Furthermore, a number of measurement techniques are presented in this thesis, which allow also to separate hysteretic and resistive losses [Yan98, MYBH00].

A question that may arise here is how the hysteresis due to flux pinning and the resistance due to flux motion can be modelled in superconductor of different properties obtained in measurements. Before we address the modelling of superconductors, we first consider hysteresis and its modelling in general.

1.2 Hysteresis and its Modelling

The magnetic hysteresis in iron, which has an approximate hysteresis loop as in Fig. 1.3(a) is probably one of the best known examples of hysteresis. But what is hysteresis? This is a question that is not so easy to answer because there is no universal definition. The effect of hysteresis appears in many different disciplines of science, so each field has its own meaning, and even within the same discipline there are arguments. The concept of hysteresis will therefore be discussed in this thesis, and the main properties, such as persistent memory and the losses it implies, will be analysed. The next issue is how the hysteretic phenomenon can be modelled in order to predict output and losses. Many models of hysteresis have been suggested, and we will make a quick overview of them [MNZ93, Ber98, LPA00]. A concentration is put on the

classical Preisach model [Pre35], which is a macroscopic and phenomenological model by which a hysteresis can be expressed. In that model, the different hysteresis curves are defined by a weighted superposition of the simplest hysteresis operator, the relay operator, in Fig. 1.3(b). The 2-dimensional weighting function $w(\mathrm{L},\Gamma)$ decides the amount the hysteresis changes at each up- (Γ) and down-switch (L), and so the superposition gives the total output:

$$y(t) = \iint_{\mathrm{L}\leq\Gamma} w(\mathrm{L},\Gamma)\mathbf{R}_{\mathrm{L}\Gamma}[u(t)]d\Gamma d\mathrm{L}\,. \tag{1.1}$$

The model's particular properties, the calculus of memory, output and losses, saturation as well as its inversion are all described in the thesis [May91, BS96].

It is well-known that most nonlinear phenomena produce *higher harmonics*, i.e. multiples of the fundamental frequency. For instance, a nonlinear system that is fed with a 50 Hz sinusoid generates the frequencies 50, 100, 150, 200 Hz, etc. Now, most natural, nonlinear systems produce *only odd harmonics* (i.e. 50, 150, 250 Hz, etc.) because the output possesses the so-called half-wave symmetry. This means that the second half of the signal equals the negative of the first part (see Fig. 5.1, p. 56). The measurements on superconductors reveals such a behaviour with only odd harmonics. A question that might come up is under what conditions the Preisach model exhibits *only odd* higher harmonics, and when does it produce *all odd* harmonics? The solutions to these two questions are investigated and formulated in the thesis, where the latter (all odd harmonics) is examined for a large class of weighting functions. The harmonics of the differentiated output from the Preisach model are expressed with help of conventional Fourier analysis. It has already been mentioned that higher harmonics can be used in measurements, but are there other ways, in which higher harmonics may be utilised in relation to hysteresis and the Preisach model?

1.3 Hysteresis Models for Superconductors

The question of how hysteresis in superconductors can be modelled was raised in the section about superconductivity. It was said then that the *critical state model* describes well the situation when flux pinning applies (no flux motion). The problems occur when the geometry of the superconductor is a bit more complicated, by which it is difficult to carry out computations with that model. Then it might instead be easier to relate input and output signals, and one could use many of the phenomenological hysteresis models mentioned in the thesis. Nevertheless, we concentrate on the Preisach model.

A good reason to do so is the following: the hysteresis in the critical state model possesses the necessary and sufficient properties of a hysteresis to be represented by the Preisach model [May91, May96]. Now, the critical state model applies very well to high temperature superconductors in self-field for transport currents below 80% of the critical current, above which flux creep losses start to appear for some specimens [Ash94, FMAO94]. Therefore, the Preisach model is at least applicable below this limit. It is also important to remember that the Preisach model is phenomenological and does not explain physical causes of hysteresis in high temperature superconductors; it rather relates experimental data [May91].

A parameterised Preisach model is proposed in this thesis, which makes the model concise, accurate and quick. The consequent question is of course whether the parameterised Preisach model can be applied to all superconducting specimens and materials, and if a weighting function can be obtained for any superconducting specimen, and what is the procedure to identify the parameters? First it is understood that these parameters must be changed in order to take into account different materials, number of filaments, geometry, etc. Then, the applicability

is ascertained as long as the critical state model applies, i.e. the main part of the losses is hysteretic. Conventionally, the weighting function is experimentally found by measuring first order transition curves [May91]. This is difficult, if not impossible, with the data obtained in electric measurements. For this reason, some different methods have been developed and are presented in later chapters. They all make estimations using data from different kinds of measurements with various quality of the results. This is demonstrated by using measurements on different high temperature superconducting specimens.

Now, many questions arise when a new model is proposed. First of all, how general is the model in the sense that either voltage or current can be a function of the other, or is there no inverse of the model? Furthermore, can losses be computed for any input current, once the model has been identified for a specimen, and at what cost? And can any engineer use these models? It has been revealed that the model may be advantageous compared to the critical state model when geometry is complicated, but what other advantages are there with the suggested model compared to other methods? A very important issue is how well the parameterised Preisach model can be applied to high temperature superconductors at the limits of flux pinning and the start of flux motion. Measurements have disclosed a saturation of hysteresis losses and an increase of resistive losses at this limit. The question is whether the model can still be applied and if it may be extended to include the effect of the flux motion? This problem has been addressed in the thesis, which proposes an equivalent circuit for superconductors that would be possible to apply in many different situations, a few of which are demonstrated.

When considering modelling of superconductors, one cannot avoid mentioning another model that has become very popular lately. It is an approximation of the critical state model that uses a power-law relationship between electric field E and current density J. It implies a material that is quasi-hysteretic, quasi-resistive, where the disposition depends on the value of the power-law exponent [Rhy93, May98]. The success of this model is due to its excellent agreement with many different kinds of measurement data. A disadvantages is, however, that simulations must be carried out in specialised finite element software, which includes this $E - J$ model, or in a self-made program using an easier integration description. Thus it requires the knowledge of such programs. Another drawback is the extensive simulation time needed to achieve the results, which is due to the large number of evaluation points inside the superconductor geometry that is required to obtain details about the global electromagnetic behaviour. It is the conviction of the author that a general but simpler model would be appreciable, especially when a superconductor is studied in combination with other elements in a larger system.

1.4 Aim and Outline of the Thesis

Many questions have appeared in this introduction to the subject of hysteresis modelling of high temperature superconductors. The aim of the thesis is therefore to closer investigate the possibilities and limitations for such a modelling and to the search for the answers of these uncertainties. In particular, it will be calculated under what circumstances the Preisach model yields only odd harmonics, as well as when all odd harmonics are produced for the very general case of a polynomial weighting function. It will further be examined how the Preisach model can be applied to superconductors, especially those of high critical temperature, where validity and limitations are kept in mind. The generalisation to materials of different characteristics and geometries will also be demonstrated by applying the proposed parameterised Preisach model to high temperature superconductors, where the parameters will be estimated from different kinds of measurements. Moreover, it is the scope of the thesis to show how simulations using the estimated weighting functions allow for computation of different outputs, including losses, for an 'arbitrary' input signal. The exploration of possibilities for a model generalisation in

order to include the effects of flux motion is also part of the thesis. This is put in the context of an equivalent circuit of a superconductor, which would serve as an engineering tool that can be applied in a larger system, of which the superconductor is part, where no special knowledge about superconductivity, finite element methods, etc. should be required.

The thesis is outlined as follows. First, an introduction to superconductivity, its recognised modelling and the cause of hysteresis exhibited by the material is given. Then, a chapter about electric measurements presents various techniques to characterise a superconductor and to separate resistive and hysteretic losses. A discussion about hysteresis and its modelling in general follows, where the Preisach model is considered in particular. It provides a base for the next chapter that investigates the higher harmonics produced by the Preisach model, and how the knowledge thereof can be utilised. Chapter 6 demonstrates the possibilities and limitations of using the Preisach model with superconductors by showing its link with the critical state model and how the parameters can be estimated from different kinds of measurements. It deals also with the inverse model and the saturation when the flux motion starts. The next chapter contains the description of a generalised equivalent circuit for superconductors, whose applicability is demonstrated in a number of examples. A conclusion summarises thereafter the main results of the thesis. An appendix provides a more detailed derivation of the symmetry description of the Preisach model, which may be used as a basis for an implementation. A second appendix presents the basics of least square estimations. A summary can be found after each chapter, which recapitulates its most important contents. The bibliography found towards the end of the thesis contains references to previous work and further reading in the different fields. It does not always refer to the original works, even if an attempt is made to find primary sources, but it is rather intended as reference for the interested reader to probe further. Finally, a biography of the thesis' author is given.

Chapter 2

Superconductivity

The term superconductivity comes from that a material has a conductivity *beyond* the normal. It was given by Kamerlingh Onnes in 1911 when he discovered that for some materials the resistance, not only decreases with temperature, but has a sudden drop at some critical temperature T_c. He called this a *superconducting state* in contrast to a *normal state*, and materials that exhibit such a behaviour are consequently called *superconductors* [Kam11a, Kam11b, Kam11c].

As research evolved, it was found that *perfect conductivity* (i.e. zero resistance, $R = 0$) is not the only characteristic of a superconductor. Meissner and Ochsenfeld noted in 1933 that the magnetic flux is expelled from the interior of a superconductor, which cannot be fully explained by perfect conductivity. They verified that *perfect diamagnetism* (i.e. expulsion of magnetic flux, $B = 0$) is a fundamental property of superconductors [MO33]. It has later been confirmed through theories and experiments that there is a third basic feature of superconductors: the magnetic flux passing through a superconducting coil can only take certain values of *quantified flux*, $\Phi = n \cdot \Phi_0$. All these features are, however, destroyed when the temperature surpass T_c or when the magnetic field exceeds a temperature-dependent critical magnetic field $H_c(T)$. For practical applications, it is also important that the current density stays below a critical value $J < J_c$. These critical values are all related and depend further on material and pressure.

In this chapter, we start by looking at the physical aspects of the superconductor characteristics, and continue to discuss some models that explain its behaviour. We consider then the classification in type-I and type-II (soft and hard) superconductors, which exhibit very different magnetic properties. A concentration is made on the latter type, which possesses a mixed state with both microscopic superconducting and normal state regions. The traversing flux tubes are pinned to certain positions where the *pinning force* must be overcome in order to move them. This is the intrinsic reason for *hysteresis* in type-II superconductors. Thermal effects in the material structure may further give rise to a *flux creep* and transport currents can start a *flux flow* that induces a *resistive voltage*. It follows then the description of a few models that take the hysteretic and the flux movement effects into account. Bednorz and Müller discovered in 1986 a new type of ceramic materials at much higher T_c than the traditional metallic superconductors. These new so-called *high temperature superconductors* are extreme cases of type-II superconductivity, which is treated in Section 2.11. Finally, there is a short discussion about cryogenic issues and possible applications of superconductors.

This chapter does in no way reflect all aspects of superconductivity and is rather intended as a motivation and an explanation for the coming chapters. Further reading about superconductors can instead be found for instance in [Tin75, RR78, Wil83, Car83, She94].

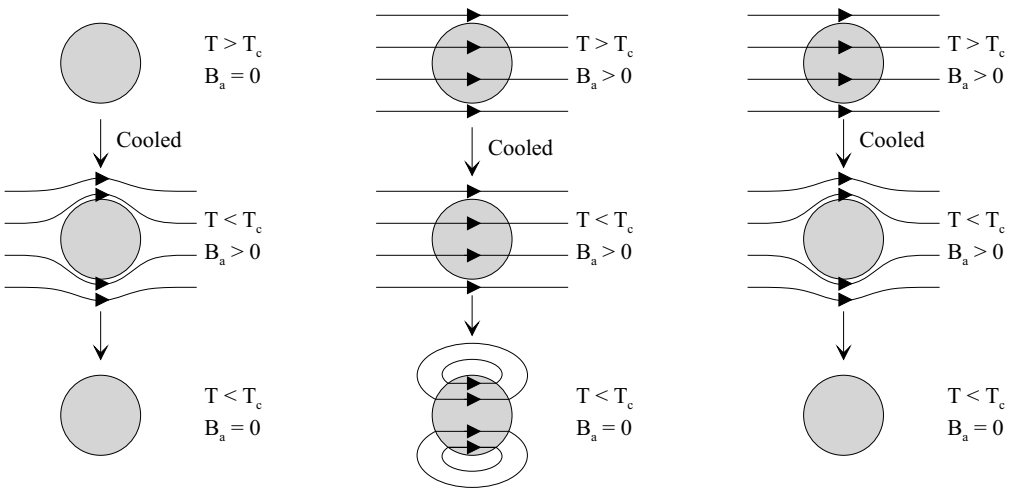

(a) $\dot{B} = 0$, $B = 0$ (b) $\dot{B} = 0$ (c) $B = 0$

Figure 2.1: The difference between materials that become perfect conductors or perfect diamagnets below a critical temperature T_c is $\dot{B} = dB/dt = 0$ for the former and $B = 0$ for the latter. (a) If there is no applied magnetic flux $B_a = 0$ *before* the material is cooled, both materials has zero internal flux below T_c. (b) A perfect conductor traps a flux that was applied before the cooling. (c) The internal flux is always expelled by a perfect diamagnet below T_c, whether an field was applied before cooling or not.

2.1 Perfect Conductivity and Perfect Diamagnetism (Meissner)

The *perfect conductivity* (zero resistance) that is occurring for superconductors is not the whole story about their properties, as mentioned above. Meissner and Ochsenfeld noted in 1933 that (type-I) superconductors are *perfect diamagnets* with the consequence that all magnetic field is expelled from the interior of the superconductor, $B = 0$ [MO33]. Let us look at an example that illustrates the difference.

Perfect conductivity implies that a change in magnetic flux enclosed in the material is not possible, $dB/dt = 0$. So, when taking a material with zero resistance below a critical temperature T_c and lowering the temperature below this T_c, and thereafter apply a magnetic field, *screening currents* will be induced in order to have an unchanged magnetic field in the interior of the material, see Fig. 2.1(a). If, however, the magnetic field were applied when the material is in normal state (i.e. *before* the temperature was lowered below the critical temperature) then the magnetic field in a material with zero resistance would again remain unchanged, and the magnetic field is trapped inside, see Fig. 2.1(b). This is quite different from how a diamagnetic material performs. In the first case when magnetic field were applied after cooling below the critical temperature, there is no difference since the magnetic field is zero for both the materials (Fig. 2.1(a)). In the second case, the magnetic field is *expelled* from the interior of the material ($B = 0$) as it is cooled below the critical temperature, see Fig. 2.1(c).

The Meissner effect so consists of expulsion of any magnetic field from the interior of a superconductor, whether it was there before the specimen became superconducting or not. The perfect diamagnetism is an intrinsic property of a superconductor, which, however, is only valid if the temperature and the magnetic field are below their critical values $T < T_c$, $H < H_c$ everywhere, where the latter depends on the temperature as

$$H_c(T) = H_c(0)\left[1 - \left(\frac{T}{T_c}\right)^2\right]. \tag{2.1}$$

2.2 Penetration Model (London)

These two fundamental electrodynamic features were well expressed by the brothers F. and H. London 1935 [LL35] with two equations dealing with the electric and magnetic fields:

$$\frac{\partial}{\partial t}\mathbf{J}_s = \frac{n_s e^2}{m}\mathbf{E} = \frac{1}{\mu_0 \lambda_L^2}\mathbf{E} \tag{2.2}$$

$$\nabla \times \mathbf{J}_s = -\frac{1}{\mu_0 \lambda_L^2}\mathbf{B} \tag{2.3}$$

where n_s is the number of superelectrons per unit volume, m and e their mass and electric charge, respectively, and μ_0 the permeability in vacuum. The London penetration depth $\lambda_L = \sqrt{m/(\mu_0 n_s e^2)}$ expresses how much the magnetic flux penetrates into the (type-I) superconductor, as will be seen.

The first London equation (2.2) is a consequence of perfect conductivity ($R = 0$) combined with Maxwell's equations and describes the acceleration of the supercurrents due to an electric field. It implies for low frequencies that the variations in the magnetic field $\dot{\mathbf{B}} = d\mathbf{B}/dt$, parallel to the material surface, penetrates the superconductor according to

$$\dot{B}(x) = \dot{B}_a \mathrm{e}^{-x/\lambda_L} \tag{2.4}$$

where $\dot{B}_a$ is the change in the applied magnetic flux density outside the superconductor.

Now, not only $\dot{B}$ but also B must decline rapidly in the superconductor in order to comply to the perfect diamagnetism property. The London brothers suggested therefore that the magnetic flux density itself also declines in a similar manner in the superconductor:

$$B(x) = B_a \mathrm{e}^{-x/\lambda_L} \tag{2.5}$$

where B_a is the applied magnetic flux density. It is now understood why λ_L is called the penetration depth because when $x = \lambda_L$, 63% of the flux density has declined. This drop in intensity of the magnetic flux density may be expressed by (2.3) for more general shaped specimens and for magnetic flux densities in an arbitrary direction.

One should remember that the London equations have been suggested in order to approximately describe the behaviour of a (type-I) superconductor. Hence, they are not exact but give a good result in most cases.

2.3 Quantum Mechanics Model (Bardeen-Cooper-Schrieffer)

The trio Bardeen, Cooper and Schrieffer [BCS57] developed a theory that explains a superconductor in terms of quantum mechanics, which was a major step in the evolution of the understanding of superconductors. It considers energy gaps and excitation spectrum for the electrons and predicts that the conducting superelectrons form so-called *Cooper pairs* because the electrons interact with mechanical vibrations in the crystalline lattice that bear a resemblance to sound waves. This atom movement in the lattice has a tendency to neutralise the normal repulsion between electrons and instead generate an attraction between them, which is only possible below a certain critical temperature.

The BCS-theory predicts a penetration depth that is very close to the London penetration depth for different superconducting materials. This combination of electrons in pairs determines also the coherence length, which is a measure how likely it is that a Cooper pair is formed, and corresponds to the distance between the electrons within the Cooper pair.

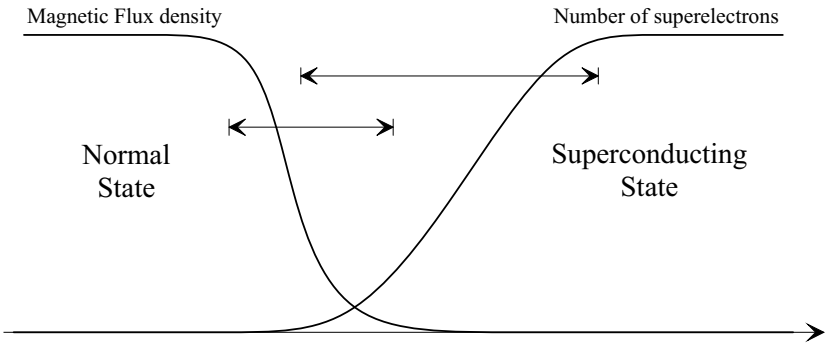

Figure 2.2: The surface energy between normal and superconducting state is *positive* when $\lambda < \xi$, as in the figure. For a *negative* surface energy ($\lambda > \xi$), it is more favourable for normal and superconducting state to co-exist in a *mixed state*.

2.4 Wave Function Model (Ginzburg-Landau)

Ginzburg and Landau presented already in 1950 a phenomenological theory for superconductivity [GL50] that concentrated entirely on superconducting electrons and not on excitations as in the BCS-theory. They introduced a pseudo-wave function that is related to the number of superelectrons per unit volume, and which can be considered as the centre-of-mass motion of the Cooper pairs. The triumph of the model is that it may handle an *intermediate state* of superconductors, where normal and superconducting state coexist in presence of a magnetic field $H \approx H_c$. It has later been shown that the pseudo-wave function is proportional to a parameter of the energy gap in the BCS-theory, which makes the Ginzburg-Landau theory a "masterstroke in physical intuition" [Tin75].

Ginzburg and Landau introduced a temperature-dependent *coherence length* ξ, which is related to, but distinct from, the coherence length introduced by Pippard in 1953 [Pip53]. It characterises the distance over which the superelectron density changes from its maximal value (superconducting state) to zero (normal state). The *penetration depth* λ that describes the strength of the Meissner effect (c.f. Londons' equations) is the shortest distance over which the magnetic field can change in a superconductor, and it influences the density of normal electrons. It has a temperature dependence as $\lambda(T) = \lambda_0(1 - (T/T_c)^4)^{-0.5}$, which corresponds approximately to the temperature dependence of the coherence length ξ. The Ginzburg-Landau ratio $\kappa = \lambda/\xi$ is therefore approximately independent of temperature.

2.5 Surface Energy – Type-I and -II Superconductors (Abrikosov)

The Ginzburg-Landau ratio takes very small values ($\kappa \ll 1$) for typical pure superconductors. This leads to a *positive surface energy* in a small domain between normal and superconducting regions in the material, see Fig. 2.2. The appearance of normal regions is then energetically unfavourable, and so the material stays superconducting throughout until the magnetic field reaches the critical value H_c.

In 1957, Abrikosov presented a theoretical work on what would happen if κ is instead very large [Abr57]. This implies a *negative surface energy*, which gives a very different magnetic behaviour of the material. Abrikosov named, therefore, the then conventional superconductors *type-I* and these new superconductors *type-II*. He showed further that the exact breakpoint is at $\kappa = 1/\sqrt{2}$. Instead of the breakdown of superconductivity at H_c as for type-I superconductors, the new type-II obeys the perfect diamagnetism property up to a *first critical field*, $H_{c1} \sim H_c/\kappa$,

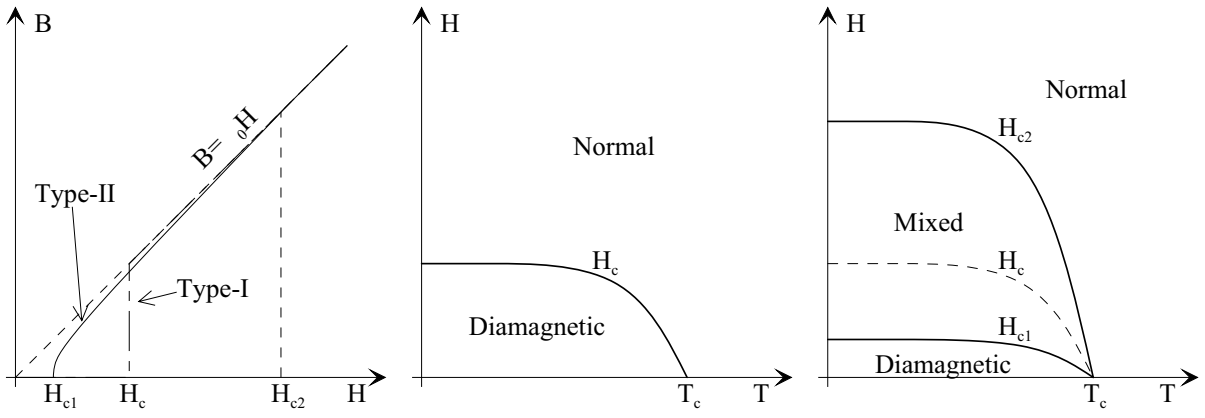

(a) (b) (c)

Figure 2.3: (a) Type-I superconductors have a break-down of superconductivity at a critical magnetic field H_c, whereas type-II superconductors have continuous increase in flux starting at H_{c1} (decreasing with κ) until the penetrated field H reaches the magnitude of the applied field H_a at H_{c2} (increases with κ) and superconductivity is lost. (b) Phase-diagram for type-I superconductors: only superconducting (diamagnetic) and normal states are present. (c) Phase-diagram for type-II superconductors: there is also a mixed state where superconducting and normal state regions co-exist.

after which it has a continuous increase in flux penetration. This diffused flux B fully penetrates the specimen at a *second critical field*, $H_{c2} \sim \kappa H_c$, whereby the superconductivity is lost, see Fig. 2.3(a). Between these critical values, normal state regions co-exist with superconducting regions in a so-called *mixed state*, see next section. The difference in phase-diagrams as functions of applied field and temperature for type-I and type-II superconductors are given in Fig. 2.3(b) and 2.3(c). The former graph is given by (2.1).

Among the low temperature type-I superconductors there are mainly pure metals, such as Lead (Pb), Mercury (Hg), Niobium (Nb) and Tin (Sn). Typical low temperature type-II superconductors are alloys, e.g. Niobium-Tin (Nb_3Sn), Titanium-Niobium (Ti_2-Nb) and Molybdenum-Rhenium (Mo_3-Re). The former group of materials is less brittle than the latter, so the two groups are equally called *soft* and *hard* superconductors, respectively. High temperature superconductors are all of type-II but have some special features that will be treated in Section 2.11.

2.6 Mixed State of Type-II Superconductors

The negative surface energy (i.e. energy is release when the interface is formed) for type-II superconductors leads to a large number of small normal regions being produced in the superconducting material when a magnetic field $H_{c1} < H < H_{c2}$ is applied. This *mixed state* (or Schubnikov phase) is an intrinsic feature of type-II superconductors.

It was foreseen by Abrikosov that the flux would penetrate in a regular array of flux tubes, all of which having the quantum of flux $\Phi_0 = h/(2e) = 2.6678 \cdot 10^{-15}$ Wb (h = Planck's constant, e = electron charge), passing through its normal state interior, see Fig. 2.4. A change in the applied field must consequently cause a modification of the density of these flux tubes. The flux tube diameters are very small ($\sim \xi$) because that increases the ratio between surface and volume, which acts beneficially on the energy state of the material. In each tube, there is a vortex of supercurrents strengthening the flux towards the centre. This supercurrent shields the

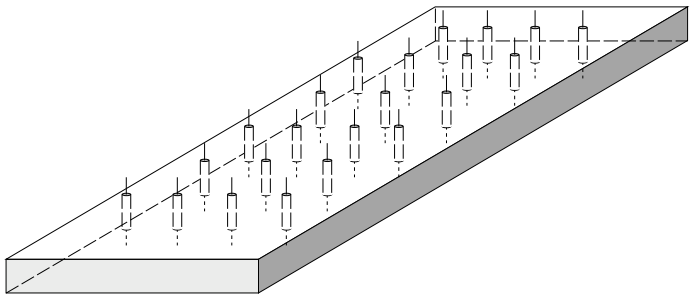

Figure 2.4: Superconducting and normal state regions co-exist in the mixed state. There is a flux quantum Φ_0 passing through each tube of normal region, and a supercurrent shields the surrounding superconducting regions from flux and so assures the diamagnetism property.

surrounding superconducting regions from flux and so assures the diamagnetism property.

2.6.1 Flux-pinning and Hysteresis

The flux tubes in type-II superconductors should in principle be able to move freely and adjust their density according to the applied field. However, inhomogeneities in the superconductor due to grain boundaries and lattice defects make that an energy barrier must be overcome in order to move the vortices. Due to this so-called *flux-pinning*, the magnetic flux in the superconductor will not change in a reversible manner as the externally applied field changes, and the work needed to overcome this *pinning force* is connected with some losses in the superconductor. Flux-pinning is therefore the fundamental reason why superconductors of type-II exhibit hysteresis with related AC-losses. Further explanation of how the pinning force produce a hysteretic behaviour is found in conjunction with the critical state model in Section 2.8.

2.7 Transport Current – Flux Flow and Flux Creep

The vortex region is, as mentioned, about the diameter of the coherence length ξ, which in a type-II superconductor is smaller than the penetration depth λ. Furthermore, the flux tubes repel each other. This leads to that a superconducting path is left open in which a current may pass.

2.7.1 Critical Current

A current that passes the flux lines produces a Lorenz-force $\mathbf{F}_L = \mathbf{J} \times \mathbf{\Phi}_0$ upon each vortex. The vortices will, however, remain in their place as long as this Lorenz-force is inferior to the pinning force F_p. At some critical current density J_c, the Lorenz-force overcomes the pinning force and the vortices starts to move. This is called *flux flow*. The critical current I_c of a type-II superconductor is so approximately J_c times the cross-section through which the current flows. (In practice, the critical current is often defined to be the current, at which an induced electric field reaches 10^{-4} V/m, c.f. Section 3.1.) The vortices can also start to move because of a reduced pinning force that has its origin in thermal activation of the lattice. The motion is then normally more sporadic and much slower. This has hence been named *flux creep*.

2.7.2 Nonlinear Resistivity

When the vortices are in motion due to an electric current in the superconductor, there is a local change in flux within the superconductor and an electric field **E** is induced in the same direction as the current. For an external observer, this electric field is viewed as if the superconductor possesses a resistivity. Hence, this nonlinear resistivity is zero below the critical current and then increases rapidly as the flux motion becomes more important. (In fact, the resistivity is not exactly zero, just extremely small, due to the thermally activated flux motion.)

This resistivity is undesirable, so it has become common to introduce "defects" into the superconductor lattice in order to increase the pinning force and so also the critical current density. Practical applications of type-II superconductors are therefore limited not only by the critical field H_{c2} and the critical temperature T_c, but also by the critical current density J_c.

2.8 Critical State Model (Bean)

Bean presented in 1962 a model that was based on experimental observations [Bea62, Bea64]. It was noted that the current density J takes only the value of zero, where the perfect diamagnetism property holds, or a critical critical value J_c, in the mixed state:

$$J = \begin{cases} 0\,, & E < E_c \\ J_c\,, & E \geq E_c \end{cases}, \tag{2.6}$$

where E_c is the electric field at the critical current density.[1] The model allows only two states, perfect diamagnetism or mixed state, with a sharp transition and it has thus been named the *critical state model*.

The model has later been explained as a consequence of having an equally strong pinning force, using the following arguments [Tin75]: when a magnetic field H is applied to a superconducting specimen that has no prior magnetic flux, there will be shielding currents induced on the superconductor surface in order to expel the magnetic field from the inner of the specimen. (The microscopic shielding currents in the individual flux tubes are not considered in the critical state model.) These currents can be very large, which then means that the Lorenz-force at the surface becomes very large too. If it is larger than the pinning force, pinned vortices are displaced inwards, into the specimen from the surface. Hence, the surface current is spread out over a larger area, and the current density is diminished. This displacement of vortices continues until the Lorenz-force is smaller than the pinning force $F_L < F_p$, which occurs when the shielding current has a density equal to J_c everywhere. For the example of an infinite slab of width $2a$ with a magnetic field applied parallel to the long side of the slab (Fig.2.5(a)), the macroscopic magnetic field distribution $h(x)$ and the current distribution $j(x)$ (both as functions of the slab width) take the values shown in Fig. 2.5(b). (The current is flowing into the slab on the right-hand side.) The flux density and the current distribution is somewhat different for an infinitely thin superconducting tape, a strip,(thickness $d \to 0$, Fig. 2.6(a)), because the applied field can act on the top side of the tape as well, see Fig. 2.6(b) [BI93].

The vortices in the specimen are now pinned where they are, and they remain therefore unchanged unless they are forced to move by a Lorenz-force. Suppose now that the magnetic field decreases from the situation in Fig. 2.5(b). A surface current in the opposite direction is then induced, which forces the flux vortices with opposite direction to enter into the specimen,

[1] In order to use the critical state model in numerical simulations, the expression (2.6) can be re-formulated as: $\mathbf{J} = \mathbf{E}\, J_c/E_c$ if $E \neq 0$ and $\partial\mathbf{J}/\partial t = 0$ if $E = 0$ [SHM91, UYTM93].

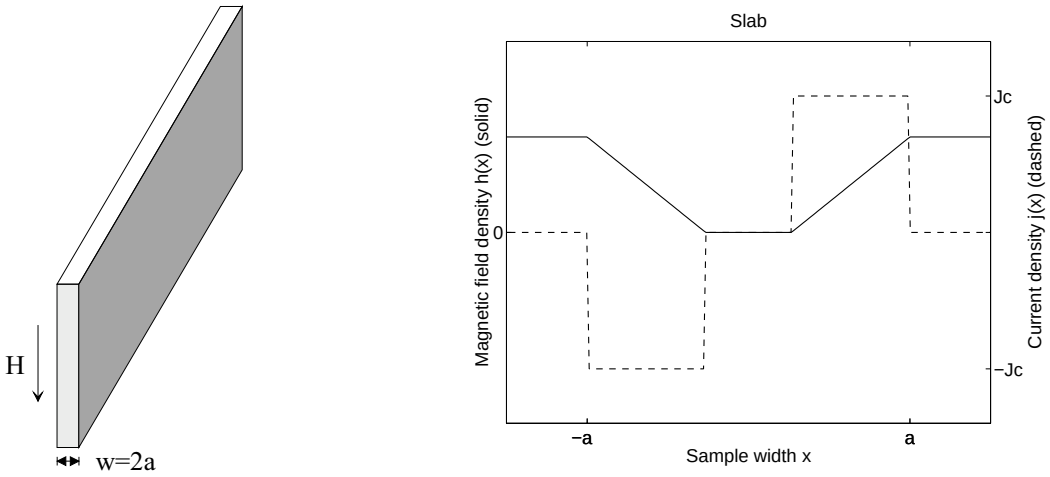

(a) (b)

Figure 2.5: (a) An infinite slab of width $2a$ with an applied magnetic field H parallel to the long side of the slab. (b) Magnetic field and current distributions in the slab for an applied magnetic field H.

and these replace the formerly pinned vortices. The flux density and the current distribution in the slab are then as in Fig. 2.7(a). The superconductor has thus a *memory* of former applied magnetic field, which is erased by a changed field. If we plot the mean magnetic flux density in the specimen $\bar{B} = \frac{\mu_0}{2a}\int_{-a}^{a} h(x)\,dx$ versus applied field H with amplitude H_0, we get a typical loop of a *hysteresis*, see Fig. 2.7(b). Hence, it is understood that the critical state model exhibits hysteresis. More about how the hysteresis in the critical state model works with a transport current is found in Section 6.1, and an extension to currents larger than a fully penetrated sample is considered in Section 6.7. The flux density and the current distribution in the case of both an applied magnetic field and a transport current have been computed in [BI93].

2.8.1 Preisach Model of Hysteresis

The Preisach model of hysteresis is a general model that describes hysteresis with different shapes of the hysteresis loop. It is demonstrated in Chapter 6 how it with certain weighting functions corresponds exactly to the results of the critical state model. This relationship to the modelling of superconductors was first shown by Mayergoyz [May91, May96].

2.9 Power-Law Approximation ($E - J$ Model)

It was assumed in the critical state model that all flux tubes are subject to the same pinning force giving a sharp transition between zero current and J_c at an electric field E_c as in (2.6). That is an approach that does not always apply to actual specimens of superconductors: the thermal activation may give rise to a flux creep already before E_c is attained. It has therefore become common to model the transition by the nonlinear relationship between the current density and the electric field expressed by the power-law:

$$\mathbf{E} = E_c \left(\frac{J}{J_c(\mathbf{B})} \right)^{n(\mathbf{B})} \frac{\mathbf{J}}{J}\,, \tag{2.7}$$

where $J = |\mathbf{J}|$ and both the critical current density $J_c(\mathbf{B})$ and the power-law exponent $n(\mathbf{B})$ depend on the local magnetic flux density. This model was firstly applied as a phenomenological

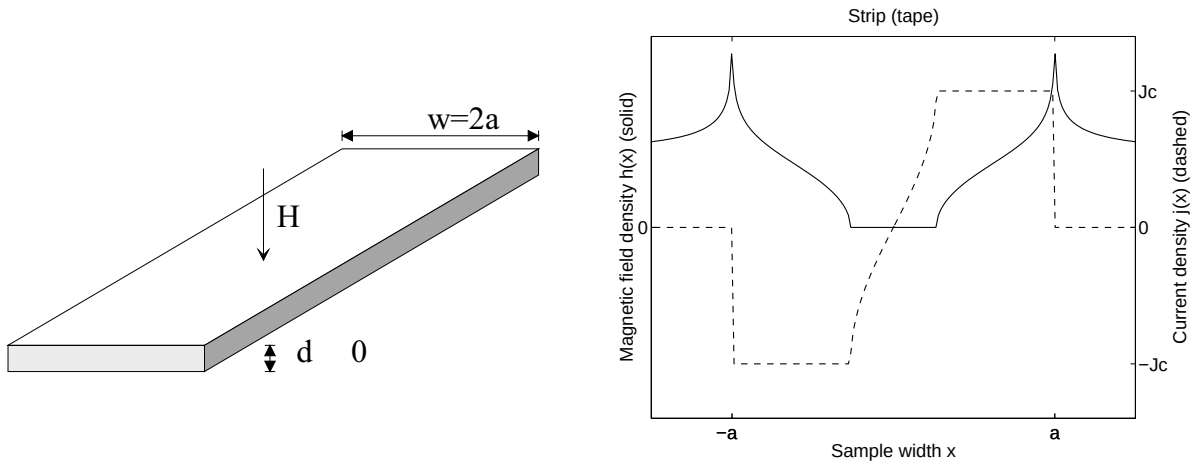

(a) (b)

Figure 2.6: (a) An infinitely thin tape (strip) of width $2a$ with an applied magnetic field H perpendicular to the flat side of the strip. (b) Magnetic field and current distributions in the strip.

approach to describe the soft transition of the current density, but it has later been justified by arguments of flux creep [VFG91, BG96, Bra96b]. (See also [May98].) The full electromagnetic description of the superconducting material also requires a constitutive law between flux density $\mathbf{B}$ and magnetic field distribution $\mathbf{H}$. The following approximate relationship was suggested in [Bra96b]:

$$\mathbf{B} = \mu_0 \mathbf{H}\,, \tag{2.8}$$

which is particularly good for a large value of the Ginzburg-Landau ratio κ, c.f. Section 2.5. The combination of (2.7) and (2.8) with Maxwell's equation so constitutes a tool to compute the electromagnetic behaviour of a superconductor of arbitrary shape with arbitrary applied magnetic field and arbitrary transport current.

The behaviour of the $E-J$ model has been theoretically investigated in [Rhy93] and [May98], in which it is demonstrated that the model corresponds to a nonlinear diffusion. The former paper shows further that the limit $n = 1$ corresponds to a purely resistive material, and $n = \infty$ to a material with a rate-independent hysteresis with no resistance. The latter reference demonstrates also that $n > 7$ is large enough to produce a field penetration close to a sharp transition for a large class of functions of the applied field, meaning that it close to the critical state model. Further explanation how the $E - J$ model exhibits hysteresis for $n > 1$ is found in Section 4.2.3.

Numerical simulations of the $E - J$ model can be made with either finite element methods [AMBT97, PL97] or with an integration formulation [Bra96a, Rhy98]. It has turned out to be a handy tool because of its good compliance with measurements on superconductors both when it comes to DC, AC and loss characteristics [Ame98, LPME98, NSD+00]. It has also been used as reference for development of new measurement techniques [MYBH00], see Section 3.7. The problem with the model is, however, that it is computationally heavy.

As an alternative to have the nonlinearity described in the $E-J$ relationship, one can suppose that there are no surface currents flowing in the superconductor and describe the nonlinearity by the relationship between $B - H$ only [VSM+98]:

$$\mathbf{J} = 0 \tag{2.9}$$

$$\mathbf{B} = \mu_0 \mathbf{H} + \mathbf{M}(\mathbf{H})\,. \tag{2.10}$$

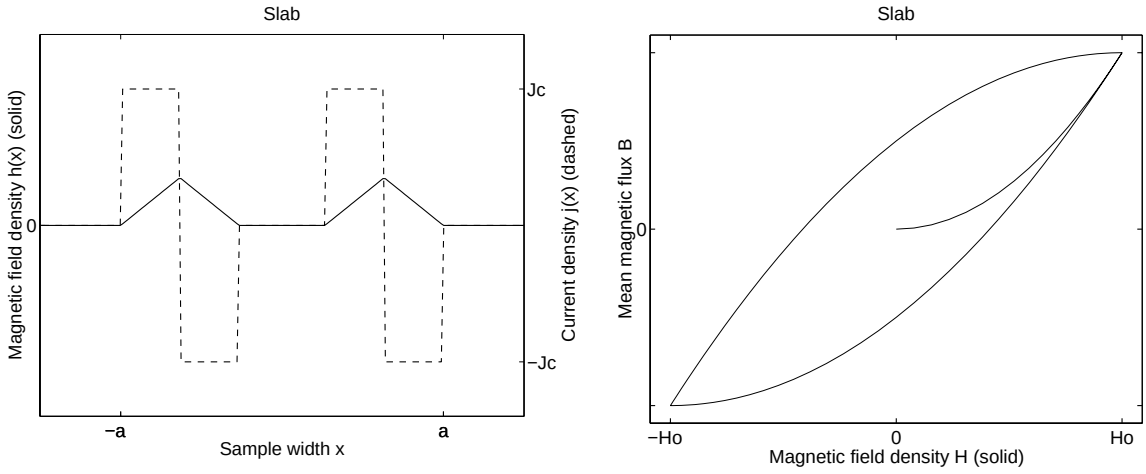

(a) (b)

Figure 2.7: (a) Magnetic field and current distribution in the slab when the applied magnetic field has decreased. Note that the applied field $H = 0$ here. (b) The typical hysteresis loop occurs when the mean magnetic flux density $\bar{B} = \frac{\mu_0}{2a}\int_{-a}^{a} h(x)\,dx$ in the superconductor is plotted versus the applied magnetic field H.

This method has mainly been used for modelling where the magnetic behaviour is of importance.

2.10 Magnetic field dependence (Kim)

Another problem with the critical state model is that the critical current density J_c has shown to be dependent on the magnetic flux density $\mathbf{B}$ and the temperature T. This has been demonstrated in numerous experiments and it was also recognised by Bean [Bea64]. Later, it has also been shown in experiments that the transition from zero current to critical current becomes smoother with a stronger field. This means that the exponent n in the power-law approximation is influenced by the magnetic flux.

One of the first models to describe the influence on the critical current by the magnetic flux was given by Kim and his team [KHS62, KHS63b, KHS63a]. The model, which is based on experiments on type-II low temperature superconductors, states that the current density decreases with local magnetic flux density according to

$$J_c(B,T) = J_{c0}(T)\left(1+\frac{B}{B_0}\right)^{-1}, \tag{2.11}$$

where $B = |\mathbf{B}|$ is the magnitude of the magnetic flux density, B_0 is a constant and $J_{c0}(T)$ is the current density at zero field, which is a temperature dependent constant of the material. Anderson developed at the same time a theory based on flux creep, i.e. thermally activated motion of flux tubes, which predicted the constant $J_{c0}(T)$ [And62, AK64].

The current distribution in a slab (Fig. 2.5(a)) is no longer constant when (2.11) is combined with the critical state model. The current distribution is then slightly smaller at the edges and somewhat larger close to the field-free region in the centre of the slab [KHS62].

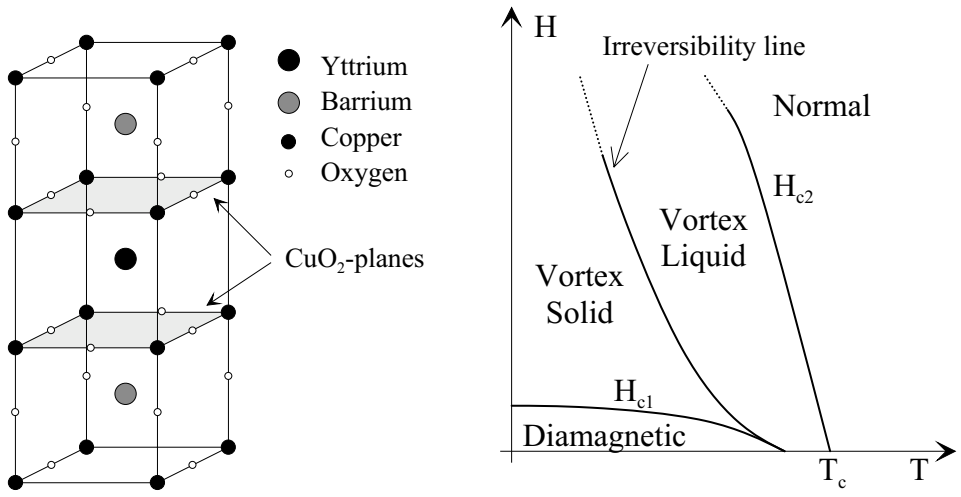

(a) (b)

Figure 2.8: (a) In the layered crystal structure of high temperature superconductors (here $YBa_2Cu_3O_7$), it is the copper-oxide planes that carries the current. This structure is also responsible for the anisotropy in critical magnetic fields and critical current. (b) High temperature superconductors has a very large region of mixed state, but thermal fluctuations in the lattice causes a *vortex liquid state*, which is especially accentuated closer to the critical current.

2.11 High Temperature Superconductors

The BCS-theory predicts that superconductivity can only appear below a critical temperature of about 32 K, so it was a big surprise to the scientific world when Bednorz and Müller in 1986 discovered a ceramic that becomes superconducting at a critical temperature of 35 K [BM86]. This discovery of *high temperature superconductors* (HTS) started the search for even higher critical temperatures and soon new materials had been discovered that have today (year 2001) critical temperatures up to 135 K.[2]

It is until today not quite clear how the superconductivity in the high temperature superconductors work, but experiments have shown that the supercurrents consists of paired electron as for the metallic low temperature superconductors. These ceramic superconductors consists of layered crystal structures, see Fig. 2.8(a), where copper-oxide planes are responsible for the current transport. The more copper-oxide planes are gathered together before another metal oxide layer appears, the larger the critical temperature has turned out to be. The layered structure is further the explanation why high temperature superconductors exhibit an extreme anisotropy in critical magnetic fields and critical current. The material, being a ceramic, is also mechanically brittle, which complicates its application. Furthermore, the crystal grains are difficult to make large, and the coupling between them is fairly poor, which reduces the ability of carrying a transport current, especially when the temperature approaches its critical value for the material. It has also turned out that the conductivity is further diminished when the grains are at an angle [She94].

High temperature superconductors have a very short coherence length (10-100 times shorter than low temperature type-II superconductors) and a very deep penetration depth, which makes them to extreme samples of type-II superconductors. The Ginzburg-Landau ratio κ is therefore very large, and so the first critical magnetic field H_{c1} is very low and H_{c2} can be extremely high.

[2] Superconductors at room temperature can today only be found in front of an orchestra or a choir.

The high temperature superconductors have consequently a very large region of mixed state, but large thermal fluctuations in the lattice may cause the vortex structure to "melt" into a *vortex liquid state*, which is especially accentuated closer to the critical current, see Fig. 2.8(b). The flux tubes are then free to move when being subject to the Lorenz force, since they are no longer pinned. This affects the resistivity and gives a very small critical current density. In order to overcome this problem, impurities are introduces in the superconductor during its production so that the vortices will be pinned at these contaminations. There is then no longer a consistent pattern of flux tubes, but the position of the flux tubes forms rather an irregular pattern, which is called the *vortex glass state*. The irregular pattern does predominantly not influence the macroscopic density of vortices. This signifies that with a mean pinning force at these vortices, the critical state model (Section 2.8) can still be applied to values up to the irreversibility line (Fig. 2.8(b)) with a mean critical current density J_c. However, an exponentially decreasing flux creep has been noted in experiments, even if the applied field is constant and no transport current flows. This suggests that the nonlinear diffusion implied by the $E-J$ model in Section 2.9 represents well the behaviour of high temperature superconductors. Moreover, the large κ makes the first critical magnetic field H_{c1} very small so that the approximation $\mathbf{B} = \mu_0\mathbf{H}$ becomes very close to reality.

2.11.1 HTS Materials

There are in principle two types of high temperature superconducting materials: those that include rare earths and those that do not. The most common from the former group is Yttrium-Barium-Copper-Oxide ($YBa_2Cu_3O_7$) or YBCO for short. It has a critical temperature of 95 K and is best suited for thin films. YBCO has a good resistance against magnetic field, but possesses weak links between grains. A widespread material from the latter group is Bismuth-Strontium-Calcium-Copper-Oxide, which is abbreviated to BSCCO. It comes in two different mixtures, $Bi_2Sr_2CaCu_2O_8$ (Bi-2212) and $Bi_2Sr_2Ca_2Cu_3O_{10}$ (Bi-2223) that have a critical temperature of about 110 K. The latter combination can be deformed and shaped more easily due to the shearing along the Bismuth-oxide planes, which makes it useful to produce tapes that contain one (mono-) or several (multi-) filaments of superconducting material. A well-developed production method helps also to align the crystals, and so increases the conducting ability. Bi-2212 is better aimed for bulk superconductors. The main problem with Bismuth-based superconductors is however its tendency of flux creep.

2.11.2 Anisotropic Parametric Model

The model presented by Kim et.al. worked well on the low temperature type-II superconductors used in their experiments, but it does not always correspond well to measurements on high temperature superconductors. The latter has also an anisotropic dependence on the magnetic flux density, which is due to the atomic structure. (See Section 2.11 for an introduction to high temperature superconductors.) Different attempts have been made to find a model that express this angular dependence of the flux density, see for instance [TT89, TBK94, Ste98].

We present here a phenomenological model that was firstly presented in [DSS99], and which was developed in order to have a good correspondence between predicted and measured data. It is intended to be used in computer simulations rather than to give a physical explanation. The model is based on (2.11) and was then empirically developed to fit measurement results, where the critical current $I_c(B, \varphi)$ depends on the amplitude of the magnetic flux density B and on the angle of the applied field φ. ($\varphi = \pi/2$ when the field is applied *perpendicular* to the flat side of the tape, as H in Fig. 2.6(a); $\varphi = 0$ when the field is applied *parallel* to the flat side, i.e.

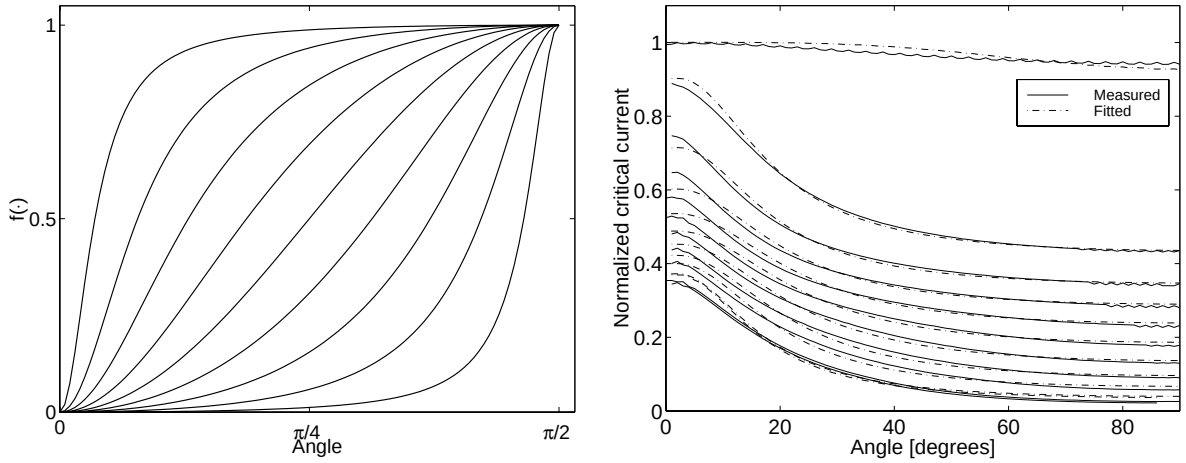

(a) (b)

Figure 2.9: (a) The function $f(\varphi, z_1)$ can move the transition to larger or smaller angels with the parameter $z_1 \in (-1, 1)$. From left to right: $z_1 = 0.8, 0.6, \ldots, -0.8$. (b) Normalised critical current I_c/I_{c0} as a function of the angle of the applied magnetic field between 2 and 400 mT, as measured and fitted from (2.12) – (2.14).

vertical to the thin, long side of the tape.) The model is constructed in such a way that some parameters, $\theta_0 = \{B_1, B_2, p_1, p_2\}$, are linked with the parallel direction ($\varphi = 0$), and others, $\theta_{\pi/2} = \{B_3, B_4, B_5, p_3, p_4, p_5\}$, with the perpendicular direction ($\varphi = \pi/2$). The two are then related with a smooth function $f(\varphi, z_1)$, whose transition may be varied with a parameter z_1. Compared to (2.11), a better fit is achieved for small fields when a term $(B/B_x)^{p_x}$ is added in the numerator in each direction. Another such term in the denominator for the perpendicular direction enables a good fit for the whole measured range. (The term $[1-f(\varphi, z_1)]$ restricting the influence of θ_0 when $\varphi = \pi/2$ may be replaced by 1 (unity) in order to simplify the expression, as the consequent difference in $I_c(B)$ is minimal.)

$$I_c(B) = I_{c0} \cdot \frac{1 + \left(\frac{B}{B_1}\right)^{p_1} \cdot [1 - f(\varphi, z_1)] + \left(\frac{B}{B_3}\right)^{p_3} \cdot f(\varphi, z_1)}{1 + \left(\frac{B}{B_2}\right)^{p_2} \cdot [1 - f(\varphi, z_1)] + \left[\left(\frac{B}{B_4}\right)^{p_4} + \left(\frac{B}{B_5}\right)^{p_5}\right] \cdot f(\varphi, z_1)} \tag{2.12}$$

The function $f(\varphi)$ is restricted by $f(0) = 0$, $f(\pi/2) = 1$, and it must further be smooth and monotonically increasing. Measured data do not show a symmetrical transition around $\pi/4$, so a function that can be adjusted with the additional parameter z_1 was constructed:

$$f(\varphi, z_1) = \frac{1 - \cos(\alpha(\varphi))}{2} \tag{2.13}$$

$$\alpha(\varphi) = \arg\left(\frac{e^{j2\varphi} - z_1}{e^{j2\varphi} - 1/z_1} \frac{1 - 1/z_1}{1 - z_1}\right) = \arg\left(\frac{e^{j2\varphi} - z_1}{1 - z_1 e^{j2\varphi}}\right), \tag{2.14}$$

where $\arg(\cdot)$ stands for the angle argument of the complex value within the brackets. This function moves the transition to larger or to smaller angles when the parameter z_1 is varied between -1 and 1, see Fig. 2.9(a). The parameters $\{\theta_0, \theta_{\pi/2}, z_1\}$ in (2.12)–(2.14) are identified by minimising the mean square error between measured and estimated data. The results from such a fit, using the measured critical current with externally applied field of different application angle (0 to $\pi/2$) and amplitudes between 2 and 400 mT (c.f. Section 3.1 and 3.4), are depicted in Fig. 2.9(b).

The power-law exponent n in (2.7) depends also on the on the magnitude of the local flux density and its direction. Measurements have shown that its dependence on the magnetic flux density is very similar to the critical current's dependence of the same variables. Hence, the model (2.12)–(2.14) has also been applied to $n(B)$ with success. However, this model has been criticised because it contains too many parameters to reflect the physics behind the phenomenon it describes.

2.12 Cryogenics

All superconducting materials must be cooled below its critical temperature in order to exhibit superconductivity, which can be a costly business. The low temperature superconductors are usually operated in a cryostat full of liquid helium, whose boiling temperature is 4.2 K at normal pressure. Sophisticated cryogenic plants are then needed to produce and maintain that temperature, and security measures must be taken in order to avoid a possible quench, i.e. a sudden re-heating of the superconductor and the surrounding cryogenic system, which is mainly due to a low heat capacity at such temperatures. The refrigeration of high temperature superconductors is much simpler and less costly. A superconductor with critical temperatures of about 100 K, such as YBCO or BSCCO, can without difficulty be cooled by a fairly simple cryo-cooler, or alternatively by liquid nitrogen (LN_2), which has a boiling-point of 77.4 K. Liquid nitrogen has the advantages of being much more available and many times cheaper to produce than liquid helium. The practical cooling capacity needed to cool the same heat loss at 77 K is also from 25 to 100 times less than for a system at 4.2 K. Capital and operational costs may then be reduced considerably. Another advantage of a higher operation temperature is the better heat capacity of the materials. It has the consequence that the thermal stability is improved and quenches are hence avoided more easily.

2.13 Applications

There are a number of areas where superconductors may be applied [See98]. The list presented here shows the diversity of present and possible future products, which apply different characteristics of superconductivity. The list is far from exhaustive and the applications are not fully described; the intension of the present section is rather to give an idea about the applicability of this seemingly theoretic area of science.

2.13.1 Small Scale Applications

Examples of small scale applications are mainly in the area of ultra fast microelectronics or instrumentation, of which most are based on the Josephson effect, a quantum phenomenon [vDT99]. Superconducting *low noise detectors* are used for antennas, and *microwave filters* with very steep skirts are now applied in the field of mobile telecommunications. SQUIDs (superconducting quantum interference devices) are highly sensitive magnetic flux detectors that are used in precision instruments, e.g. in MEG (magnetoencephalography) for detecting the brain's magnetic activity. Finally, there have also been attempts to produce digital memory and circuits based on the Josephson effect.

2.13.2 Large Scale Applications

Large scale application use preferably the characteristic of low resistivity in order to lower losses and to reduce size of conventional electric equipment [DWS90]. One of the first applications was *superconducting magnets*, which are used in physics experiment and medical equipment in in order to produce extremely high magnetic fields, e.g. MRI (magnetic resonance imaging). *SMES* (superconducting magnetic energy storage) is a new possibility to store energy by letting a supercurrent circulate in such a magnet. Efforts has also been made to introduce superconducting magnets into *motors* and *generators*. *Transformers* with superconducting windings and *cables* are two other applications where reduction of losses and size are foreseen. There are also new technological opportunities that make use of the transition between superconducting and normal states in *fault current limiters*. The magnetic property of superconductors have been suggested to be used in *bearings* of fly-wheel energy storage systems. Likewise, there are *magnetically levitated (MagLev) trains* that use this property.

The future for superconducting applications look very optimistic from a technological point of view (even if some obstacle exist), but so far it is rather expensive to produce the superconductor. There is also a hesitation to introduce new technologies in some domains, so although there might also be environmental advantages, there are only some niches where these new products are profitable [NO99, SP01, PSSR01].

2.14 Chapter Summary

This chapter has addressed the fundamental characteristics of superconductors (perfect conductivity, perfect diamagnetism and quantified flux) and models that describe them at different levels. A large portion has been dedicated to type-II superconductors, which have a partial penetration of magnetic flux. It has been explained how the pinning of these flux lines is the intrinsic reason for *hysteresis* in such superconductors, and that flux flow and flux creep give rise to a *resistive voltage*. It has further been elucidated that high temperature superconductors are extreme cases of type-II superconductors. Practical aspects, such as cryogenics and possible applications, have also been mentioned.

In particular, the author has proposed a parametric model that may be used to describe accurately the measured dependence of critical current and power-law exponent on both perpendicular and parallel magnetic field. A special function that produces a smooth transfer from 0 to 1 when the angle changes from 0 to $\pi/2$ was necessary for this behaviour. The latter function was invented by the author. This parametric model has, however, been criticised for having too many parameters to describe the physics behind the modelled phenomenon.

Chapter 3

Measurements

There are different methods of measuring losses in superconductors: calorimetric, magnetisation and electric methods. Here we only consider the latter one.

The electrical measurement method is advantageous for specimen in form of tapes that have short lengths (50-10 cm) in order to evaluate their AC-losses. This is because once the experimental configuration is correctly tuned, it allows simple and quick measurements, where specimen may be changed without major effort. However, the electrical method has some inherent difficulties with large currents (10–40 A) and low voltages (10–100 nV) present in the same experimental set-up. This requires high-quality, low-distortion and low-noise amplifiers. It is also extremely important to prevent coupling between the low voltage circuit and the current circuit. Another difficulty is the large inductive component that occurs in lock-in measurement (see Section 3.3), which makes the phase-angle that decides the losses extremely difficult to deduce with precision.

The electrical measurements used in this thesis are carried out on Bi-2223 tapes with sheaths of silver and silver-gold alloys. The number of superconducting filaments in the tapes are 1, 7, 19, 37 and 55. A transport current is driven through these specimen, either in self-field or with an additional externally applied magnetic field. The latter may be applied at different angles with respect to the larger surface of the HTS tape, c.f. Section 2.10. The current is given for each of the different measurements. Even so, it is also measured in order to know the true current that actually flows through the specimen. The tapes are immersed in liquid nitrogen during the measurements in order to keep a constant temperature of 77 K, which is about 30 K below their critical temperature, see Fig. 3.1. For large supercritical currents, the dissipation in the superconductor can increase considerably so that bubbles of nitrogen may occur on the specimen's surface. The produced heat is then not removed in a homogeneous manner, meaning that temperature of the superconductor is not properly controlled. Hence, the temperature dependence of the specimen's characteristics enters the measurement data in an uncontrolled way. Such large currents must therefore be avoided. The data describing the measurements can be found in Table3.1

Current amplitude I_0 [A]	$0 \rightarrow 0.8I_c$
	$0 \rightarrow 1.5I_c$
Measured length l_t [m]	0.050
Current frequency ω_0 [rad/s]	$2\pi \cdot 59$
Sampling frequency f_s [kHz]	10
Temperature T [K]	77

Table 3.1: Measurement Specification

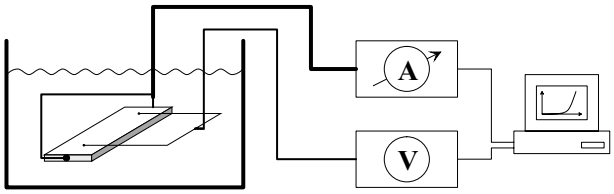

Figure 3.1: The electrical measurements are carried out with the superconductor immersed in liquid nitrogen. A current is forced through the specimen, whereby the voltage, but also the current, is measured, and finally the data are treated in a computer program.

3.1 Direct Current Measurements

These measurements are carried out in order to characterise the specimens from a DC point of view. The current I is slowly increased whereby the current and voltage V_{dc} are registered over the measurement length l_t with a voltmeter (or with time-series if many consecutive measurements should be carried out). Afterwards, the critical current I_c is defined to be the current that produces a voltage drop of $V_0 = 1.0\mu\text{V/cm}$, which is a generally accepted definition. The data are then fitted to a global power-law between voltage and current,

$$V = V_0 \cdot \left(\frac{I}{I_c}\right)^n , \tag{3.1}$$

defining the power-law exponent n.

3.2 Time-series Measurements

All measurements in the applied set-up are, in fact, recorded as time-series by sampling at a frequency of 10 kHz and then treated in a computer program. The treatment may consist of retrieving the DC characteristics as described above or of extracting amplitude and phase information with the lock-in method presented in the next section, before the data are stored. But time-series as such are also stored for later treatment. The latter are either with a sinusoidal current or with an 'arbitrarily' shaped current.

The measurements with a sinusoidal current (59 Hz) are repeated for different amplitudes and are later used for identification of a model of the superconductor, which will be presented in Section 6.3. The final time-series measurement of voltage induced from an 'arbitrarily' shaped transport current is utilised in the validation of the parametric Preisach model in Section 6.4.3. The 'arbitrary' current consists of the following: a null and a linear part, then a sinusoid with decreasing amplitude and increasing frequency (approximately 50–90 Hz) followed by a square root decrease, and finally an exponential increase, see Fig. 3.2. The last decrease (the square root part) is such that all memory in the superconductor (i.e. pinned flux) is wiped out except for the one corresponding to the largest amplitude. The maximum amplitude of this 'arbitrary' signal is always chosen to $0.8 \cdot I_c$ for each measured specimen.

3.3 Lock-in Measurements

The lock-in method is a common applied technique that is utilised in order to enhance the quality of measured data that are distorted by a noisy environment. The method allows to either reconstruct the signal or to deduce its amplitude and phase for a certain frequency. In

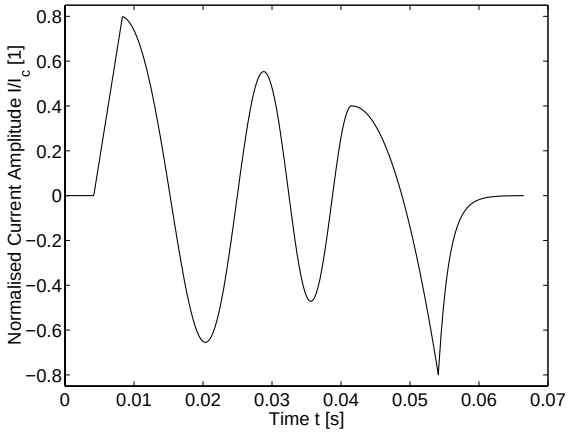

Figure 3.2: The shape of the 'arbitrary' current used to validate the parametric Preisach model presented in Chapter 6.

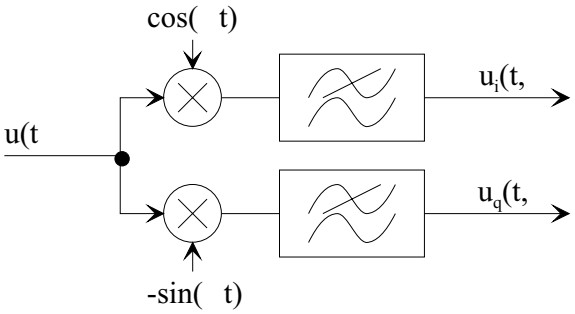

Figure 3.3: The principle of lock-in measurements is to capture the in-phase $u_i(t,\omega)$ and quadrature $u_q(t,\omega)$ terms of the signal $u(t)$ at a certain frequency ω. These terms may then be used to reconstruct the signal or extract its amplitude and phase.

the latter case, the measurements can be carried out for longer time intervals so that the signals can be averaged. Hence, the results have a better quality.

The method consists of extracting the orthogonal in-phase $u_i(t,\omega)$ and quadrature $u_q(t,\omega)$ terms for a certain frequency ω of the investigated signal $u(t)$. This is accomplished by multiplying the signal with respectively a cosine and a sine and extract the DC-component by low-pass filtering, see Fig. 3.3. The low pass filtering is necessary because the multiplication produces the double frequency as well. We consider here only pure harmonics h of the principal frequency ω_0 and so retrieve the following formulas:

$$u_i(t,h) = 2 \cdot LP\{u(t)\cos(h\omega_0 t)\} \tag{3.2}$$
$$u_q(t,h) = -2 \cdot LP\{u(t)\sin(h\omega_0 t)\}\,. \tag{3.3}$$

The original signal can be *reconstructed* if it consists of a finite number of frequencies or harmonics. In the case when there are infinite harmonics, an estimate $\hat{u}(t)$ can be obtained by including as many harmonics as possible; usually with an amplitude above some noise level:

$$\hat{u}(t) = \sum_h u_i(t,h)\cos(h\omega_0 t) + u_q(t,h)\sin(h\omega_0 t)\,. \tag{3.4}$$

This estimate has so excluded all noise at frequencies between the harmonics. Such a 'filtering' is applied to the voltage signal measured on a superconductor in Section 5.6 and 6.3

It is though more customary to use the in-phase and quadrature information to calculate the *amplitude* and *phase* of each harmonic. Commonly, the obtained signals are then averaged over very long times in order to cancel out statistical errors due to noise. This is possible when the principal frequency is constant, e.g. the case when a sinusoidal current is forced through a superconductor giving a voltage with many harmonics. The average in-phase and quadrature signals are here denoted $u_i(h)$ and $u_q(h)$, respectively. (Note the close relationship this averaging has to the Fourier transform at the frequency $\omega = h\omega_0$.) The amplitude and phase of each harmonic of the original signal are straightforward to calculate from the in-phase and quadrature signals:

$$U_h = |u_h| = \sqrt{u_i^2(h) + u_q^2(h)} \tag{3.5}$$

$$\varphi_h^u = \arg(u_i(h), u_q(h)) = \arctan\left(\frac{u_q(h)}{u_i(h)}\right) \pm \pi \tag{3.6}$$

(The last adding or subtracting of π in the expression for the phase applies only when the phase is in the 2nd or 3rd quadrant, and it is due to the output limitations of the arctan function.) Noteworthy is that this phase-angle is with respect to the cosine signal used in the lock-in procedure, see Fig. 3.3. This means that if the in-phase and quadrature signals are sought relative to another signal, the phase-difference between these signals must be considered. This is the case when measuring the voltage drop over the measured length l_t of a superconductor $v(t)$ and wanting to relate it to the transport current $i(t)$ flowing through the specimen:

$$i(t) = I_0 \cos(\omega_0 t + \varphi_I) \tag{3.7}$$

$$v(t) = \sum_h V_h \cos(h\omega_0 t + \varphi_h^v)\,. \tag{3.8}$$

The amplitude is of course indifferent of which phase is considered as reference.

The quantities retrieved by the lock-in measurements on superconductors enable us to calculate the *power losses*. The amplitudes of the first harmonic voltage drop V_1 and the transport current I_0 and their phase-difference $(\varphi_1^v - \varphi_I)$ retrieved at measurements are used to give the following expression of power losses per cycle and unit length:

$$\hat{\bar{Q}}_c(I_0) = \frac{\pi I_0 V_1}{\omega_0 l_t} \cos(\varphi_1^v - \varphi_I)\,, \tag{3.9}$$

where $l_t = 50$mm is the length over which the voltage was measured. Note that the energy losses are determined only by the principal frequency of the output because the integration over a cycle for the higher harmonics gives zero, i.e. harmonics are orthogonal. For all loss measurements utilised in this thesis, a principal frequency of $\omega_0 = 2\pi \cdot 59$ rad/s was used with a sample frequency of $f_s = 10$ kHz. For the subcritical loss measurements, the transport current amplitude I_0 is varied from 0.6 A to $0.8 \cdot I_c$ in consecutive measurements. Supercritical loss measurements are also carried out, whereby the current amplitude is brought up to $1.5 \cdot I_c$.

The lock-in measurements further allows us to retrieve the *reactive amplitude*, which is defined as the part of the measured voltage $v(t)$ that has no contribution to the losses. Hence, it has an exact phase of $\pi/2$ after the input current. It is therefore nothing else than the quadrature term of the voltage w.r.t. the current, which can be expressed as

$$\hat{\bar{v}}_r(I_0) = \frac{V_1}{l_t} \sin(\varphi_1^v - \varphi_I)\,, \tag{3.10}$$

when it is normalised with respect to the length over which the voltage measurement took place l_t. The reactive voltage (3.10) is used to adjust the parametric model to the reactive part of the measured voltage, see Section 6.4.2.

3.3.1 Problems with the method

There are some difficulties related with the lock-in measurements. First of all, a correct phase difference is very important to give an accurate result. Any uncertainty on the phase of the current or the voltage across the sample results in a large error in the in-phase component of the voltage. It is quite challenging to go around this problem because the voltage tap geometry (see Section 3.5) includes a large inductive (quadrature) component, which leads to a large error in losses for a small phase error. The measurements includes, therefore, simultaneous recording of the current and the voltage using a dual channel lock-in measurement configuration in order to take into account the phase-difference in (3.9) and (3.10) and so minimise phase-errors. The accuracy of the phase also depends on the precision of the lock-in frequency. For this reason, the same sample clock is used by the unit for generating the transport current and the sampling of measured quantities. The large inductance also provokes a large difference between in-phase and quadrature voltages (several orders of magnitude), which may lead to troubles with the dynamic reserve of the used low-signal amplifier. The use of a large dynamic reserve in the amplifier has shown to introduce less noise in the phase than a reactive voltage compensation would do [DSS99].

3.4 Applied Magnetic Field

The superconductors are sensitive to excessive magnetic field as pointed out in Section 2.10. The results presented there were measured in an externally applied magnetic field, whose application angle can be varied in order to observe the consequences in the superconductor. The field amplitude may be varied from 0 (self-field) to 400 mT but must be fixed during the measurements for this set-up.

3.5 Resistive-Inductive Measurements

The common way to carry out electric measurements on superconducting tapes is with what we here call the *resistive-inductive* technique. The reason for the name is that voltages due to both resistance and flux-changing is recorded, which will be clear in a moment. Hence, the method includes the total losses, both resistive and hysteretic (and also eddy-current losses in the sheath at high frequencies).

This measurement configuration is depicted in Fig. 3.4(a): two taps are soldered to the specimen a distance l_t apart, from which the connecting leads are placed perpendicularly to the tape side and connected to a voltmeter a distance w_m out from the specimen. It is important that this loop width w_m is large enough in order to include all flux changes, by which hysteretic losses are recorded. In order to understand this, we use the fact that a voltmeter measures the gradient of a scalar electric potential, ∇V, at its connectors. Now, exploiting Maxwell's equations [Che84], this gradient can be expressed with the electric field $\mathbf{E}$ and the vector magnetic potential $\mathbf{A}$:

$$\nabla V = -\mathbf{E} - \frac{\partial \mathbf{A}}{\partial t}\,. \tag{3.11}$$

The voltage v_m at the voltmeter can be calculated with some simple vector algebra: it is the integral of the scalar electric potential along the measurement circuit. By replacing it with (3.11) and applying Stoke's theorem, it turns out that the measured voltage consists of the electric field along the imaginary line between the soldered taps *and* of the flux-change through the measurement loop surface $S_m = l_t \times w_m$, i.e. a resistive voltage v_r and flux-dependent voltage

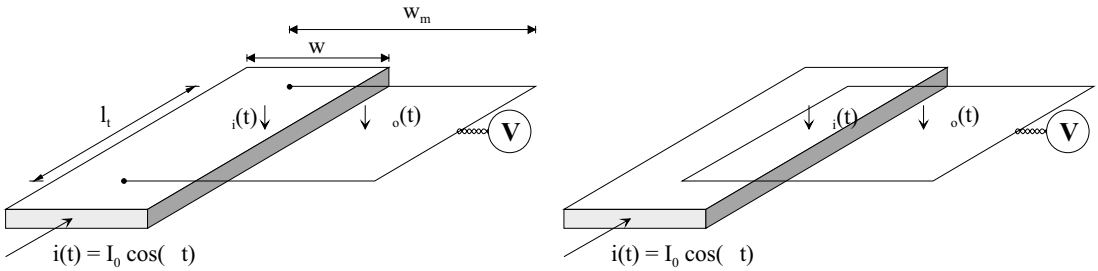

(a) (b)

Figure 3.4: (a) The resistive-inductive measurement configuration has soldered taps onto the specimen. Therefore, it picks up all voltage contributions, i.e. resistive, hysteretic, eddy-current and pure inductive voltages, for an applied transport current in self-field. (b) The inductive measurement configuration has a closed measurement circuit. As a result, the resistive voltage over the specimen is excluded from the measurement. It is very important to place the circuit return in the centre of the specimen where the flux is zero.

v_l:

$$v_m = \oint -\nabla \mathbf{V} \cdot d\mathbf{l} = \oint (\mathbf{E} + \frac{\partial \mathbf{A}}{\partial t}) \cdot d\mathbf{l} \tag{3.12}$$

$$= \oint \mathbf{E} \cdot d\mathbf{l} + \frac{\partial}{\partial t} \iint_{S_m} \mathbf{B} \cdot d\mathbf{s} = E \cdot l_t + \frac{d\Phi_{S_m}}{dt} = v_r + v_l \,. \tag{3.13}$$

The flux $\Phi_{S_m}(t)$ through this measurement loop surface consists of both the flux passing through the specimen $\Phi_i(t)$ *and* outside $\Phi_o(t)$: $\Phi_{S_m}(t) = \Phi_i(t) + \Phi_o(t)$. If the taps were soldered on the edges of the specimen, there would be no internal flux, but the electric field between the taps at this position would have changed accordingly so that the voltmeter would display the same value. The placement of the taps are therefore not crucial [YHB+96, Vin00]; one tap may even be placed at the centre and the other at the edge! However, it is important to have parallel leads going out from the specimen in order to have a well-defined surface S_m. Furthermore, it is also essential that the width w_m of the measurement loop is next to infinite from a flux point of view, i.e. the width must be large enough to include practically all flux-changes. In practice it suffices to have a loop width of 3–5 times the specimen width, by which about 95% of the magnetic field due to the superconductor is recorded. In order to obtain good measurement results, it is in general better to put the loop parallel to the larger tape surface as in Fig. 3.4(a) than having it perpendicular to the tape. The reason is that the flux lines are more dense at the short side of the superconducting tape, so a much smaller loop width is required in order to comprise most of the flux [Cam95].

When the configuration is set up in a correct manner, the total voltage over the specimen is recorded. It includes voltage due to a resistivity in the specimen, voltage due to a hysteretic behaviour, voltage induced by eddy-currents at high frequencies and a pure inductive voltage. The three former are all related to some losses, so applying the lock-in method on the measured total voltage includes all these contributions giving the total losses dissipated in the specimen when a transport current flows through it. The inductive voltage does not contribute to the losses because it is a pure quadrature voltage w.r.t. the phase of the current. It is normally much larger than the loss-producing in-phase voltage. This leads to the difficulties in the lock-in method that were presented in the preceding section. The only way to diminish its amplitude would be to reduce the width of the measurement loop, but that implies that the hysteretic and eddy-current losses are not properly picked up.

3.6 Inductive Measurements

Another possibility of measurements on superconducting tapes is the *inductive* technique. It is in principle the same as the resistive-inductive method, just that the resistive part has been excluded [Yan98].

The exclusion of the resistive voltage is possible by closing the measurement circuit along the centre of the specimen, see Fig. 3.4(b). The leads should not have electric contact with the tape surface in order to avoid any currents passing between the measurement and superconductor circuits. It is also very important that the lead along the centre of the specimen is well placed; it must be along a line where there are no flux-changes in the vertical direction in order to reflect a correct voltage. This criticality is not present for the resistive-inductive measurements because a bad placement is compensated by an electric field between the taps, which of course is not possible with the inductive measurement configuration. Furthermore, only specimen with a symmetric flux-distribution w.r.t the central line may be measured with this technique. The reason is the same as before: the vertical flux-changes must be zero along the central lead. It is so understood that twisted filaments cannot be measured with the inductive method.

Looking at the measurement circuit equations, there is no longer any electric field in the part at the centre of the specimen, so the voltage v_m measured by the voltmeter registers only the flux-changes:

$$v_m = \oint -\nabla \mathbf{V} \cdot \mathbf{dl} = \oint \frac{\partial \mathbf{A}}{\partial t} \cdot \mathbf{dl} = \frac{d\Phi}{dt} = v_l \tag{3.14}$$

The voltage due the losses in the specimen are recorded by the voltmeter, but now only inductive losses, such as hysteretic and eddy-current losses. In all the measurements used in this thesis, the frequency of the transport current ω_0 has always been kept low enough in order to keep eddy-current losses negligible. The losses measured with the lock-in measurement and the inductive method contains therefore only losses due to hysteresis. It is so clear that resistive and hysteretic losses can be separated by employing both the resistive-inductive and the inductive methods, where the resistive losses are obtained by subtracting the resistive losses from the total losses.

3.7 Use of Higher Harmonics

The hysteretic behaviour in a superconductor produces higher harmonics. (This is further discussed in Chapter 5.) So, for a more a complete characterisation of the electric behaviour of the superconductor, simultaneous measurements of several harmonics are required. The used measurement set-up records all data as time-series, which are then treated as required, c.f. Section 3.2. Hence, there is no problem to extract also higher harmonics.

Now, only nonlinear phenomenon produce higher harmonics, i.e. eddy-current and coupling losses produce only first harmonic voltages. The latter voltages are, due to a pure phase-shift of the voltage, such that the in-phase voltage becomes non-zero and so losses are produced [Yan98]. The third harmonics is most suitable to use because the third harmonic is much larger than harmonics of even higher order, which therefore become less reliable.

For *magnetic measurements* where a magnetic field is applied perpendicular to the superconductor

$$H(t) = H_0 \cos(\omega_0 t + \varphi_H)\,, \tag{3.15}$$

the losses in the superconductor can be expressed by [MYBH00]:

$$Q_s = \frac{\pi^2 w_c H_0}{l_t \omega_0} V_1 \cos(\varphi_1^v - \varphi_H) = \frac{\pi^2 w_c H_0}{l_t \omega_0} V_3 \, f_m(H_0, n) \tag{3.16}$$

where w_c is the width of the pick-up coil, $V_1 \cos(\varphi_1^v - \varphi_H)$ is the part of the voltage that is in phase with the applied magnetic field and V_3 is the magnitude of the third harmonic. The magnitude is used because both the in-phase and the quadrature components of the third harmonics are related to the magnetic hysteresis. The factor $f_m(H_0, n) = V_1 \cos(\varphi_1^v - \varphi_H)/V_3$ must be a slowly changing function of the applied field and the exponent n of the $E - J$ characteristics (or measured $I - V$ characteristics) in order to make this method reliable. Furthermore, it must not have a strong dependence on the superconductor geometry. Numerical simulations with the $E - J$ power law have been used to identify this factor function for a strip geometry under perpendicular fields in [MYBH00]. It demonstrates that $f_m(H_0, n)$ is close to constant with a weak dependence on the exponent n for magnetic fields below full penetration. Above full penetration, it decreases quickly to unity, which all can be summarised in an analytical expression as follows:

$$f_m(H_0, n) = 1 + \frac{r(n)}{\sqrt{1 + (\mu_0 H_0 / B_p)^{2.5}}} \tag{3.17}$$

where B_p is the magnetic field at which a maximal loss is observed in the superconductor, i.e. at full flux penetration. Values of $r(n)$ varies between 0.5 ($n \to \infty$), 1.0 ($n = 20$), 1.4 ($n = 10$) and infinity ($n = 1$), i.e. for a linear resistance with absence of a third harmonic. The method of using the third harmonic in magnetic measurements can be used to extract the hysteretic losses produced by the superconductor. The resistive losses are retrieved by deducting the hysteretic losses from the total losses.

The method of higher harmonics is also applicable in *measurements with transport currents*. The resistive-inductive measurements contains not only hysteretic losses from the superconductor, but also resistive, which are due to the nonlinear resistivity of the superconductor. Both these nonlinearities produce higher harmonics, which are detected and included in the superconductor losses. In order to measure only the hysteretic losses, the inductive measurement technique must be applied. These measurements register voltages due to changes in magnetic flux, so the nonlinear resistance does not occur. The losses registered by higher harmonics then contain contributions from only the hysteretic behaviour of the superconductor, since eddy-currents loss is due to a pure phase-shift. A corresponding factor function with a dependence on power-law exponent n and on current amplitude,

$$f_e(I_0, n) = \frac{V_1 \cos(\varphi_1^v - \varphi_I)}{V_3}\,, \tag{3.18}$$

must be identified, for instance with numerical simulations, in order to use higher harmonics with electric measurements.

3.8 Chapter Summary

The chapter contains a description of electrical measurements on superconducting tapes and refers particularly to the measurement configuration used for the measured data in this thesis. It considers characterisation of the superconductor from a DC and AC perspective, time-series and loss measurements as well as special techniques to separate loss contributions. Its contents have been retrieved from scientific articles and private communications.

The DC measurements give the critical current I_c and the power-law exponent n, which are qualitative measures of the superconducting specimen. Time-series measurements for 'arbitrary' currents have been recorded in order to validate models in later chapters. A thorough description of the lock-in method reveals its ability to improve measurement data for loss measurements. It has also been used to identify the reactive voltage, i.e. the inductive part. It is further shown that

the resistive-inductive measurement technique comprises all losses dissipated in the specimen. The more sensitive inductive method excludes the resistive voltage so that only hysteretic losses are recorded. Hence, a separation of resistive and hysteretic (flux-dependent) losses is possible to carry out. The two flux-dependent hysteretic and eddy-current losses can also be distinguished by considering higher harmonics.

Chapter 4

Hysteresis and the Preisach Model

It was concluded in Chapter 2 that the type-II superconductors exhibit hysteresis. But what really is that, and how can it be modelled? The concept of hysteresis and its mathematical description is considered in this chapter. We start the chapter by comparing how different authors characterise hysteresis and then adopt one of these definitions. It follows an account for different common mathematical models to express the hysteretic output as a function of the input. The rest of the chapter is devoted to one such hysteresis model: the classical Preisach model. It is reported how the memory function works and how the output and the energy losses can be computed. The necessary and sufficient conditions of a hysteresis to be described by this model are also pointed out, and the cases when an inverse model exists are described. Finally there is an account for what kind of generalised Preisach models have been developed and in what cases they are to be applied.

4.1 Hysteresis – a Matter of Definition

If you ask your colleagues or friends to define hysteresis, you will most probably get as many answers as there are persons. There is no clear answer to that question also when searching in the scientific literature. The word *hysteresis* originates in the Greek word *hysterein*, which means to be behind, to come later or to lag behind. The related Greek word *hysteresis* is translated as shortcoming, deficiency or need. This gives an idea of what hysteresis is, but in order to have a definition of the phenomenon, it is important to consider the observable effects of systems with hysteresis. A good overview of different phenomena that are related to ferromagnetic hysteresis in particular is provided by [Ber98], but these phenomena may be applied to the many areas of science where hysteresis appears due to physical conditions, such as elasto-plasticity and superconductivity, or where it is voluntarily introduced as in thermostats (engineering).

Hysteresis can generally be described as a hysteresis transducer with an input signal $u(t)$ and an output signal $y(t)$. First, it is noted that hysteresis is connected with some lagging in time. This is however not exclusive to hysteretic systems. Take the example of a sinusoid as input and an output with a phase-shift ϕ:

$$u(t) = U_0 \cos(\omega t)\,, \qquad y(t) = Y_0 \cos(\omega t + \phi(\omega)) \tag{4.1}$$

The phase shift may be frequency-dependent, i.e. rate-dependent, as in most linear filters. Such a system produces a *loop* in the input-output phase-plane as shown in Fig. 4.1(a). But is the system (4.1) a hysteretic system? No, not in the opinion of the author of this thesis, because this input-output relationship may be produced by a fully linear system; a system with hysteresis is a *nonlinear* system.

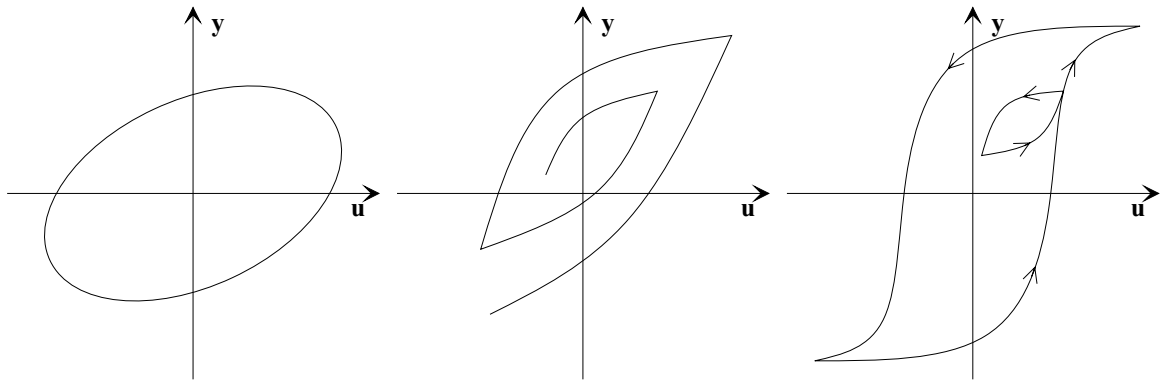

(a) (b) (c)

Figure 4.1: (a) A system with a phase-shift produces an elliptic loop in the input-output phase-plane. (b) Branching is typical for hysteresis and constitutes a basic feature. (c) The Madelung property means that the inner loop is closed and the outer loop continues as if the minor loop had never existed.

A common way to describe hysteresis is to consider the loops that are closely connected with its behaviour. These loops return often to the same point in the input-output plane, but in reality there are many hysteretic effects that do not form such closed loops. It would therefore be better to talk about *looping* as a basic feature of hysteresis. This statement is contradicted by [May91], which expresses that *branching* constitutes the essence of hysteresis because loops may not be closed. Furthermore, branching, with singularity points (dy/du non-existent) where the input changes signs, is typical for hysteresis, and takes the form as in Fig. 4.1(b). Thus, hysteresis is always related to some functions with asymmetry with respect to input-reversal, such that there exist at least one point where dy/du takes different values depending on if the input is increasing or decreasing, i.e. the sign of du/dt. Madelung noticed in his experiments [Mad05] that if the input was changed in such a way that minor loops were created within a larger loop, the inner loop was closed and the outer loop then continued as if the minor loop never had occurred. This *Madelung property* is depicted in Fig. 4.1(c). This phenomenon is closely related to the *wiping out property* of the memory function that will be described more in detail in Section 4.3.2.

Typical is the *rate-independent* or *static* hysteresis, where the output does not depend on how fast the input changes. The rate-independent hysteresis is a good approximation for many hysteretic phenomena, such as some ferromagnetic hystereses [Ber98] and superconductive hysteresis (see [May96] and Chapter 6), as long as the input changes neither too fast nor too slow. It is often to this static hysteresis that the common engineer relates the word hysteresis, and in [Vis94] hysteresis is actually defined as a rate-independent memory effect. (The reference mainly considers rate-independent hysteresis.) However, rate-independence is an idealised situation, which only approximately comply to certain hysteretic effects, so defining it in this way would be too restrictive. It turns out that when the hysteresis is rate-independent, the output is related to the input by a hysteresis operator

$$y(t) = \Upsilon[u(t)]\,, \tag{4.2}$$

whose output is completely defined by the local extrema of the input [BS96]. The hysteresis is then due to a persistent memory, which consists of the input's local extrema [Ber98]. Such a hysteresis operator was firstly introduced by the group of Krasnoselskii, which described its mathematical behaviour in [KP89].

We note that hysteresis is a *memory effect*, which may be rate-independent or rate-dependent. In the former case, the scale is of little importance, but for the latter case, the output is

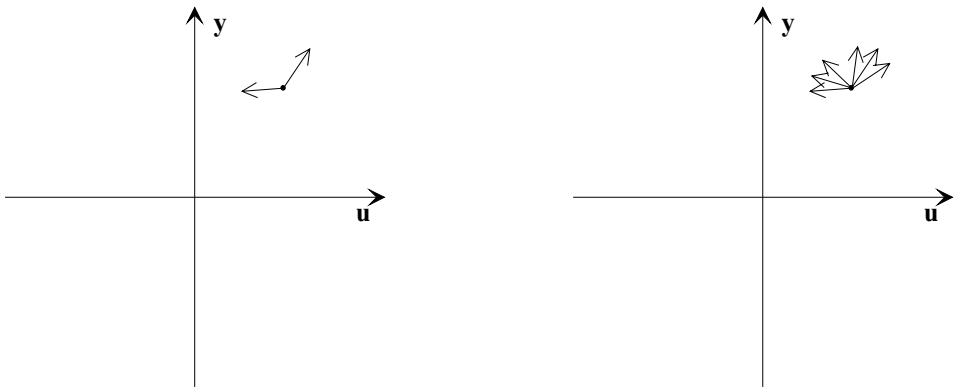

(a) (b)

Figure 4.2: (a) A system with a local memory has only two possible future behaviours of the output at each point depending on the derivative of the input. (b) A system with a nonlocal memory has infinitely many possible future behaviours of the output at each point depending on the history of the input.

scale dependent [Vis94]. Indeed, a basic property of hysteresis is its memory, including the initial memory state. (Ref. [Vis94] insists that also rate-independence is a basic property for hysteresis.) The input-output relationship described by the hysteresis operator (4.2) includes therefore a memory effect. All static (rate-independent) hysteresis have either a *local memory* or a *nonlocal memory* [May91]. The latter is equivalent with a persistent memory that can only be erased under certain conditions. The local memory hysteresis has an output that only depends on the present output and input values and the derivative of the input. In this way, the input and the output defines a state that is enough to decide the future output. The local memory hysteresis has only two possible future behaviours of the output at each point: one when the input increases, the other when it decreases, see Fig. 4.2(a). A nonlocal memory hysteresis does not only depend on the present values of output, input and the derivative of the input, but also on the history of the input [Ber98]. It turns out that the output will not depend on all the history of the input, but only on its past extrema for rate-independent hysteresis systems [BS96], as mentioned earlier in this section. Thus, the nonlocal memory hysteresis has an infinite number of future behaviours at each point in the input-output $(y - u)$ diagram, where the direction depends on the global input history, see Fig. 4.2(b). Branching at reversal points (extrema) can be expected for systems with persistent memory [Ber98], which brings us back to the discussion of looping and branching. This shows the importance of the existence of memory in a system with hysteresis.

So can then a hysteretic system be defined as *a system with persistent memory* [Ber98], since it produces branching at reversal points of the input? This is not so good because a simple system (e.g the *relay operator* presented in Fig. 4.4(a)) does truly exhibit hysteresis, but it does not have a nonlocal memory. Local memory is not consistent with experimental facts according to [May91], but this does not change that such simple operators exhibit hysteresis. Hence, taking a definition based on persistent memory is not acceptable. At the same time, we must remember that absolutely persistent memory cannot exist in reality, even if some physical effects, such as low temperature superconductivity, come very close to it. The memory of many hysteretic systems is very complex, especially when it comes to nested loops. There is thus need for an update of the memory as time passes, which is done with a memory function. Many hysteresis operators comply to the so-called Preisach memory, which is described in Section 4.3.2.

A completely different matter is the physical reason to the hysteretic behaviour of a system. Already mentioned is the flux-pinning in superconductors in Chapter 2. More generally one

can talk about metastability in the material. When the external field is changed such that it distorts the energy profile, the equilibrium can be moved to an inflection point and a spontaneous jump, so-called Barkhausen jump, to nearest local minimum takes place. The energy then suddenly decreases, which results in an energy loss. When changes are quicker, so that significant field variations occur during the Barkhausen jumps, then rate-independence is not valid any more [Ber98]. The discussion on metastability takes us into details about the physical origins of hysteresis, but a mathematical system, e.g. the relay operator, may also exhibit hysteresis, so defining hysteresis from physics would not be a good idea. Further discussion about metastability lies outside of the scope of this thesis.

We continue the discussion of how to define hysteresis. It was mentioned that hysteresis is always related to some irreversible functions. The derivative dy/du must therefore be different at least one point, when du/dt change signs, i.e. at input extrema. Hysteresis is referred to a "whole set of intimately connected phenomena arising from the simultaneous existence of metastable states, dissipation mechanisms with characteristic time scales, and thermal relaxation" in [Ber98]. This description is very general and includes most, if not all, physical hysteresis effects. It is, however, referred to a physical system and so excludes any artificial system that exhibit hysteresis, e.g. a computer program with introduced hysteresis. It is so preferable to consider hysteresis as a phenomenological effect, which may however have its origin in physical effects. The definition in the literature that best (according to the author) describes hysteresis as a phenomenological effect was found in [May91]. It is general enough to include all the cases, which we here call hysteresis, yet restrictive enough to exclude hysteresis-similar phenomena such as the phase-shifted system. It states: *"a system is called a hysteretic system if its input-output relationship is a multi-branch nonlinearity for which branch-to-branch transitions occur after input extrema."* This is what we mean by hysteresis in this thesis.

4.2 Mathematical Models of Hysteresis

The tool for an engineer to describe the real world is normally with some kind of mathematical model. Many different descriptions of hysteresis has so been developed during the past years, which started around the end of the 19^{th} century, and there is still an ongoing research in this field. Notes on the history of hysteresis modelling can be found in [Vis94]. A number of books that present the different possible mathematical models of hysteresis has been published in the last few years [KP89, May91, Vis94, BS96, Ber98, Del99]. There is also an infinity of articles presented in the field, where the following articles present a comparison of some of the models: [MNZ93, LPA00].

A short presentation of the main models follows in this section. It is a non-exhaustive list of models that only considers the main features of some scalar output models. Many of these only relates the output to the input and do not explain the origin for the hysteresis. This phenomenological notion of hysteresis also goes well with the definition adopted in Section 4.1. The presented models describe only the hysteretic behaviour. They can then be combined with other linear or nonlinear systems in order to describe a larger system, e.g. in differential equations [BS96].

It will be concentrated upon one model in this thesis: the classical Preisach model of hysteresis, which was firstly invented by F. Preisach in 1935 [Pre35]. He used an intuitive approach to model the hysteresis of magnetism, but it has later been applied in many fields of hysteresis. The Preisach model will be discussed in detail in Section 4.3 and is hence not included in this section.

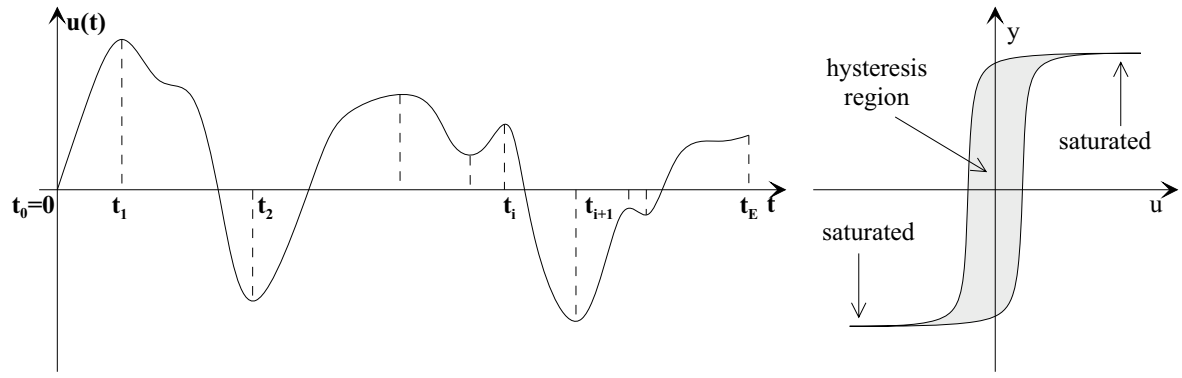

(a) (b)

Figure 4.3: (a) Piece-wise monotone input signal. The local extrema of the input signal are when the hysteretic output changes behaviour, so the total time interval for the input signal $[t_0, t_E]$ is partitioned such that the input is monotone in each interval. (b) The hysteresis region is bounded by the major ascending and descending curves. The irreversible behaviour appears within this region. The hysteresis is said to be saturated when the reversal (non-hysteretic) parts are horizontal.

4.2.1 Model Input and Hysteresis Region

It was mentioned in the discussion of hysteresis definition in Section 4.1 that a hysteretic system changes its behaviour only when the input derivative changes signs. These time instants and their corresponding input values are therefore very important. They are recorded by letting the total time interval for the input signal, $[t_0 = 0, t_E]$, be partitioned such that the input is monotonely increasing or monotonely decreasing on each of the subintervals $[t_i, t_{i+1}]$, see Fig. 4.3(a). Such signals are said to be piece-wise monotone. (A mathematically more rigorous definition is given in Chapter 6, where it is required for the context.)

The output of a rate-independent hysteresis operator is fully defined by the local extrema of the input [Vis94, BS96]. In most cases, this ensemble of data may also be reduced and yet the output is fully defined. Section 4.3.2 describes this reduction procedure for the Preisach memory.

The *hysteresis region* is the part of the input-output diagram that is enclosed by the major ascending and descending bounding curves, see Fig. 4.3(b). It is thus the region where the hysteresis transducer has an irreversible behaviour. In the case when the reversal parts are horizontal (dy/du=0), the hysteresis is said to have reached *saturation*.

4.2.2 Differential Equation (Duhem model)

A way to describe hysteresis is by means of differential equations. Duhem was probably the first one to do so [Duh97], and so these kinds of models are usually referred to as *Duhem models*. He postulated a phenomenological model using that the output can only change characteristics when the input changes direction. The Duhem model can be expressed in many different manners, but we satisfy us in giving it in a general form with the common assumption of multiplication between time-derivative of input $u(t)$ and the descriptive functions f_1 and f_2 [MNZ93]:

$$\frac{dy}{dt} = f\left(y(t), u(t), \frac{du}{dt}\right) = \begin{cases} f_1(y(t), u(t))\frac{du}{dt}, & \frac{du}{dt} \geq 0 \\ f_2(y(t), u(t))\frac{du}{dt}, & \frac{du}{dt} \leq 0 \end{cases} \tag{4.3}$$

This equation describes the interior of the hysteresis region. Boundary curves enclosing this hysteresis region may be included in the model by adding some constraints to the differential equation (4.3) [KP89, MNZ93]. It is clear from the equation above that the Duhem model works with a local memory. The Duhem model is further investigated in a mathematical-theoretic approach in [Vis94].

Many other scientists have followed in the footsteps of Duhem [Bab59, Bou71, CH87, Hod88] and produced similar models. *Jiles and Atherton* have developed a sophisticated version of the Duhem model based on physical observations and reasoning around magnetic domains and the pinning of the domains' walls in ferromagnetic materials [JA83, JA86]. Although the model has local memory, both major and minor loops can be obtained by adjusting integration constants defined by initial and final values to be reached on the curves [Jil92]. The *Stoner-Wohlfarth model* [SW48] consists of a sum of non-interacting particles whose magnetic value is determined by a bistable energy function. Transition curves may be more or less smooth depending on the number of particles and on parameter values. The model has local memory, but minor loops can be obtained by introducing pinning effects in the particles, meaning that a certain magnetic field must be surpassed before there is a change in magnetisation [LPA00].
Chua and Stromsoe used another approach and introduced a hysteresis model based on circuit theory [CS70]. It was later improved to include both rate-independent and rate-dependent phenomena [CB72].

4.2.3 Nonlinear Partial Differential Equation ($E - J$ model)

The nonlinear constitutive power law between electric field $\mathbf{E}$ and current density $\mathbf{J}$ was introduced in Section 2.9 in order to describe the behaviour of a superconductor:

$$\mathbf{E} = E_c \frac{\mathbf{J}}{J} \cdot \left(\frac{J}{J_c(\mathbf{B})} \right)^{n(\mathbf{B})} \tag{4.4}$$

where $J = |\mathbf{J}|$ and E_c are constants. The argument $\mathbf{B}$ (magnetic flux density) to the critical current density J_c and the power-law exponent n accounts for the material's sensitivity to magnetic flux and for effects of a possible anisotropy. This power law in combination with Maxwell's equations (μ_0 denotes the permeability of vacuum)

$$\nabla \times \mathbf{E} = -\frac{\partial \mathbf{B}}{\partial t} \tag{4.5}$$

$$\nabla \times \mathbf{B} = \mu_0 \mathbf{J} \tag{4.6}$$

and appropriate boundary conditions constitute what we here call the $E-J$ *model* for superconductors. This is a three-dimensional nonlinear partial differential equation, where the results of simulations are dependent on the power law parameters and the geometry of the object. In order to remove the dependence of geometry and to simplify the problem, a semi-infinite material has been considered in [Rhy93, May98]. It is shown that the $E-J$ model simplifies to the following one-dimensional nonlinear partial differential equation under the assumption that the electric field and the current distribution only vary along one direction (the direction of the y-axis) and that J_c and n are constants:

$$\frac{\partial^2 J_y^n}{\partial z^2} = \frac{\mu_0 J_c^n}{E_c} \operatorname{sgn}(J_y) \frac{\partial J_y}{\partial t} \,. \tag{4.7}$$

The current density depends on the penetration direction z and on the time, $J_y = J_y(z,t)$. This is nothing but a nonlinear diffusion equation considering the current density penetration into a nonlinear material. (The diffusion equations for the magnetic flux density and for the electric field was considered in [Rhy93].)

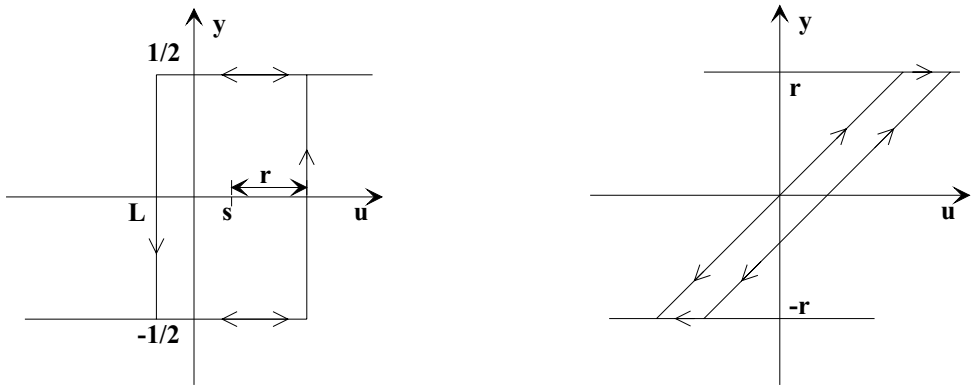

(a) (b)

Figure 4.4: (a) The output due to the relay operator $\mathbf{R}_{\mathrm{L}\Gamma}$ (simplest hysteresis operator for the Preisach model) is a rectangular loop in the output-input diagram which possesses an 'up'-switch at Γ and a 'down'-switch at L. (b) The stop operator works with a stress-strain behaviour; the linear stress is immediately recovered when the input is reduced below the yield value.

The $E-J$ model implies a resistive-hysteretic behaviour where losses in the material cannot be clearly separated in resistive or utter rate-independent hysteretic losses. The material is purely resistive (linear case) for a power law exponent $n = 1$, by which (4.7) describes the so-called skin-effect; a sheer rate-independent hysteresis is obtained when $n = \infty$. However, any value of the exponent in between these extremes, $1 < n < \infty$, implies a rate-dependent resistive-hysteretic behaviour [Rhy93]. Analytical solutions to the special case of a semi-infinite slab have been deduced for a periodic applied magnetic field [Rhy93] and for a monotonically increasing magnetic field [May98]. However, numerical simulations must be carried out for more general geometries by means of integration methods, such as with integration formulation [Bra96a, Rhy98], or finite element methods [AMBT97, PL97, Ame98, LPME98, Nib99, NSD+00].

4.2.4 Basic Hysteresis operators

We consider here three basic hysteresis operators: *relay*, *stop* and *play*. They are basic because they constitute the simplest hysteresis operator for some other hysteresis models, such as the Prandtl model and the Preisach model. All the three operators are rate-independent and have local memory. The latter does not prevent, however, that when they are superimposed for instance in the Preisach model, the new model has a nonlocal memory. This will be demonstrated in Section 4.3.2.

Relay operator

The *relay* or *switch operator* $\mathbf{R}_{\mathrm{L}\Gamma}$ is characterised by two threshold-values L and Γ and two output values, here $\pm 1/2$. (Sometimes the mean $s = (\mathrm{L}+\Gamma)/2$ and the half-width $r = (\Gamma-\mathrm{L})/2$ may be used instead.) Fig 4.4(a) depicts how the operator output switches to $+1/2$ at input equal to Γ and to $-1/2$ at L, but otherwise stays the same. This operator is mathematically defined as

$$y(t) = \mathbf{R}_{\mathrm{L}\Gamma}[u(t)] = \begin{cases} +1/2, & u > \Gamma \quad \text{or} \quad [u \in (\mathrm{L},\Gamma) \quad \text{and} \quad u(\tau) = \Gamma] \\ -1/2, & u < \mathrm{L} \quad \text{or} \quad [u \in (\mathrm{L},\Gamma) \quad \text{and} \quad u(\tau) = \mathrm{L}] \end{cases} \tag{4.8}$$

where τ indicates the time instant at which either of the thresholds, L or Γ, was attained. If τ is not defined, an initial operator state $\mathbf{R}_0 = \pm 1/2$ must be defined. The problem with the relay operator is the ambiguity at the threshold values; it is not clearly defined what happens if a switching threshold is merely attained. This causes mainly problems when considering continuity from a mathematical point of view. In this engineering approach, this ambiguity has no influence.

A *generalised relay operator* can also be defined by letting the upper and lower limits be functions instead of constants. These functions attain commonly bounded values as the input reaches $\pm\infty$. The general relay operator then becomes a mapping between function spaces.

Stop operator

The *stop operator* $\mathbf{S}_r$ can be considered as the relation of an ideal elastic-plastic material, and it is therefore also called the *elastic-plastic operator*. The relationship between output and input is as the stress y relates to a strain u: as long as the modulus of the stress is smaller than a certain yield stress r, it is linearly related by Hooke's law. But when the stress reaches this yield value, it remains constant even under an increased strain. The linear elastic behaviour is again recovered once the strain is decreased, see Fig. 4.4(b). This behaviour can be analytically expressed by the stop operator:

$$y(t) = \mathbf{S}_r[u(t)] = \min\{r, \max\{-r, (u(t) - u(\tau_i) + y(\tau_i))\}\} \tag{4.9}$$

where τ_i is the last time instant when the piece-wise monotone input reached an extreme, i.e. the input has been monotone since time instant τ_i. No such time instant exists at time zero, so allowed initial values for the input $u(t_0) = u_0$ and the output $y(t_0) = y_0$ must replace $u(\tau_i)$ and $y(\tau_i)$, respectively, in (4.9).

Play operator

Just as the stop operator has its origin in an elastic-plastic relation, the *play operator* $\mathbf{F}_r$ is closely related to a mechanical play between two elements, see Fig 4.5(a). The input variable $u(t)$ controls the position of element 1. The position of the output $y(t)$ stays constant so long as $u(t)$ moves in the interior of the play, i.e. within $\pm r$ of the central point of element 2. Now, if element 1 hits the boundary, it will drag along element 2 and so change the output value. The input-output diagram produced by such a mechanical play is given in Fig. 4.5(b).

A direct formula to describe the relationship between the output and the input of the play operator can be expressed as follows:

$$y(t) = \mathbf{F}_r[u(t)] = \max\{(u(t) - r), \min\{(u(t) + r), y(\tau_i)\}\}\,, \tag{4.10}$$

where as before τ_i is the last time instant the piece-wise monotone input reached a local extreme. An initial value of the play output $y(t_0) = y_0$ is used instead of $y(\tau_i)$ before the first input extreme is reached. This formula shows that the play operator is very similar in its behaviour to the stop operator, which also can be seen from Fig. 4.4(b) and 4.5(b). The two hysteresis operators are related according to the equation

$$\mathbf{F}_r[u] = u - \mathbf{S}_r[u]\,. \tag{4.11}$$

The play operator can also be expressed by the relay operator. If is is assumed that the initial value of the outputs of both play and relay operator are zero, their relationship is expressed as:

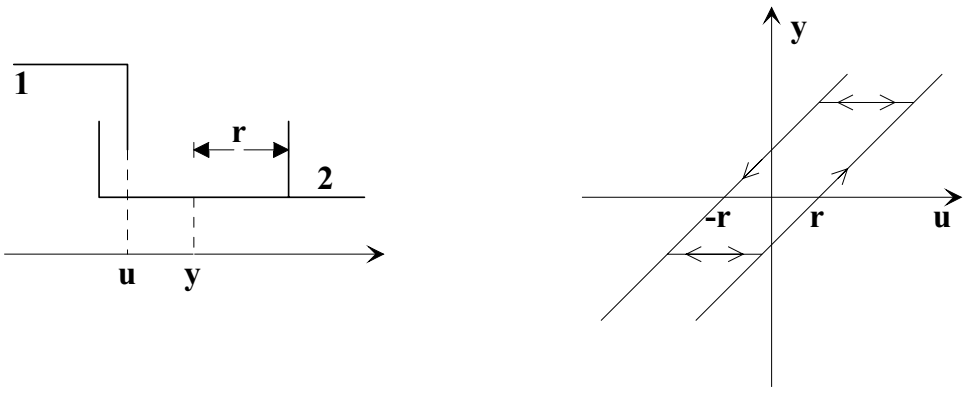

(a) (b)

Figure 4.5: (a) A mechanical play represents the behaviour of the play operator. Element 2 remains still until element 1 moves outside $\pm r$, which then drags element 2 along. (b) The corresponding input-output diagram of the play operator.

$$\mathbf{F}_r[u] = \int_{-\infty}^{\infty} \mathbf{R}_{s-r,s+r}[u]\, ds\,. \tag{4.12}$$

4.2.5 Krasnoselskii-Pokrovskii Hysteron

A *generalised play operator* $\mathbf{G}(g_a, g_d)[u]$ was introduced by Russian scientists [KP89], by which the 45 degree lines in Fig. 4.5(b) are replaced by arbitrary functions, $g_a(u)$ and $g_d(u)$; a and d stands for ascending and descending curves, respectively. These functions must not cross each other in the output-input $(y-u)$ diagram. These scientists so defined a hysteresis operator, now called the *Krasnoselskii-Pokrovskii hysteron*, which can be represented in the form

$$y(t) = \mathbf{H}[u(t)] = f(u(t), \mathbf{G}(g_a, g_d)[u(t)])\,, \tag{4.13}$$

where $f(\cdot)$ is a memoryless function. This hysteron represents a class of hysteresis with arbitrary major transition curves and with a single class of functions for the interior of the hysteresis region.

4.2.6 Prandtl Model of Hysteresis (Ishlinskii Model)

The following model was firstly presented by Prandtl in 1928 [Pra28], but it was independently also formulated by Ishlinskii about 15 years later [Ish44]. It is thus not uncommon to see both these names for this model figuring in the scientific literature. The *Prandtl model* was developed to describe the hysteretic behaviour of an elastic-plastic material. It is therefore natural that the Prandtl operator $\mathbf{D}[u]$ consists of a weighted superposition of basic stop operators:

$$y(t) = \mathbf{D}[u(t)] = \int_{0}^{\infty} p(r)\, \mathbf{S}_r[u(t)]\, dr\,. \tag{4.14}$$

The basic stop operator is rate-independent, which means that this linear superposition is also rate-independent. However, the local memory of the stop operator is not transferred to the Prandtl operator. The latter has indeed a nonlocal memory that obeys the rules Madelung

set up [Mad05]. If fact, the memory function of the Prandtl model obeys the same rules as the Preisach memory, c.f. Section 4.3.2, and the model is therefore included in the class of Preisach-type models, see Section 4.5.6.

An alternative description of the input-output behaviour of the Prandtl model is given by the so-called shape function $g_P(\cdot)$ [BS96]. This continuous and odd function gives the output of the hysteresis as

$$y(t) = \frac{1}{2}\, g_P(2u_0) + \sum_{k=1}^{N(t)} g_P(u_k - u_{k-1}) \tag{4.15}$$

for a Prandtl model with zero initial value, $y_0 = 0$. The values $\{u_0, \cdots, u_{N(t)}\}$ are the extrema of the input signal (c.f. Fig. 4.3(a)) that are kept with the Preisach memory rules, see Section 4.3.2. This shape function fully characterises a hysteresis described by the Prandtl model.

4.3 The Preisach Model of Hysteresis

The classical Preisach model was firstly invented by F. Preisach in 1935 [Pre35], in which he used an intuitive approach to model the hysteresis of magnetism. It was later re-invented by D.H. Everett in 1952 [EW52, ES54, Eve54, Eve55], who applied it to adsorption hysteresis. Krasnoselskii clarified in the 1970's the phenomenological nature of the Preisach model by generalising it in a mathematical idea similar to spectral decomposition with no physical meaning [KP89]. It is now used in a wide range of scientific areas to describe hysteresis, and so it is exhaustively discussed in large number of papers and books.

A good description of the classical Preisach model of hysteresis is found in [May91]. The notation is here slightly changed and its simplest hysteresis operator (the relay operator) has been given a unit step centred around zero. Therefore, we start by describing the Preisach model, which also facilitates the comprehension of the following parts of this thesis. A more mathematical approach is given in [BS96], and important contributions concerning inversion of Preisach operators by [Kre91, BS96].

4.3.1 Superposition of Relay Operators

The Preisach model consists of a superposition of an infinite number of relay operators $\mathbf{R}_{\mathrm{L}\Gamma}$, each representing a rectangular loop in the output-input $(y-u)$ diagram, see Fig. 4.4(a). In the sequel, it is assumed that $\mathrm{L} \leq \Gamma$. Each $\mathbf{R}_{\mathrm{L}\Gamma}$ is weighted by an arbitrary weighting function $w(\mathrm{L}, \Gamma)$, the *Preisach function*, leading to the following expression for the Preisach model:

$$y(t) = \mathbf{P}[u(t)] = \iint\limits_{\mathrm{L}\leq\Gamma} w(\mathrm{L}, \Gamma)\mathbf{R}_{\mathrm{L}\Gamma}[u(t)]d\Gamma d\mathrm{L}\,. \tag{4.16}$$

The hysteresis operator $\mathbf{P}$ for the Preisach model has nonlocal memory, even if it consists of a superposition of the operators $\mathbf{R}_{\mathrm{L}\Gamma}$ that have only local memory. We consider now how to calculate the output from the Preisach model for an arbitrary input signal. First, the evolution of the nonlocal memory is presented, then the geometrical presentation is used to simplify the computation of (4.16).

4.3.2 Preisach Plane and Memory

The Preisach model can be interpreted geometrically because there is a one-to-one correspondence between the relay operator $\mathbf{R}_{\mathrm{L}\Gamma}$ and the point (L, Γ) in the $(\mathrm{L}-\Gamma)$-plane, the so called

Preisach plane. The half-plane $\mathrm{L} \leq \Gamma$ is only considered. There is a subdivision of the Preisach plane into $S^+(t)$ and $S^-(t)$, the two parts where $\mathbf{R}_{\mathrm{L}\Gamma}$ is positive and negative respectively. This division depends on extrema of past input and on the present input, and consists of a line $\mathcal{C}(t)$, the *Preisach memory function*, see Fig. 4.6(b). Its last value (L_0, Γ_0) corresponds to the present value of the input $(u(t), u(t))$ and is attached to the line $\mathrm{L} = \Gamma$ in the figure.

We consider the evolution of an invented input signal and the corresponding Preisach plane in Fig. 4.6 in order to understand the rules for updating the Preisach memory. Suppose first that no input signal has yet been applied to the hysteretic system at time $t_0 = 0$, and that the output is zero as well. The subdivision of the Preisach plane is then along the line $\mathrm{L} = -\Gamma$ with the initial input $u(t_0) = u_0 = 0$ attached to the origin, see Fig. 4.6(b). The hysteresis is then said to be in its *virgin state*, or equally the system has *no history*. A horizontal line is moving upwards in the Preisach plane when the input is increased from the virgin state up to a point 1, as depicted in Fig. 4.6(c). Note how the memory function has an additional vertex at (L_s, Γ_s). Yet another vertex is added when the input is turning to the lower value at point 2', now with a vertical line moving to the left, see Fig. 4.6(d). Let us now consider the time instant at point 5' when the input is increasing. This is after a few periods with decreasing amplitude so that a number of vertices have been added, see Fig. 4.6(e). The memory function $\mathcal{C}(t)$ makes then up a 'stair-case' line, which means that it can be represented by a number of vertices[1], e.g.

$$\mathcal{C}(t) = \{(\mathrm{L}_s, \Gamma_s), \cdots, (\mathrm{L}_1, \Gamma_2), (\mathrm{L}_1, \Gamma_1), (\mathrm{L}_0, \Gamma_1), (\mathrm{L}_0, \Gamma_0)\}. \tag{4.17}$$

The subdivision of the Preisach plane is still along the line $\mathrm{L} = -\Gamma$ for $\mathrm{L} < \mathrm{L}_s$ and $\Gamma > \Gamma_s$. We say that the hysteretic system has *no history* beyond the point (L_s, Γ_s).

Wiping-out Property

Now, if the input continues to increase from point 5', the evolution of the memory function has the same behaviour as before until it reaches the value of $u(t) = u_3$. A further increase beyond u_3 to u_5 means that the memory function looks like in Fig. 4.6(f). The memory function consists then of two vertices less. These have been wiped out from the history of the input, which means that not all extrema are saved in the memory function. A curiosity is that the memory function did not only forget about point 3, but also about point 4. That is the case, even if the absolute value of the input at point 4 is larger than at point 3, $|u_4| > |u_3|$. It is easy to understand that this behaviour will lead to forgetting of minor loops, just as the Madelung property in Fig. 4.1(c): the vertices introduced by minor loops are wiped out when returning to the major loop and the hysteresis curve will continue along the major loop.

The behaviour of the memory function described in this section is called the *wiping-out property*, and it is a particularity of the Preisach memory. The illustrated behaviour of the Preisach memory function shows its dynamic evolution, and it so contains number of vertices that may vary between one to infinity.

4.3.3 Model Output

It is clear that the memory function $\mathcal{C}(t)$ constantly changes with time (i.e. if input $u(t)$ changes with time) and hence the parts of the Preisach plane where the relays are positive, $S^+(t)$,

[1]The vertices in the memory function are at each corner of the 'stair-case' line in this thesis. This is in order to have a symmetry for increasing and decreasing input signals, which is used for the symmetry description in Appendix A. However, it is enough to record the vertices at every upper corner of 'stair-case' $\mathcal{C}(t)$ in order to fully describe the Preisach memory [May91].

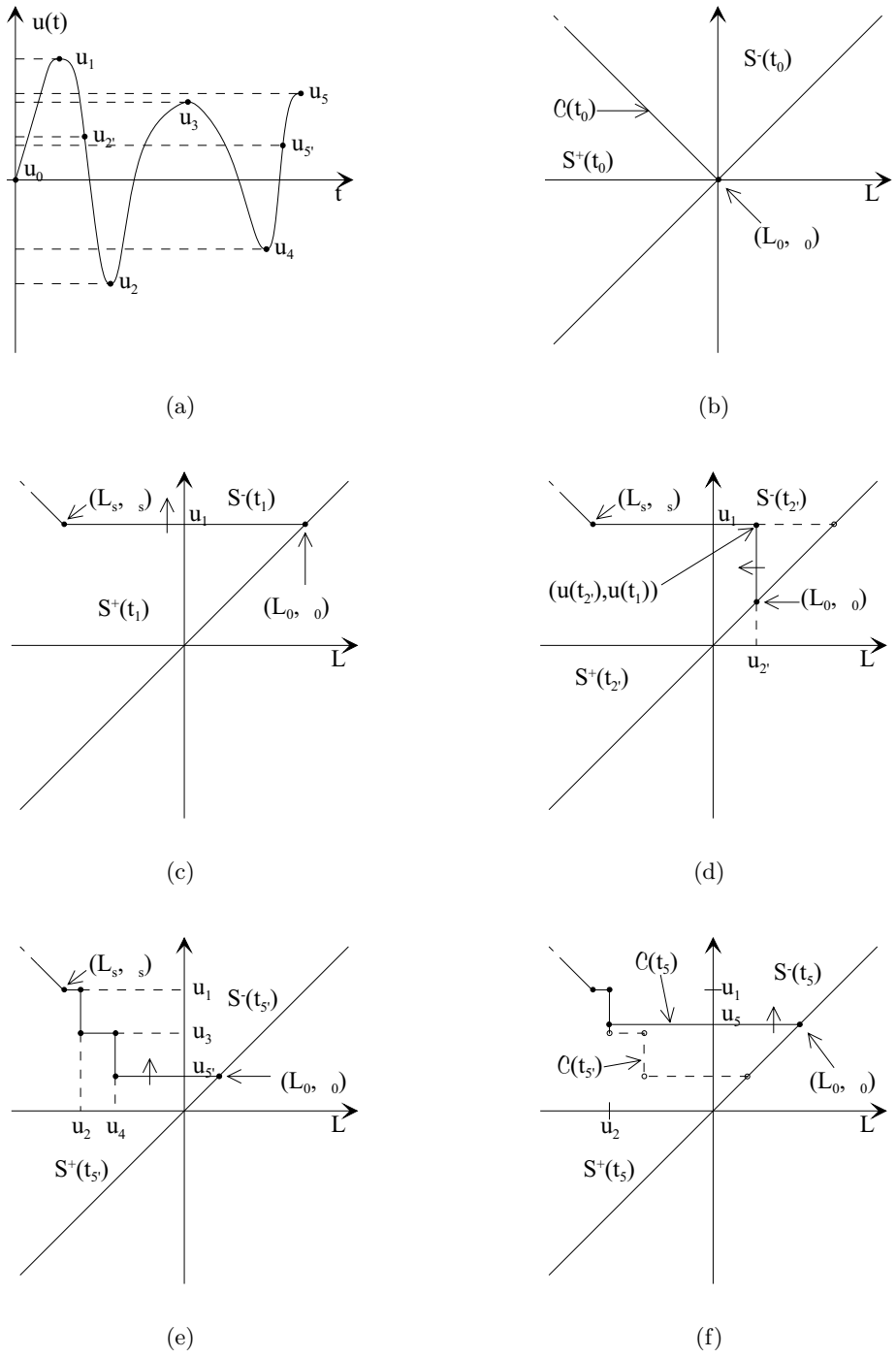

Figure 4.6: The geometric interpretation of the Preisach model can be illustrated with an input signal as in (a), which gives the memory function $\mathcal{C}(t)$ in the Preisach plane as in (b)-(f) at the indicated time instants. The line $\mathcal{C}(t)$ divides the half-plane $\mathrm{L} \leq \Gamma$ into two part, $S^+(t)$ and $S^-(t)$, where $\mathbf{R}_{\mathrm{L}\Gamma}$ is positive and negative, respectively. (b) The virgin state of the memory means that no input has been ever been applied so that the system has no history. (c) A horizontal line is sweeping the Preisach plane upwards when the input is increasing. (d) A vertical line is sweeping to the left when the input is decreasing. A new vertex has here been added to the memory function. (e) The depicted memory function with the form of a 'stair-case' has been produced by a periodic input with decreasing amplitude. (f) Two vertices are wiped out from the memory function when the input pass beyond a former memory vertex. This wiping-out property is particular to the Preisach memory. It is understood that the memory function is dynamic and contains from one to infinity number of memory points.

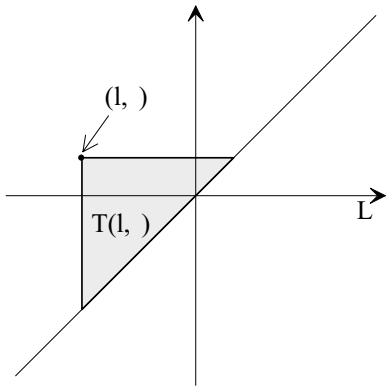

Figure 4.7: The triangle that is limited by L=Γ and the coordinate (l, γ) as in the figure defines the surface over which the Preisach function is integrated to form the Everett function $W(l, \gamma)$.

and negative, $S^-(t)$, also change. From the geometric interpretation in Fig. 4.6, it is easily understood that the output of the Preisach model (4.16) takes the following form:

$$y(t) = \frac{1}{2} \iint\limits_{S^+(t)} w(\mathrm{L}, \Gamma) d\Gamma d\mathrm{L} - \frac{1}{2} \iint\limits_{S^-(t)} w(\mathrm{L}, \Gamma) d\Gamma d\mathrm{L} \tag{4.18}$$

because $\mathbf{R}_{\mathrm{L}\Gamma}[u(t)]$ takes the values $+1/2$ and $-1/2$ in $S^+(t)$ and $S^-(t)$ respectively. Both $S^+(t)$ and $S^-(t)$ depend on previous extrema, so it is understood from this description that the output $y(t)$ also depends on past extreme values of the input $u(t)$. Hence, the model has nonlocal memory.

The Everett Function

Instead of the Preisach function $w(\mathrm{L}, \Gamma)$, we can use the *Everett function*[2] $W(l, \gamma)$ which is the integral of $w(\mathrm{L}, \Gamma)$ over a triangular domain

$$T(l, \gamma) = \{l \leq \mathrm{L}\,,\, \gamma \geq \Gamma\,,\, \mathrm{L} \leq \Gamma\} \tag{4.19}$$

as the one presented in Fig. 4.7. The Everett function is thus:

$$W(l, \gamma) := \iint\limits_{T(l,\gamma)} w(\mathrm{L}, \Gamma) d\Gamma d\mathrm{L}\,. \tag{4.20}$$

There are certain advantages for the use of the Everett function $W(l, \gamma)$, such as the output computation avoids the double integral in (4.16) and introduces a finite sum of differences in an implementation, e.g. the symmetry description in Section 4.3.7 or the one presented in [May91].

The Preisach function $w(\mathrm{L}, \Gamma)$ can be extracted from $W(l, \gamma)$ (inverse formula) by taking the derivative:

$$w(\mathrm{L}, \Gamma) = -\frac{\partial^2}{\partial\Gamma\partial\mathrm{L}} W(\mathrm{L}, \Gamma)\,. \tag{4.21}$$

The Everett function $W(l, \gamma)$ can be retrieved directly from a measured output for a periodic input with monotonicity in each half-period, or equally between two outputs for which the history $\mathcal{C}(t)$ is not influenced, i.e. such that $\Gamma_i > u(t), \mathrm{L}_i < u(t)\, \forall i > 0$. This is comprehended by considering the outputs $y(t_1)$ and $y(t_{2'})$ in Fig. 4.6(c) and 4.6(d), which are the output

[2] In [BS96] the Everett function is called the shape function of the hysteresis with Preisach memory.

extrema due to an input with extrema $u(t_1) = u_1$ and $u(t_{2'}) = u_{2'}$ respectively, presented in the form of (4.18):

$$y(t_1) = \frac{1}{2} \iint\limits_{S^+(t_1)} w(\mathrm{L}, \Gamma) d\Gamma d\mathrm{L} - \frac{1}{2} \iint\limits_{S^-(t_1)} w(\mathrm{L}, \Gamma) d\Gamma d\mathrm{L} \tag{4.22}$$

$$y(t_{2'}) = \frac{1}{2} \iint\limits_{S^+(t_{2'})} w(\mathrm{L}, \Gamma) d\Gamma d\mathrm{L} - \frac{1}{2} \iint\limits_{S^-(t_{2'})} w(\mathrm{L}, \Gamma) d\Gamma d\mathrm{L} \,. \tag{4.23}$$

The difference of these outputs is computed to be the Everett function at the point $(u(t_2), u(t_1))$:

$$y(t_1) - y(t_{2'}) = \frac{1}{2} \iint\limits_{T(u(t_{2'}),u(t_1))} w(\mathrm{L}, \Gamma) d\Gamma d\mathrm{L} + \frac{1}{2} \iint\limits_{T(u(t_{2'}),u(t_1))} w(\mathrm{L}, \Gamma) d\Gamma d\mathrm{L} = W(u(t_{2'}), u(t_1)) \,, \tag{4.24}$$

and so the Everett function is directly retrieved from a measured output.

On physical grounds (symmetry considerations), it can be expected that the decreasing and increasing transition curves are congruent w.r.t. the origin, which then has the consequence that

$$W(l, \gamma) = W(-\gamma, -l) \quad \text{and} \quad w(\mathrm{L}, \Gamma) = w(-\Gamma, -\mathrm{L}) \,. \tag{4.25}$$

The symmetry relation (4.25) is used to simplify expressions of the energy losses, in the numerical implementation in Section A.1 and in the Fourier analysis in Section 5.4.1.

In certain applications, the derivative of the output from the Preisach model is the sought measure, which we denote by

$$v(t) = \frac{dy(t)}{dt} \,. \tag{4.26}$$

Congruent minor loops

The Preisach and Everett functions are not dependent on any other parameters than their position in the Preisach plane for the classical Preisach model. Hence, they are assigned a specific value at each of these points. It is therefore clear that the difference (4.24) is constant, whatever value the *output* took at the first instant, $y(t_1)$, because this difference depends only on the value of the Everett function at the input extrema u_1 and $u_{2'}$. The shape of the output must then also take the same geometrical form when the input changes periodically between two values u_1 and u_2, independently of the starting value of the output. The latter may differ due to differences in the memory function, see Fig. 4.8(a). This *congruency of minor loops*, independent of the history $\mathcal{C}(t)$, is typical for the the classical Preisach model (4.18).

4.3.4 Necessary and Sufficient Conditions

We just concluded that congruency of minor loops[3] is a consequence of the definition of the classical Preisach model. Equally, it was demonstrated that the model implies a wiping-out property for the memory function. Hence, it is understood that these two properties are necessary conditions on a hysteresis in order to be described by the classical Preisach model. Furthermore, it has been proven in [May91] that these are indeed sufficient properties of a physical hysteresis to be described by the classical Preisach model.

[3] The congruency of minor loops is the same as assuming that an Everett function exists [BS96].

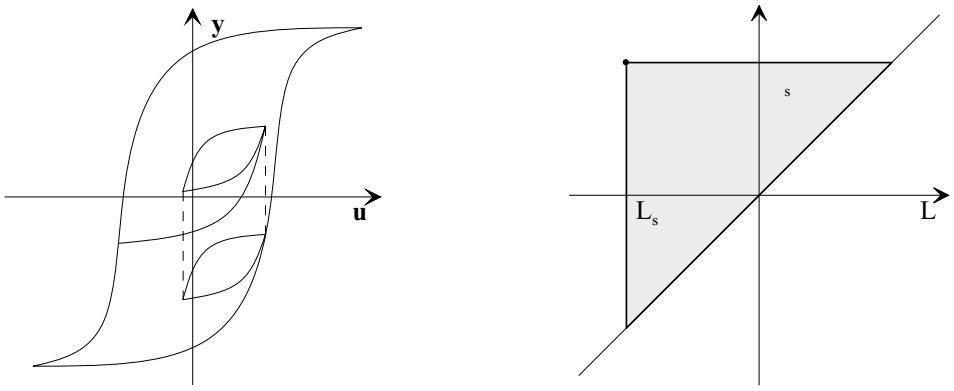

Figure 4.8: (a) Congruency of minor loops, independent of history, is an inherent property of the classical Preisach model. (b) Geometric representation of saturation in the Preisach plane: the Preisach function is non-zero only within a triangle limited by the lines $\mathrm{L} = \Gamma$, $\mathrm{L} = \mathrm{L}_s$ and $\Gamma = \Gamma_s$. The positive and negative saturations are normally symmetric with respect to zero ($\mathrm{L}_s = -\Gamma_s$) as depicted in the figure.

4.3.5 Hysteresis Saturation

A *saturation* of a hysteresis as defined in Section 4.2.1 can be modelled in the Preisach model by introducing a limitation of the Preisach function such that it is zero for inputs smaller than L_s or larger than Γ_s:

$$w(\mathrm{L}, \Gamma) = 0\,, \qquad \mathrm{L} < -\mathrm{L}_s \quad \text{or} \quad \Gamma > \Gamma_s\,. \tag{4.27}$$

In general, the positive and negative saturations appear symmetrically around zero ($\mathrm{L}_s = -\Gamma_s$) as depicted in Fig. 4.8(b). A hysteresis can also be modelled without a saturation, where it is supposed that the possible saturation is simply not attained. Such a restricted Preisach model is only valid within the defined limits. This approach is adopted in Chapter 6. A discussion what happens for, and how to model, the hysteresis saturation in superconductors are discussed in Section 6.7.

4.3.6 Losses

It is well known that hysteretic phenomena are associated with some energy dissipation. In magnetism, it has been found that the hysteresis energy losses are equal to the area enclosed by a loop resulting from a periodic input. Here the losses are considered in view of the Preisach model, partly given by [May91].

Returning to the relay operator $\mathbf{R}_{\mathrm{L}\Gamma}$ and its representation in the output-input diagram (Fig. 4.4(a)), it is realised that the horizontal lines are reversible and hence give no energy loss. Therefore, the 'up' and 'down' switching contains all energy dissipation. Symmetry considerations leads to assigning equal loss per switching [May91],

$$q = \frac{1}{2}(\Gamma - \mathrm{L})\,. \tag{4.28}$$

The energy losses for a monotonic increase of input $u_1 \to u_2$ can therefore be calculated by integrating q weighted by $w(\mathrm{L}, \Gamma)$ over the surface S swept by the memory function in the

Preisach-plane, i.e the loss is calculated for the relays that was forced to change signs:

$$Q(u_1, u_2) = \frac{1}{2} \iint_S w(\mathrm{L}, \Gamma)(\Gamma - \mathrm{L}) d\Gamma d\mathrm{L} \,. \tag{4.29}$$

An example of S is in Fig. 4.6(f), where it is the surface between the dotted line $\mathcal{C}(t_{5'})$ and the solid line $\mathcal{C}(t_5)$. The energy loss for any *closed loop* of a monotonically increasing and then monotonically decreasing input between the values u^- and u^+ has the following expression

$$Q_c(u^-, u^+) = \iint_{T(u^-, u^+)} w(\mathrm{L}, \Gamma)(\Gamma - \mathrm{L}) d\Gamma d\mathrm{L} \,, \tag{4.30}$$

where $T(u^-, u^+)$ is the triangular surface in the Preisach-plane swept by the input signal during one cycle, c.f. Fig. 4.7. An inverse formula can be derived from (4.30) by which the Preisach function $w(\mathrm{L}, \Gamma)$ can be calculated from a known energy loss per cycle [Dju97]:

$$w(\mathrm{L}, \Gamma) = -\frac{1}{\Gamma - \mathrm{L}} \frac{\partial^2}{\partial \mathrm{L} \partial \Gamma} Q_c(\mathrm{L}, \Gamma) \tag{4.31}$$

The formula (4.31) tells us that when the energy losses can be expressed analytically for a loop, the Preisach model can be derived with exact losses [DSD98]. The derived Preisach and Everett functions $w(\mathrm{L}, \Gamma)$ and $W(l, \gamma)$ then enable simulations of such systems for an *arbitrary input*.

The use of $W(l, \gamma)$ implies, by partial integration, an expression for the energy loss (4.29) over the triangle $T(u^-, u^+)$ [May91] as

$$Q_W(u^-, u^+) = \frac{1}{2}(u^+ - u^-) W(u^-, u^+) - \frac{1}{2} \int_{u^-}^{u^+} W(l, u^+) dl - \frac{1}{2} \int_{u^-}^{u^+} W(u^-, \gamma) d\gamma \,. \tag{4.32}$$

The loss by such a monotonic increase of the input equals the loss for the corresponding decrease. Therefore, the loss of the loop in (4.30) can also be calculated with the expression (4.32) according to

$$Q_c(u^-, u^+) = 2 Q_W(u^-, u^+) \,. \tag{4.33}$$

In the case when the loop is between two input values that are symmetrically placed around zero, e.g. in the case of the sinusoidal input signal with peak value U_0,

$$u(t) = U_0 \cos(\omega_0 t) \,, \tag{4.34}$$

and the symmetry (4.25) applies, then the hysteretic losses of a full loop are expressed by [Sjö98, SDD00]

$$Q_c(-U_0, U_0) = 2U_0 W(-U_0, U_0) - 2 \int_{-U_0}^{U_0} W(l, U_0) dl \,. \tag{4.35}$$

The above formula is useful when relating a parametrised $W(l, \gamma)$ and measured energy losses, so that the parameters can be identified as in Section 6.4.

4.3.7 Symmetry Description

The principle of how the classical Preisach model works has been considered so far. We note in this section that the symmetry relation (4.25) allows to express it in a manner that is advantageous for an implementation. By remarking that there is no fundamental difference of

increasing and decreasing input, a simple change of indices highly simplifies the description of the model, and therefore also the coding of an implementation. Both the output signal $y(t)$ and the energy losses between two sample occasions can be calculated in this fashion. Furthermore, the suggested description allows any initial memory function and takes the fully virgin state into account without approximation, as long as the symmetry (4.25) applies. A full derivation of this description is found in Appendix A. There it can be seen how an implementation code can be considerably simplified by using the memory function (4.17), which contains twice as many data as the memory function of the implementation suggested in [May91].

4.3.8 Higher Harmonics

As for most nonlinear systems, the Preisach model produces higher harmonics when it is fed with a sinusoidal input. A detailed frequency analysis is carried out with an arbitrary Everett function in Chapter 5. It shows that the output contains all odd harmonics of the fundamental input frequency. These results justify an extraction of all odd harmonics above noise level as filtering of time-series measurements with sinusoidal input. As a consequence, a novel identification method is suggested for the Everett function which uses sinusoids of different amplitudes as input. This identification method is simpler to apply than the conventional first-transition curve identification [May91] for certain applications, where the output signal may be difficult to extract, as for measurements on superconductors.

4.4 Inverse Models

In the sections above, we have looked at how a hysteretic behaviour between an input $u(t)$ and output $y(t)$ can be described by a hysteresis operator Υ and how it can be computed using the Preisach model. A question that may arise is whether there exist an inverse of such an operator and under what circumstances it exists. One of the first papers that investigated this problem in a systematic way was [Kre91], which has been followed by completing works. Here, we will shortly mention some of the results presented in [BS96], which we will later use in Section 6.6.

4.4.1 Composition of Hysteresis Operators

An inverse hysteresis operator is the operator that when applied on the output from a first hysteresis operator gives the identity operator, i.e. the composition of the two operators reproduces the original input signal:

$$\Upsilon_2[\Upsilon_1[u(t)]] = (\Upsilon_2 \circ \Upsilon_1)\,[u(t)] = \left(\Upsilon_1^{-1} \circ \Upsilon_1\right)[u(t)] = \mathbf{I}[u(t)] = u(t)\,. \tag{4.36}$$

Such an operator does indeed exist in some cases, but in order describe these cases, a few notions must be explained.

4.4.2 Monotone and Odd Hysteresis Operators

By a *piecewise monotone hysteresis operator* is meant an operator with an output that is a monotone function of t (monotonely increasing or monotonely decreasing) in any time interval where the input $u(t)$ is monotone with respect to t. The output of such a piecewise monotone hysteresis operator has local extrema that all correspond to the local extrema of its input $u(t)$, i.e. the local extrema of the output and the input are at exactly the same time instants, see Fig. 4.9. Furthermore, a hysteresis operator with Preisach memory, which has an Everett

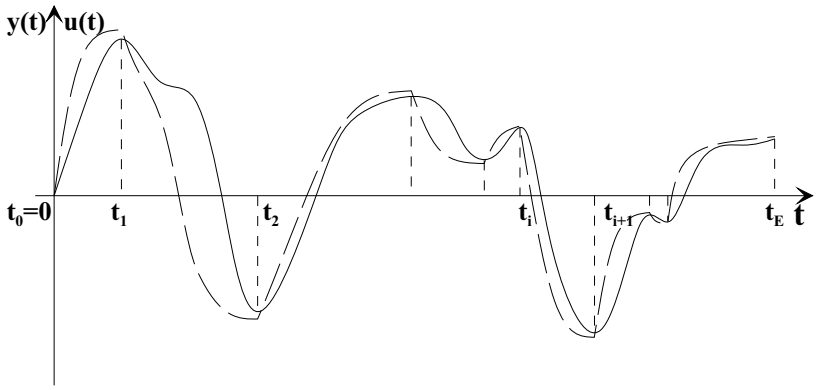

Figure 4.9: The extrema of the input (solid) and output (dashed) are at the same time instants when the hysteresis operator is monotone.

function $W(\mathrm{L},\Gamma)$, is (strictly) monotone if and only if $W(C,x)$, $W(-x,C)$ and $W(-x,x)$ are all (strictly) monotone with increasing x, where C is any constant for which the Everett function is defined. This follows from that the evolution of the Preisach memory is either vertical, horizontal respectively diagonal in the Preisach plane. The latter occurs when the memory passes beyond the point of no history, see Section 4.3.2. We call such an Everett function monotone. It is further clear from (4.20) that a (strictly) positive Preisach function $w(\mathrm{L},\Gamma)$ in the half-plane $\mathrm{L} \leq \Gamma$ implies a (strictly) monotone Everett function. Likewise, the inverse is true: a (strictly) monotone Everett function results in a (strictly) positive Preisach function by applying (4.21).

The next notion to be defined is an *odd hysteresis operator*, by which is understood an operator Υ that produces an output with the following property by a monotone input u when it has no initial history:

$$\Upsilon[-u] = -\Upsilon[u]\,. \tag{4.37}$$

A Preisach model that applies to the symmetry relation (4.25) obeys this property.

4.4.3 Inverse Hysteresis Operator

An important result presented in [BS96] is that two hysteresis operators with *Preisach memory* with no initial memory, where the first operator is piecewise monotone and odd produces a new hysteresis operator with Preisach memory with no initial memory, $\Upsilon = (\Upsilon_2 \circ \Upsilon_1)$. This means that a Preisach model that has a monotone Everett function is a good candidate to have an inverse operator. Indeed, it is shown that if the restriction (4.37) applies to a hysteresis operator with Preisach memory defined on the real axis, then there exists an inverse that is also a hysteresis operator with Preisach memory and which is an odd operator (4.37). Sometimes, a hysteresis operator is only considered or defined on a part of the real axis: a restricted model. This causes no problem because, if the hysteresis operator is limited to a certain domain, the statement above is still true within that domain.

4.4.4 Inverse Prandtl Model

Before we state the result that is really interesting for the application in Chapter 6 (i.e. the parameterised Preisach model), a property of the Everett function for a Prandtl model is enlightened: a hysteresis operator with Preisach memory having an Everett function that depends only on the difference of its arguments is a Prandtl operator and this function is the shape

function presented in (4.15),

$$W(\mathrm{L},\Gamma) = W(\Gamma - \mathrm{L}) = g_P(\Gamma - \mathrm{L})\,. \tag{4.38}$$

This understanding is very important because the inverse of a Prandtl operator is considerably easier to identify than the inverse of the more general Preisach model. The following result is proven in [BS96]: a hysteresis operator with Preisach memory with an Everett function that only depends on the difference of its arguments $W(\mathrm{L},\Gamma) = W(\Gamma - \mathrm{L})$ (i.e. a Prandtl operator), where the Everett function is strictly monotone, continuous and odd, has an inverse that is also a Prandtl operator whose Everett function is

$$W_{inv}(\mathrm{L}',\Gamma') = W^{-1}(\Gamma' - \mathrm{L}')\,, \tag{4.39}$$

where $W^{-1}(\cdot)$ denotes the inverse of the one argument Everett function $W(\cdot)$. The inverse operator has restricted domain if $W(\Gamma - \mathrm{L})$ is not defined on the whole real axis. It is therefore straight forward to identify the inverse operator in the case of Prandtl models.

4.4.5 Existence of Inverse Preisach Model

Another very important consideration is whether it is possible to find an inverse Everett function for the Preisach model defined by the more general Everett function $W(\mathrm{L},\Gamma)$. Suppose, a Preisach operator $\mathbf{P}$ (Preisach model) with zero initial state is defined by a Preisach function $w(\mathrm{L},\Gamma)$, which applies to the symmetry relation (4.25). If its inverse can be described by an Everett function $W_{inv}(\mathrm{L},\Gamma)$, then $\mathbf{P}$ is a Prandtl operator. Hence, in order to find an Everett function for the inverse, the operator $\mathbf{P}$ must be described by an Everett function that depends on the difference of its arguments, $W(\Gamma - \mathrm{L})$. This means that even if the inverse hysteresis operator exists, one can only find an inverse Everett function in certain cases.

4.5 Generalised Scalar Preisach models

The Preisach model has got some limitations: first, the congruency of minor loops does not always coincide with experiments, which means that the Preisach model does not give accurate results. When input is fast, another Preisach function might apply than when input is slow. Some hysteresis need stabilisation before it forms loops, whereas the Preisach model forms loops directly after one cycle. There are some variants of the Preisach model that deal with these issues.

4.5.1 Generalised Preisach Model

There are hysteretic systems that does not have a pure saturation outside of the hysteresis region, but that continues in an arbitrary reversible function. Such a system can be modelled with the *generalised Preisach model*, which divides the model into a reversible and an irreversible part

$$y(t) = f_{rev}(t) + \mathbf{P}[u(t)]\,. \tag{4.40}$$

It describes the same hysteresis system as the classical Preisach model within the hysteresis region, and outside, this model can describe any measured reversible behaviour, whereas the classical Preisach model only have constant output at saturation.

4.5.2 Nonlinear Preisach Model

The *nonlinear Preisach model* introduces a Preisach function that is dependent on the input, $w(\mathrm{L}, \Gamma, u)$, and it is therefore also called the *input dependent Preisach model*. The advantage by doing so, is that minor loops of a hysteresis do not necessarily need to be congruent, but they have equal vertical chords. This enables a fitting of experimentally measured first and second order reversal curves, and so the nonlinear Preisach model is expected to give more accurate results than the classical one.

4.5.3 Restricted Preisach Model

When the saturated value of the output cannot be reached, or in other words, when the whole $\mathrm{L}-\Gamma$ space cannot be measured, a *restricted Preisach model* is applicable. The model is hence only valid within measured input/output. If the maximum and minimum input values are not the same, a constant must be added to the model (4.18) in order to give a correct bias to the model. This was model was mentioned in conjunction with saturation in Section 4.3.5.

4.5.4 Dynamic Preisach Model

The previously described Preisach models are static in the sense that they do not depend on how rapidly the output changes, i.e. dy/dt. The *dynamic Preisach model* takes this measure into account by adding it to the Preisach function. In order not to make life too complicated, only the first two terms of the power series are used,

$$w(\mathrm{L}, \Gamma, \frac{dy}{dt}) = w_0(\mathrm{L}, \Gamma) + \frac{dy}{dt} w_1(\mathrm{L}, \Gamma) \tag{4.41}$$

which leads to the model

$$y(t) = \iint\limits_{\mathrm{L}\leq\Gamma} w_0(\mathrm{L}, \Gamma)\mathbf{R}_{\mathrm{L}\Gamma}[u(t)]d\Gamma d\mathrm{L} + \frac{dy}{dt} \iint\limits_{\mathrm{L}\leq\Gamma} w_1(\mathrm{L}, \Gamma)\mathbf{R}_{\mathrm{L}\Gamma}[u(t)]d\Gamma d\mathrm{L}\,. \tag{4.42}$$

The model implies that if the output has slow variations, the second term is equal to zero. This means that the first term corresponds to the rate-independent Preisach model. It is a tedious work to find both $w_0(\mathrm{L}, \Gamma)$ and $w_1(\mathrm{L}, \Gamma)$, since the measurements must both contain a dynamic part and a part with relaxation at each (L, Γ).

4.5.5 Preisach Model with Accommodation

In practical magnetism, a stabilisation process is often the case before a hysteresis produce minor loops. This is called accommodation or reptation in the literature. A model that reflect this *accommodation* can be defined by letting the Preisach function depend on the last attained local extremum of the *output*: $w(\mathrm{L}, \Gamma, y^{(m)})$. A monotonically input varied back and forth between two values u^- and u^+ will eventually form a closed minor loop in the input-output plane, if the dependence on $y^{(m)}$ is well selected.

4.5.6 Hysteresis Models of Preisach Type

It was pointed out in Section 4.2.6 that the Prandtl model has a memory evolution that coincide with the Preisach memory. In fact, the Preisach memory can be considered a general model

for describing the memory in rate-independent hysteretic systems, where all such models that comply to the Preisach memory are called *hysteresis models of Preisach type*, a term that was introduced in [BS96]. It is shown there that all such models can be divided into a part that deals solely with the memory update (according to Preisach memory) and a second memoryless part that maps the memory into the output value. The 'stair-case' formed memory function $\mathcal{C}(t)$ (see Fig. 4.6) can be expressed in the rotated coordinates $s = (\mathrm{L} + \Gamma)/2$ and $r = (\Gamma - \mathrm{L})/2$, which correspond to the mean value and the half-width of the relay operator in Fig. 4.4(a). The memory function is then given by the diagram of the function

$$s = \mathbf{F}_r[u(t)] \tag{4.43}$$

where $\mathbf{F}_r[\cdot]$ is the play operator. In this way, it is thus possible to express the memory of the hysteresis alone as a function of the play operator. The classical Preisach model (4.16) expressed in these rotated coordinates gives the following equation:

$$y(t) = \int_0^\infty f(r, \mathbf{F}_r[u(t)])\, dr \tag{4.44}$$

when it holds that

$$f(t, z) = \int_{-\infty}^{z} w(s, r) - \int_z^\infty w(s, r)\, ds\,. \tag{4.45}$$

The function $f(\cdot)$ is a memoryless function that relates the memory function to the hysteresis output. The Prandtl model can be expressed in the same manner as

$$y(t) = \int_0^\infty f_p(\mathbf{F}_r[u(t)])\, dr\,, \tag{4.46}$$

where $f_p(\cdot)$ is also a memoryless function.

We see from the presentation above how the sheer memory function can be held separately and its relationship to the output in a memoryless function. All hysteresis models that can be separated in this fashion are the so-called models of Preisach type.

An interesting application of this separation was carried out in [SV98, VSM+00]. They introduced feed forward neural networks instead of more classical functions in order to compute the hysteretic output.

4.6 Chapter Summary

The author has in this chapter recapitulated what different hysteresis definitions figure in the literature and then adopted one of the phenomenological characterisations.

A review of different mathematical models is presented and in particular the classical Preisach model of hysteresis. The manner to update the Preisach memory and to compute output and losses with the model is described. The necessary and sufficient conditions on a hysteretic system to be described by the classical Preisach model has been recapitulated. The cases when an inverse of a the Preisach model exists have been investigated and some generalised Preisach models have been presented.

In particular, the author has developed a description of the Preisach model assuming a symmetric Preisach function that allows for simple implementations for the computation of output,

differentiated output and losses. This description is based on the numerical implementation presented in [May91], but further permits arbitrary initial conditions of the input and the memory function. Details of this symmetry description is found in Appendix A.

Chapter 5

Higher Harmonics in Classical Preisach Model

Most nonlinear systems produce higher harmonics when they are excited with a sinusoidal input. Most often there are only odd harmonics present, which is due to the half-wave symmetry of the signal. In the classical Preisach model this is also true with some conditions on the Preisach (or Everett) function. The necessary and sufficient conditions on the Preisach and Everett functions in order to have a half-wave symmetry on the output are derived for the case when the input signal is half-wave symmetric and monotonic in each half-period. The conditions for producing *all* odd harmonics when the input is the special case of a sinusoid are then investigated for an Everett function described by a polynomial of infinite degree. Such an Everett function includes a large class of functions via MacLaurin-series [Sjö99].

The analysis of the restrictions on the Everett function and a general polynomial Everett function (Section 5.1–5.2) was firstly presented in [Sjö99]. The analysis of Everett function of polynomial of difference $(\Gamma - \mathrm{L})$ (Section 5.4.1) was described in [SD98] for the first time, but it has been complemented with an analysis by Fourier-series here.

The advantage of knowing that the output contains all odd and only odd harmonics of the principal input signal is that these may be extracted from a noisy measured signal. In this way the signal quality may be enhanced. The relationship between the free parameters in the polynomial Everett function and the frequency contents can also be applied to estimate these from measurements. This can be exploited to separate data in a process that contains linear and hysteretic elements because the latter are the only ones that contribute to higher harmonics in the measured signal.

5.1 Half-wave Symmetric Signals

A half-wave symmetric signal has the same shape in each half-period, except that it has a negative sign compared to the half-period before. An example of a half-wave symmetric signal is given in Fig. 5.1. A signal with half-wave symmetry is defined as follows.

Definition 5.1 (Half-wave symmetry).
A periodic signal $s(t)$ with period T is half-wave symmetric *if and only if it obeys*

$$f(t + T/2) = -f(t)\,. \tag{5.1}$$

Another special case of the half-wave symmetric signal is when it is monotonically increasing and monotonically decreasing in each respective half-period.

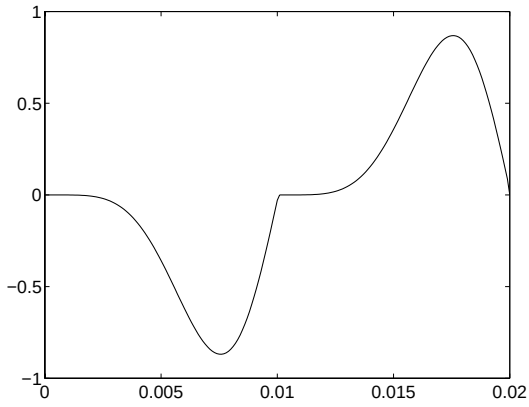

Figure 5.1: Example of a half-wave symmetric signal.

Definition 5.2 (Monotonic half-wave symmetry).
A half-wave symmetric signal $s(t)$ with $\frac{ds}{dt} \geq 0$ in one half-period and $\frac{ds}{dt} \leq 0$ in the other is called a monotonic half-wave symmetric signal.

We continue to remind that half-wave symmetry produces only odd harmonics. It is well known that a periodic signal of period $T = 2\pi/\omega_0$ can be described by the Fourier series expansion:

$$f(t) = a_0 + \sum_{h=1}^{\infty} 2\left(a_h \cos(h\omega_0 t) + b_h \sin(h\omega_0 t)\right) \tag{5.2}$$

where

$$a_h = \frac{1}{T}\int_0^T f(t)\cos(h\omega_0 t)dt \qquad \text{and} \qquad b_h = \frac{1}{T}\int_0^T f(t)\sin(h\omega_0 t)dt \tag{5.3}$$

for all harmonics $h \geq 0$. The direct term a_0 is a simple shift of the signal amplitude.

A signal that possesses the half-wave symmetry has no contribution to the even harmonics, which is straight forward to calculate from (5.3): $a_{2n} = b_{2n} = 0$. Hence, there exist only odd harmonics. On the contrary, if a signal consists of only odd harmonics, it is a superposition of signals that all obey the half-wave symmetry (5.1), and so the signal must also be half-wave symmetric. Thus, the well known result is established:

Lemma 5.1. *A periodic signal consists of only odd harmonics if and only if half-wave symmetry applies.*

5.2 Restrictions on Everett function – Only Odd Harmonics

Next, the conditions on the Preisach function are derived in order to have half-wave symmetry on the output signal. The considered cases have an input signal $u(t)$ with the following restrictions:

Definition 5.3 (Monotonic half-wave symmetry with additive direct term).
A monotonic half-wave symmetric signal with an additive direct term consists of a direct term $a_{0,u}$ and a dynamic part $\tilde{u}(t)$:

$$u(t) = a_{0,u} + \tilde{u}(t) \tag{5.4}$$

where the dynamic part $\tilde{u}(t)$ with amplitude U_0 is monotonic half-wave symmetric.

Note that a sinusoid is a special case of Definition 5.3 with $a_{0,u} = 0$. The considered output $y(t)$ should have the following characteristics:

Definition 5.4 (Half-wave symmetry with additive direct term).
A half-wave symmetric signal with an additive direct term consists of a direct term $a_{0,y}$ and a dynamic part $\tilde{y}(t)$:

$$y(t) = a_{0,y} + \tilde{y}(t) \tag{5.5}$$

where the dynamic part $\tilde{y}(t)$ is half-wave symmetric.

The direct term is necessary for a generalisation of the output as will become clear in the sequel.

5.2.1 Input without Direct Term

First the case when $a_{0,u} = 0$ is considered. An input signal as in Definition 5.3 has an output that can be expressed using (4.24) leading to the following formula:

$$y(t) = \begin{cases} y_{-U_0} + W(-U_0, u(t)), & du/dt \geq 0 \\ y_{U_0} - W(u(t), U_0)), & du/dt < 0, \end{cases} \tag{5.6}$$

where y_{U_0} and y_{-U_0} are the outputs at maximum and minimum of the input $u(t)$, respectively. Now, due to the characteristics of the input signal in Definition 5.3 with $a_{0,u} = 0$ the upper and lower equations in (5.6) are applied exactly half a period apart. For the time being, we consider the dynamic output $\tilde{y}(t)$ only, and so by subtracting the direct part $a_{0,y}$ we have

$$\tilde{y}(t) = \tilde{y}_{U_0} - W(u(t), U_0) \tag{5.7}$$

and half a period earlier:

$$\tilde{y}(t + T/2) = \tilde{y}_{-U_0} + W(-U_0, u(t + T/2)) \tag{5.8}$$

The input maximum and minimum also appear exactly half a period apart, whereby the Everett function is equal to zero, $W(\mathrm{L}, \mathrm{L}) = 0$, by definition. This implies that $\tilde{y}_{U_0} = -\tilde{y}_{-U_0}$ for the half-wave symmetry to hold. By taking this relationship and combine it with (5.7), (5.8), the half-wave symmetry of the input and of the the output, it turns out that it is necessary for the Everett function to obey $W(\mathrm{L}, U_0) = W(-U_0, -\mathrm{L})$. This is valid for all amplitudes of the input if:

$$W(\mathrm{L}, \Gamma) = W(-\Gamma, -\mathrm{L}) \tag{5.9}$$

which is equivalent to having a Preisach function $w(\mathrm{L}, \Gamma) = w(-\Gamma, -\mathrm{L})$. This is nothing else but the symmetry relation (4.25)

$$W(l, \gamma) = W(-\gamma, -l) \quad \text{and} \quad w(\mathrm{L}, \Gamma) = w(-\Gamma, -\mathrm{L}), \tag{5.10}$$

which is therefore a necessary condition to have half-wave symmetry on the dynamic output. The actual output of the model is, however, $y(t) = a_{0,y} + \tilde{y}(t)$. The direct term is retrieved by combining this equation with (5.7), (5.8), the half-wave symmetry of the dynamic output, and is given by:

$$a_{0,y} = \frac{y(t) + y(t + T/2)}{2} = \frac{y_{U_0} + y_{-U_0}}{2} \tag{5.11}$$

Next, it is clarified that the direct term is necessary for a generalisation. The symmetry relation (5.10) implies that the maximum output of the Preisach model can be expressed as (use (A.18) with $\mathrm{L}_s = -U_0$ and $\Gamma_s = U_0$)

$$y_{U_0} = \frac{W(-U_0, U_0)}{2} \tag{5.12}$$

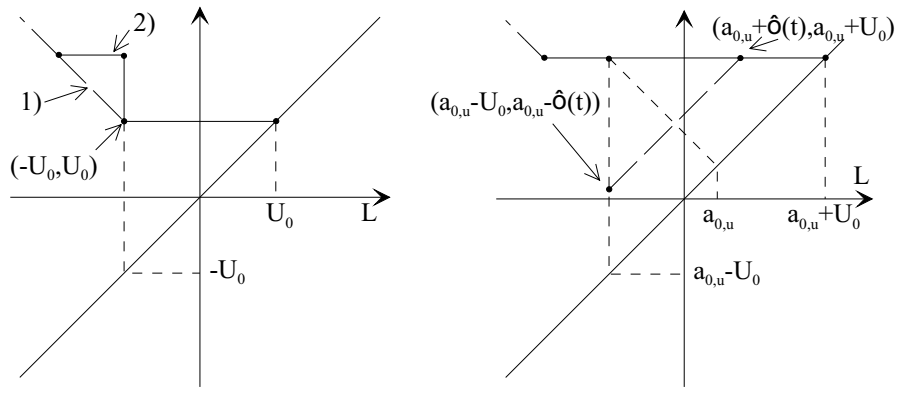

Figure 5.2: (a) The direct term of the output is history dependent. History 1) implies a direct term equal to zero, for 2) it is non-zero. (b) The oscillation around an offset $a_{0,u}$ described in the Preisach-plane. It is then necessary to have $W(a_{0,u}+\tilde{u}(t), a_{0,u}+U_0) = W(a_{0,u}-U_0, a_{0,u}-\tilde{u}(t))$ for an output with half-wave symmetry except for an offset $a_{0,y}$.

if there is no history beyond point $(-U_0, U_0)$ as in Fig. 5.2(a)– 1. (No history means that the model is in a virtue state as explained in Section 4.3.2.) In that case the direct term $a_{0,y}$ is equal to zero since $y_{U_0} = -y_{-U_0}$. However, (5.12) is not true when there is a history beyond the point $(-U_0, U_0)$ as in Fig. 5.2(a)– 2, whereby the direct term must be added. The direct term is therefore history dependent and it is necessary for a generalisation. Note that (5.12) can always be used to calculate $\tilde{y}_{U_0}$, since that corresponds to an output with $a_{0,y} = 0$.

It is easy to see that the symmetry relation (5.10) is also a sufficient condition for half-wave symmetry, since it directly produces $W(u(t), U_0) = W(-U_0, -u(t)) = W(-U_0, u(t+T/2))$ and $\tilde{y}_{-U_0} = -\tilde{y}_{U_0}$, and so (5.7) is equal to the negative of (5.8) and the half-wave symmetry for the dynamic output is a fact. When there is history beyond $\mathrm{L} < -U_0$ or $\Gamma > U_0$, a direct term according to (5.11) then gives a correct output. The following Proposition can therefore be stated:

Proposition 5.1. *When the input to a classic Preisach model obeys Definition 5.3 and $a_{0,u} = 0$, the output is half-wave symmetric, except for a possible history-dependent direct term as in Definition 5.4, if and only if the symmetry relation (5.10) applies.*

Note that the output is not necessarily monotone. In order to have a monotone output, the Everett function must also be monotone, as defined in Section 4.4.2. Next follows a corollary that is a direct consequence of Lemma 5.1.

Corollary 5.1.1. *The output from such a Preisach model contains only odd harmonics, except for the possible direct term.*

5.2.2 Input with Direct Term

Now we consider when the input also has a non-zero direct term, $a_{0,u} \neq 0$. Otherwise, the same input and output condition as in Definition 5.3 and 5.4 are taken into account. This means that the input is oscillating around an offset $a_{0,u}$ which is described by Fig. 5.2(b) in the Preisach-plane. The conditions on the weighting function in this case are obtained in the same way as before. First, the equations of the dynamic output for descending and ascending inputs half a

period apart are respectively

$$\tilde{y}(t) = \tilde{y}_{a_{0,u}+U_0} - W(a_{0,u} + \tilde{u}(t), a_{0,u} + U_0) \tag{5.13}$$
$$\tilde{y}(t + T/2) = \tilde{y}_{a_{0,u}-U_0} + W(a_{0,u} - U_0, a_{0,u} + \tilde{u}(t + T/2)) \tag{5.14}$$

and the relation $W(\mathrm{L}, \mathrm{L}) = 0$ at maxima and minima of the input directly gives that $\tilde{y}_{a_{0,u}+U_0} = -\tilde{y}_{a_{0,u}-U_0}$ for the half-wave symmetry to hold. Taking this last formula and re-combining it with (5.13), (5.14) and the half-wave symmetry of dynamic input $\tilde{u}(t)$ and output $\tilde{y}(t)$, it turns out that it is necessary for the Everett function to obey:

$$W(a_{0,u} + \tilde{u}(t), a_{0,u} + U_0) = W(a_{0,u} - U_0, a_{0,u} - \tilde{u}(t)) \tag{5.15}$$

These two points of the Everett function are marked in Fig. 5.2(b). It is therefore clear that the Everett function must be equal in all points parallel to the line $\mathrm{L} = \Gamma$ in order to have the conditions on input and output valid for all input amplitudes U_0 or for all input offsets $a_{0,u}$. This is the same as to state that the Everett function must depend only on the difference of its arguments:

$$W(\mathrm{L}, \Gamma) = W(\Gamma - \mathrm{L}) \tag{5.16}$$

which is equivalent to having a Preisach function $w(\mathrm{L}, \Gamma) = w(\Gamma - \mathrm{L})$. As before, the direct term of the output $y(t)$ can always be calculated according to:

$$a_{0,y} = \frac{y(t) + y(t + T/2)}{2} = \frac{y_{a_{0,u}+U_0} + y_{a_{0,u}-U_0}}{2} \tag{5.17}$$

When there is no further input history beyond the point $(-|a_{0,u}|-U_0, |a_{0,u}|+U_0)$ in the Preisach-plane, the direct term can also be expressed as

$$a_{0,y} = \frac{W(2(|a_{0,u}| + U_0)) - W(2U_0)}{2} \cdot \mathrm{sgn}(a_{0,u}) \tag{5.18}$$

For an input history beyond this point the direct term is history dependent as before.

It is straightforward to see that the relation (5.16) is sufficient to have the half-wave symmetry on the output except for a direct term when the input obeys Definition 5.3 with $a_{0,u} \neq 0$. When (5.16) applies, the relation (5.15) follows and the different half-periods of the output given by (5.13) and (5.14) are half-wave symmetric, except for a constant $a_{0,y}$ given by (5.17). The result is gathered in the following proposition:

Proposition 5.2. *When the input to a classic Preisach model obeys Definition 5.3 with $a_{0,u} \neq 0$, the output is half-wave symmetric, except for a direct term $a_{0,y}$, if and only if the weighting function depends only on the difference of its arguments:*

$$w(\mathrm{L}, \Gamma) = w(\Gamma - \mathrm{L}) \quad \textit{or} \quad W(\mathrm{L}, \Gamma) = W(\Gamma - \mathrm{L}) \tag{5.19}$$

As before, this relates to the frequency contents using Lemma 5.1:

Corollary 5.2.1. *The output from such a Preisach model contains only odd harmonics and a direct term (zero frequency).*

Another interesting consequence of Proposition 5.2 in combination with the odd harmonics given in Lemma 5.1 is the inverse problem:

Corollary 5.2.2. *A measured signal that can be described by the classical Preisach model, and which contains only odd harmonics except for a direct term for all input offsets $a_{0,u}$, has a weighting function that depends only on the difference of the arguments (5.19).*

5.3 Frequency Analysis for Polynomials – All Odd Harmonics

So far it has been shown that the output from the Preisach model contains only odd harmonics under certain conditions (Definition 5.3 and 5.4). Next it shall be investigated what harmonics, if any, are present. To do so, it is first assumed that the input is sinusoidal with no direct term ($a_{0,u} = 0$)

$$u(t) = U_0 \cos(\omega_0 t) \tag{5.20}$$

with frequency $\omega_0 = 1/2\pi T$ and with an amplitude U_0 inferior to a possible saturation:

$$U_0 < \min(|\mathrm{L}_s|, |\Gamma_s|) \tag{5.21}$$

A sinusoid is a special case of an input according to Definition 5.3, and so Proposition 5.1 and corollary apply. The possible direct term in the output gives only a DC component and is therefore ignored here ($a_{0,u} \Rightarrow \tilde{y}(t) = y(t)$), i.e. no history beyond $(-U_0, U_0)$ is supposed,

It is necessary to know something about the structure of the weighting function to be able to investigate what harmonics are present. An Everett function with polynomial expansion is considered here, since it includes a large class of functions via MacLaurin-series:

$$W(\mathrm{L}, \Gamma) = \sum_{p=0}^{\infty} \sum_{k=0}^{\infty} c_{p,k} \mathrm{L}^p \Gamma^k \tag{5.22}$$

As there should be only odd harmonics in the output, the symmetry (5.10) must apply, and so the polynomial expansion above can be expressed by:

$$W(\mathrm{L}, \Gamma) = \sum_{p \le k} \tilde{c}_{p,k} \left((-\mathrm{L})^p \Gamma^k + (-\mathrm{L})^k \Gamma^p \right) = \sum_{p \le k} W_{p,k}(\mathrm{L}, \Gamma) \tag{5.23}$$

where $\tilde{c}_{p,k} = (-1)^p c_{p,k}$. (The summation is only for $p \le k$, but all terms in (5.22) are included as the summation here is for both $(-\mathrm{L})^p \Gamma^k$ and $(-\mathrm{L})^k \Gamma^p$.) For the frequency contents, it suffices to investigate one of the terms: $W_{p,k}(\mathrm{L}, \Gamma)$. With such an Everett function, the output is half-wave symmetric and the odd harmonic in-phase and quadrature terms can be calculated by using only the first half-period. In this first half-period, the phase of the sinusoidal input (5.20) is chosen such that the output can be expressed by (5.7):

$$y(t) = y_{U_0} - W_{p,k}(u(t), U_0) \tag{5.24}$$

where the first term can be computed according to (5.12). Therefore, the output consists of a part that depends exclusively on the output at the input extrema, $y_A(t)$, and another part that depends on the structure of $W_{p,k}(\mathrm{L}, \Gamma)$, $y_W(t)$:

$$y(t) = y_A(t) - y_W(t)\,. \tag{5.25}$$

The factors of the Fourier series are also separated accordingly, and are calculated as:

$$a_{2n-1} = a^{(A)}_{2n-1} - a^{(W)}_{2n-1} = \frac{2}{T} \int_0^{T/2} [y_A(t) - y_W(t)] \cos((2n-1)\,\omega_0 t)\, dt \tag{5.26}$$

$$b_{2n-1} = b^{(A)}_{2n-1} - b^{(W)}_{2n-1} = \frac{2}{T} \int_0^{T/2} [y_A(t) - y_W(t)] \sin((2n-1)\,\omega_0 t)\, dt \tag{5.27}$$

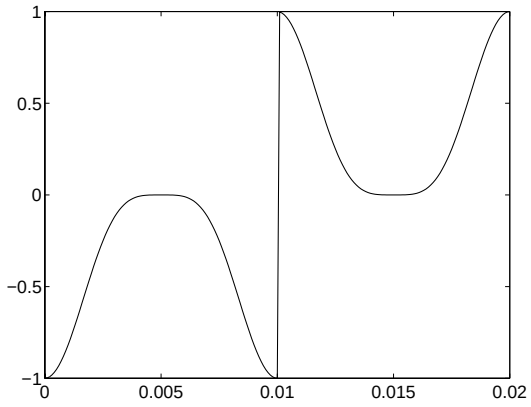

Figure 5.3: An Everett function (5.23) with an even p (or k) produces an output with even harmonics within a half period and a jump between them. Here, $p = 4$,$k = 0$.

By this separation, it is realised that $y_A(t)$ is in fact a square wave with amplitude y_{U_0}. The Fourier components for such a square wave are straight forward to calculate and take the following form:

$$a_{2n-1}^{(A)} = 0 \tag{5.28}$$

$$b_{2n-1}^{(A)} = \frac{2y_{U_0}}{\pi(2n-1)} = \frac{W_{p,k}(-U_0, U_0)}{\pi(2n-1)} = \frac{2\tilde{c}_{p,k}U_0^{p+k}}{\pi(2n-1)} \tag{5.29}$$

The last equality is obtained by applying (5.12) on $W_{p,k}(\mathrm{L}, \Gamma)$. The expressions reveal that the square wave has sinusoidal contributions at *all* odd harmonics.

Now, the second part y_W is considered. The cosine-function to the power of p can be expressed by higher harmonic cosines by applying Euler's formula $\cos(x) = (\mathrm{e}^{jx} + \mathrm{e}^{-jx})/2$ and binomial expansion, by which the following relationship is achieved:

$$\cos^p(x) = \begin{cases} 2^{1-p} \sum_{r=0}^{\frac{p-1}{2}} \binom{p}{r} \cos\left((p-2r)x\right), & p \quad \text{odd} \\ 2^{-p}\binom{p}{p/2} + 2^{1-p} \sum_{r=1}^{p/2} \binom{p}{p/2+r} \cos\left(2rx\right), & p \quad \text{even} \end{cases} \tag{5.30}$$

That is, when p is odd, all odd harmonics up to the p's harmonic are present, and when it is even, there are even harmonics up to the p's harmonic plus a constant term. Note that the Everett function (5.23) was chosen such that the output is half-wave symmetric. Thus, even harmonics cannot be present. The output by an even p (or k) gives only an even harmonic within each half period and then jumps between these half periods, see Fig. 5.3. It is straightforward to compute $a_{2n-1}^{(W)}$ from (5.26) and (5.30): it is zero for even p and k and for all harmonics larger than $\max(p, k)$, and non-zero otherwise. Mathematically, this is expressed by

$$a_{2n-1}^{(W)} = -\tilde{c}_{p,k}U_0^{p+k}[g(p) + g(k)] \tag{5.31}$$

where

$$g(x) = \frac{1-(-1)^x}{2} 2^{-x} \binom{x}{\frac{x-2n+1}{2}} s(x-2n+1) \tag{5.32}$$

and $(1-(-1)^x)/2$ is zero for all even x and $s(\cdot)$ is the step function:

$$s(x) = \begin{cases} 1, & x \geq 0 \\ 0, & x < 0 \end{cases} \tag{5.33}$$

Similarly, the quadrature term $b_{2n-1}^{(W)}$ is found to be zero for odd p's and k's when computed from (5.27) and (5.30). An even exponent present in the Everett function (5.23) produced a signal as in Fig. 5.3. Such signals with abrupt changes contains all odd harmonics, which is revealed in the evaluation of the integral (5.27):

$$b_{2n-1}^{(W)} = \frac{2\tilde{c}_{p,k}U_0^{p+k}}{\pi}\left[h(p) + h(k)\right] \tag{5.34}$$

where

$$h(x) = \frac{1-(-1)^{x+1}}{2}\left[\frac{2^{-x}}{2n-1}\binom{x}{x/2} + 2^{1-x}\sum_{r=1}^{x/2}\binom{x}{x/2+r}\frac{2n-1}{(2(n+r)-1)(2(n-r)-1)}\right] \tag{5.35}$$

We gather the result in a theorem:

Theorem 5.1. *A classical Preisach model, defined by the general polynomial Everett function (5.23), whose input is a sinusoid with no direct term (5.20) and with no history beyond $(-U_0, U_0)$, has a half-wave symmetric output (only odd harmonics) and the following terms in the Fourier series:*

$$a_{2n-1} = \tilde{c}_{p,k}U_0^{p+k}\left[g(p) + g(k)\right] \tag{5.36}$$

$$b_{2n-1} = \frac{2\tilde{c}_{p,k}U_0^{p+k}}{\pi}\left[\frac{1}{2n-1} - h(p) - h(k)\right] \tag{5.37}$$

where $g(x)$ and $h(x)$ are given by (5.32) and (5.35), respectively.

Proof. The proof follows from the discussion above. □

It can be concluded that $W_{p,k}(\mathrm{L},\Gamma)$ contributes to all odd harmonic up to the maximum of p and k in the in-phase part and that the quadrature part contains all harmonics in general. However, the quadrature part b_{2n-1} may not be present for specific combinations of exponents:

Corollary T 5.1.1. *When either p or k is odd, the terms b_{2n-1} in (5.37) cancel out if and only if the other exponent is equal to zero. These exponents correspond to the Everett functions:*

$$W_{0,2s-1}(\mathrm{L},\Gamma) = \tilde{c}_{0,2s-1}(\Gamma^{2s-1} - \mathrm{L}^{2s-1}) \tag{5.38}$$

Proof. This result is deduced from (5.37). The only combination of p and k that gives the terms $b_{2n-1} = 0$ is when either of them is zero and the other odd. □

It is seen that when these Everett functions (5.38) are expressed in Preisach functions $w(\mathrm{L},\Gamma)$ by applying (4.21), then they are equal to zero and do not express any hysteresis. Proposition 5.1 with corollary still holds, since the system produces odd harmonics up to $\max(p,k)$ in the in-phase term.

5.4 Frequency Analysis for Polynomials of Difference $(\Gamma - \mathrm{L})$

The case given by Proposition 5.2, when the input signal with offset gives only odd harmonics and depends only on the difference $(\Gamma - \mathrm{L})$, has first been investigated in [SD98]. We assume an Everett function as a polynomial of this difference:

$$W(\mathrm{L},\Gamma) = \sum_{p=1}^{P} c_p\left(\frac{\Gamma-\mathrm{L}}{2C}\right)^p = \sum_{p=1}^{P} W_p(\mathrm{L},\Gamma) \tag{5.39}$$

where a normalisation of the difference by $2C$ is applied. The contribution for each $W_p(\mathrm{L},\Gamma)$ to the Fourier coefficients is now computed.

The analysis with the Everett function (5.39) is completely analogous with one in the preceding section, and the calculus is also very similar. We consider the same external conditions as before, i.e. a single sinusoid (5.20) with an amplitude inferior to a saturation (5.21) is input to the Preisach model. Proposition 5.2 is then applicable, so there are only odd Fourier coefficients, which can be computed from the first half-period using (5.26) and (5.27) due to the half-wave symmetry of the model output. The components of the first part (square wave) only differs in the amplitude in comparison with (5.28) and (5.29):

$$a_{2n-1}^{(A)} = 0 \tag{5.40}$$

$$b_{2n-1}^{(A)} = \frac{2y_{U_0}}{\pi(2n-1)} = \frac{W_p(-U_0,U_0)}{\pi(2n-1)} = \frac{2c_p}{\pi(2n-1)}\left(\frac{U_0}{C}\right)^p \tag{5.41}$$

Next, the second part y_W is calculated. First, it is understood that the Everett function (5.39) with the defined sinusoidal input may be written as follows in the first half-period. It turns out to be a sinusoid to an even power of half the input frequency:

$$W_{p,k}(u(t),U_0) = c_p\left(\frac{U_0 - U_0\cos(\omega_0 t)}{2C}\right)^p = c_p\left(\frac{U_0}{C}\right)^p \sin^{2p}(\frac{\omega_0}{2}t)\,. \tag{5.42}$$

It is therefore useful to rewrite the sinus-function to the power of p using Euler's formula $\sin(x) = (\mathrm{e}^{jx} - \mathrm{e}^{-jx})/2j$ and binomial expansion in a similar way as was made with the cosine-function:

$$\sin^p(x) = \begin{cases} 2^{1-p}\sum\limits_{r=0}^{\frac{p-1}{2}} (-1)^{\frac{p-1}{2}+r}\binom{p}{r}\sin\left((p-2r)x\right)\,, & p \quad \text{odd} \\ 2^{-p}\binom{p}{p/2} + 2^{1-p}\sum\limits_{r=1}^{p/2}(-1)^r\binom{p}{p/2+r}\cos\left(2rx\right)\,, & p \quad \text{even} \end{cases} \tag{5.43}$$

Note that the exponent is always even for the Everett function (5.42) and that the frequency is *half* the input frequency. There exist therefore contributions to all odd harmonics up to the p^{th} harmonic of ω_0 in the in-phase part $a_{2n-1}^{(W)}$, contrary to was found in the previous section where even exponents gave no contribution. This is easily verified by evaluating the integral (5.26) using the re-written Everett function (5.42) and the power expansion of the sinusoid (5.43), which gives

$$a_{2n-1}^{(W)} = -c_p\left(\frac{U_0}{C}\right)^p \tilde{g}(p) \tag{5.44}$$

where

$$\tilde{g}(x) = 2^{-2x}\binom{2x}{x+2n-1}s(x-2n+1)\,. \tag{5.45}$$

and $s(\cdot)$ is again the step function.

Likewise, the quadrature term $b_{2n-1}^{(W)}$ is computed with the integral (5.27) and the power expansion of the re-written Everett function. The expressions of the power expansions of the cosine- and sine-functions look very alike, so it can be understood that the output signal is similar to the one in Fig. 5.3, and so contains all odd harmonics. The evaluated quadrature term takes the following form:

$$b_{2n-1}^{(W)} = \frac{2c_p}{\pi}\left(\frac{U_0}{C}\right)^p \tilde{h}(p) \tag{5.46}$$

where

$$\tilde{h}(x) = \left[\frac{2^{-2x}}{2n-1} \binom{2x}{x} + 2^{1-2x} \sum_{r=1}^{\lfloor x/2 \rfloor} \binom{2x}{x+2r} \frac{2n-1}{(2(n+r)-1)(2(n-r)-1)} \right] \tag{5.47}$$

and $\lfloor \cdot \rfloor$ denotes rounding off to the first smaller integer. The results are summarised in the following theorem:

Theorem 5.2. *A classical Preisach model, defined by the Everett function of polynomials of difference* (Γ − L) *(5.39), who has an sinusoidal input with no direct term (5.20) and with no history beyond* $(-U_0, U_0)$*, has a half-wave symmetric output (only odd harmonics) and the following terms in the Fourier series:*

$$a_{2n-1} = c_p \left(\frac{U_0}{C} \right)^p \tilde{g}(p) \tag{5.48}$$

$$b_{2n-1} = \frac{c_p}{\pi} \left(\frac{U_0}{C} \right)^p \left[\frac{1}{2n-1} - 2\,\tilde{h}(p) \right] \tag{5.49}$$

where $\tilde{g}(x)$ *and* $\tilde{h}(x)$ *are given by (5.45) and (5.47), respectively.*

Proof. The proof follows from the preceding discussion. □

We can summarise that a Preisach model defined by an Everett function with the structure (5.39) has contributions to the odd harmonics up to the p^{th} harmonic in the in-phase term and to all harmonics in the quadrature term. There exists one exception for the quadrature terms, which then all are zero:

Corollary T 5.2.1. *The quadrature terms* b_{2n-1} *in (5.49) are all equal to zero if and only if the exponent* $p = 1$.

Proof. This result is deduced from (5.49). The only exponent p that gives zero for the coefficients $b_{2n-1} = 0$ is 1. □

The exception mentioned in Corollary T 5.2.1 corresponds to $W_{0,1}(\mathrm{L}, \Gamma)$ in (5.38). The Everett function of the kind (5.39) has another advantage; it allows the parameters c_p to be identified from the higher harmonics, which will be clarified in Section 6.5.

5.4.1 Fourier Transform

It is possible to express the frequency contents of the Preisach model output derived above in terms of the Fourier transform as well. We consider the case with the Everett function (5.39).

We assume again a single sinusoidal input signal (5.20) with an amplitude inferior to the saturation level (5.21), which gives two different expressions for the output signal (5.6), depending on the the derivative of $u(t)$. Again using the symmetry (5.10), the output signal from the Preisach model in (5.6) can be merged into

$$y(t) = \operatorname{sgn}(-\frac{du}{dt}) \left[y_{U_0} - W(\operatorname{sgn}(-\frac{du}{dt})\, u(t), U_0) \right], \tag{5.50}$$

where the function $sgn(\cdot)$ is defined as

$$\operatorname{sgn}(x) = \begin{cases} 1\,, & x > 0 \\ 0\,, & x = 0 \\ -1\,, & x < 0\,. \end{cases} \tag{5.51}$$

It is now possible to directly apply the Fourier transform on the output:

$$Y(\omega) = \int_{-\infty}^{\infty} y(t)\mathrm{e}^{-j\omega t}\,. \tag{5.52}$$

As noted already in (5.25), the output consists of a part that depends on the output at the input extrema exclusively, $y_A(t)$, and another part that depends on $W(l,\gamma)$, $y_W(t)$. The same subscript is used for their corresponding Fourier transforms:

$$Y(\omega) = Y_A(\omega) - Y_W(\omega) \tag{5.53}$$

The first part $y_A(t)$ is the well known square wave. The Fourier transform for such a square wave is straight forward to calculate and takes the following form:

$$Y_A(\omega) = -j\frac{4y_{U_0}}{\omega}\sum_{k=-\infty}^{\infty}\delta(\frac{\omega}{\omega_0} - 2k + 1) \tag{5.54}$$

where $\delta(\cdot)$ is the Dirac δ-function, c.f. (5.29).

A general expression for the Fourier transform of the second part of the output signal, $y_W(t)$, cannot be retrieved without further information about $W(l,\gamma)$. However, it can be somewhat simplified since the integral can be divided into a sum of partial integrals whose signs are determined by the negative derivative of the input signal, c.f. (5.50),

$$Y_W(\omega) = \sum_{k=-\infty}^{\infty}\Big[-\int_{(2k-1)\frac{\pi}{\omega_0}}^{2k\frac{\pi}{\omega_0}} W(-u(t),U_0)\mathrm{e}^{-j\omega t}dt + \int_{2k\frac{\pi}{\omega_0}}^{(2k+1)\frac{\pi}{\omega_0}} W(u(t),U_0)\mathrm{e}^{-j\omega t}dt\Big] \tag{5.55}$$

and the input signal is half-wave symmetric (5.1). The most general expression of $Y_W(\omega)$ without any assumptions on $W(l,\gamma)$ is expressed by

$$Y_W(\omega) = (1-\mathrm{e}^{j\pi\frac{\omega}{\omega_0}})\sum_{k=-\infty}^{\infty}\int_{2k\frac{\pi}{\omega_0}}^{(2k+1)\frac{\pi}{\omega_0}} W(u(t),U_0)\mathrm{e}^{-j\omega t}dt\,. \tag{5.56}$$

By applying the Everett function (5.39) to this expression, the Fourier transform can be written as a sum of the contribution for each p:

$$Y(\omega) = \sum_{p=1}^{P} c_p\, Y^{(p)}(\omega) \tag{5.57}$$

so that $c_p\, Y^{(p)}(\omega)$ is the contribution from $W_p(\mathrm{L},\Gamma)$. Then the Fourier Transform is obtained by using trigonometric rewriting, applying binomial expansions and some cumbersome calculus, which we summarise in a theorem:

Theorem 5.3. *A classical Preisach model, defined by the polynomial Everett function (5.39) and whose input is a single sinusoid has an output with a Fourier transform that has a contribution from each term in the polynomial according to (5.57). These frequency contributions are separated in a real and imaginary part:*

$$Y^{(p)}(\omega) = c_p\left(\frac{U_0}{C}\right)^p \cdot \left[Y^{(p)}_{Re}(\omega) + j\cdot Y^{(p)}_{Im}(\omega)\right] \tag{5.58}$$

$p\backslash\omega$	ω_0	$3\,\omega_0$	$5\,\omega_0$
1	$(\frac{\pi}{2} + j\,0)/\omega_0$	0	0
2	$(\frac{\pi}{2} - j\,\frac{2}{3})/\omega_0$	$(0 + j\,\frac{2}{15})/\omega_0$	$(0 + j\,\frac{2}{105})/\omega_0$
3	$(\frac{15\pi}{32} - j)/\omega_0$	$(\frac{\pi}{32} + j\,\frac{1}{5})/\omega_0$	$(0 + j\,\frac{1}{35})/\omega_0$
4	$(\frac{7\pi}{16} - j\,\frac{6}{5})/\omega_0$	$(\frac{\pi}{16} + j\,\frac{22}{105})/\omega_0$	$(0 + j\,\frac{2}{45})/\omega_0$
5	$(\frac{105\pi}{256} - j\,\frac{4}{3})/\omega_0$	$(\frac{45\pi}{512} + j\,\frac{4}{21})/\omega_0$	$(\frac{\pi}{512} + j\,\frac{4}{63})/\omega_0$
6	$(\frac{99\pi}{256} - j\,\frac{10}{7})/\omega_0$	$(\frac{55\pi}{512} + j\,\frac{10}{63})/\omega_0$	$(\frac{3\pi}{512} + j\,\frac{94}{1155})/\omega_0$

Table 5.1: Values of the Fourier transform $Y_{Re}^{(p)}(\omega) + j \cdot Y_{Im}^{(p)}(\omega)$ for some frequencies ω and values of p.

and the real and imaginary parts are:

$$Y_{Re}^{(p)}(\omega) = \frac{2\pi}{4^p \omega_0} \sum_{s=0}^{\lfloor (p-1)/2 \rfloor} \binom{2p}{p-2s-1} \times \left[\delta\left(\frac{\omega}{\omega_0} - 2s - 1 \right) + \delta\left(\frac{\omega}{\omega_0} + 2s + 1 \right) \right] \tag{5.59}$$

$$Y_{Im}^{(p)}(\omega) = \left[\left(\binom{2p}{p} \frac{1}{4^{p-1}} - 2 \right) \frac{1}{\omega} + \sum_{s=1}^{\lfloor p/2 \rfloor} \binom{2p}{p-2s} \frac{2}{4^{p-1}} \cdot \frac{\omega}{\omega^2 - (2\omega_0 s)^2} \right] \times \sum_{k=-\infty}^{\infty} \delta\left(\frac{\omega}{\omega_0} - 2k + 1 \right) \tag{5.60}$$

where $\lfloor \cdot \rfloor$ denotes rounding off to the first smaller integer.

Proof. The expansion in (5.57) is a consequence of the linearity of the Fourier transform and that the output from the Preisach model can be expressed linearly with the Everett function, c.f. (4.24), when no memory points are 'wiped out', as when the input signal is oscillating between two values, e.g. for a sinusoid. The continuation of the proof was originally proved by applying the definition of the Fourier transform (5.52), but this is extremely long and tedious. It is better to employ the connection between the Fourier transform $F(\omega)$ and the Fourier coefficients a_k and b_k of the principal frequency ω_0,

$$F(\omega) = \frac{2\pi}{\omega_0} \sum_{k=1}^{\infty} a_k \left(\delta\left(\frac{\omega}{\omega_0} - k \right) + \delta\left(\frac{\omega}{\omega_0} + k \right) \right) - j \cdot b_k \left(\delta\left(\frac{\omega}{\omega_0} - k \right) - \delta\left(\frac{\omega}{\omega_0} + k \right) \right), \tag{5.61}$$

and use the result of Theorem 5.2. The Fourier transform of the model output (5.58)-(5.60) follows directly by introducing the odd harmonic Fourier coefficients of the output (5.48)-(5.49) in (5.61). □

The formula (5.57) reveals the linear relationship between the parameters and all harmonics. An identification of the parameters is thus straight forward, which be enlightened in Section 6.5. Some values of $Y_{Re}^{(p)}(\omega) + j \cdot Y_{Im}^{(p)}(\omega)$ are given in Table 5.1. Note that the output contains only odd harmonics and that some p's do not contribute to all frequencies or only to the imaginary part.

5.5 Frequency Analysis for Differentiated Output

Next, we reflect on how to retrieve the Fourier coefficients for the time-derivative of the output $v(t)$. These may be obtained by continuing in the same manner as in the previous two sections:

by applying the definitions. However, that is unnecessary tedious because the frequency contents of the outputs for the two Everett functions (5.23) and (5.39) are already retrieved and their differentiated versions are closely related. We exploit instead the connection between the Fourier coefficients and the Fourier transform (5.61) and use a standard relationship between a signal and its time-derivative in order to retrieve these coefficients. We state the outcome in a theorem for a general signal and its time-derivative:

Theorem 5.4. *Let a signal $y(t)$ have the principal frequency ω_0 and the Fourier coefficients a_k and b_k. The time-derivative of this signal, $v(t) = dy/dt$, has then the following Fourier coefficients:*

$$\tilde{a}_k = \omega_0 k b_k \tag{5.62}$$

$$\tilde{b}_k = -\omega_0 k a_k \tag{5.63}$$

Proof. Common Fourier analysis tells us that the Fourier transform $V(\omega)$ of the time-derivative is related to the signal's Fourier transform $Y(\omega)$ as

$$V(\omega) = j\omega\, Y(\omega) \tag{5.64}$$

where $j\omega = \sqrt{-1}\omega$. The Fourier coefficients are directly identifiable from this relationship when the transforms are expressed with (5.61). Whence the theorem follows. □

5.6 Filtering of Time-series

Data are often contaminated by noise so that their quality must be enhanced by some filtering technique. The frequency analyses in the previous sections then give useful information. It was made clear that the frequency contents of the output and its differentiated version contain only odd harmonics of the principal input frequency ω_0:

$$Y(\omega) = \sum_{k=0}^{\infty} Y((2k+1)\omega_0)\,, \quad V(\omega) = j\omega Y(\omega)\,, \tag{5.65}$$

where $j\omega$ relates the two Fourier transforms. An example of the output's Fourier transform of a numerical simulation is given in Fig. 5.4(a). This means that in a noisy time-series measurement, these frequencies can be extracted as long as their components are larger than the noise. This greatly enhances the signal to noise ratio. The method to extract the odd harmonics from the signal is by computing the in-phase $y_i(t)$ and quadrature $y_q(t)$ terms of the signal $y(t)$ for a the harmonic frequencies $(2n-1)\cdot\omega_0$ at each time instant, and then reconstructing the signal by adding all desired harmonics. The extraction can for instance be carried out with a numerical lock-in method, which was presented in Section 3.3. The filtered signal is reconstructed by summing all the extracted harmonics in the following manner:

$$y_{odd}(t) = \sum_n y_i(t)\cos((2n-1)\omega_0 t) + y_q(t)\sin((2n-1)\omega_0 t) \tag{5.66}$$

The resulting data $y_{odd}(t)$ can be used to give raw estimates of the weighting functions $w(\mathrm{L},\Gamma)$ and $W(l,\gamma)$. A disadvantage with truncating the sum in (5.65) is, however, that the signal cannot be fully reconstructed, and so it has some anomalies at the singularities, as seen in Fig. 5.4(b).

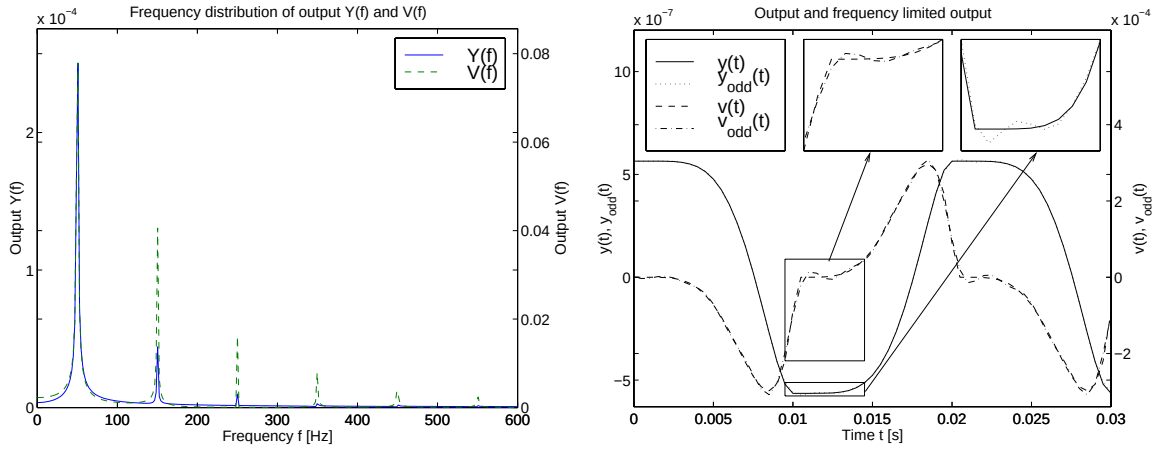

(a) (b)

Figure 5.4: (a) Digital Fourier transform of simulated output from the Preisach model. The output $y(t)$ and $v(t)$ contain frequencies at all odd and only at odd harmonics of the fundamental input frequency, here 50 Hz. (b) Outputs $y(t)$ and $v(t)$ from a simulation of the Preisach model in time domain. The solid and dashed lines present correct outputs, whereas higher harmonics have been removed in the dotted and dash-dotted lines, resulting in incomplete reconstruction, as seen in the enlargements.

5.7 Chapter Summary

The chapter started by giving a review of half-wave symmetric signals and how these contain only odd harmonics of the principal frequency. It continued to derive the sufficient and necessary conditions on a Preisach model in order to produce a half-wave symmetric output, which then only contains odd harmonics. The result is that the model output is half-wave symmetric when the Preisach model complies to the symmetry relation for the Preisach function (and so also the Everett function)

$$W(l,\gamma) = W(-\gamma,-l) \quad \text{and} \quad w(\mathrm{L},\Gamma) = w(-\Gamma,-\mathrm{L}) \tag{5.67}$$

and the input is monotonic half-wave symmetric with no direct term. The output may then also have a direct term (offset), which is history-dependent. Furthermore, the model output also complies to the half-wave symmetry when the monotonic half-wave symmetric input has an arbitrary direct term and the Preisach function (or the Everett function) depends on the difference of its arguments:

$$w(\mathrm{L},\Gamma) = w(\Gamma-\mathrm{L}) \quad \text{or} \quad W(\mathrm{L},\Gamma) = W(\Gamma-\mathrm{L})\,. \tag{5.68}$$

A frequency analysis of the output was then carried out in assuming a polynomial Everett function that complies to the symmetry relation (5.67). Such an Everett function includes a large class of functions via MacLaurin-series. Its Fourier coefficients are given in Theorem 5.1, which tells that all odd harmonics are present, except in a few certain cases. An analogous computation of the Fourier coefficients for an Everett function (5.68). The result may be found in Theorem 5.2. Noteworthy is that the Fourier coefficients are directly proportional to the free parameters in the assumed polynomial Everett functions. An estimation of the parameters from e.g. a measurement of harmonics is therefore straightforward. The relationship between the Fourier transform and the Fourier coefficients has been reviewed in order to express the frequency contents with the Fourier transform (Theorem 5.3). This relationship also allows

to easily retrieve the Fourier coefficients for the time-derivative of the model output. The connection between the frequency contents of a signal and its differentiated version is summarised in Theorem 5.4.

Knowing that the output signal contains only odd and all odd harmonics of the principal frequency may be used to enhance its quality. Measurements are never free from noise, so filtering the signal by extracting the odd harmonics above the noise level gives a better appearance. However, the signal cannot be fully reconstructed when all harmonics are not retrieved, so small discrepancies may be observed.

The contents of this chapter are unique, which had never been presented in a scientific journal before the articles [SD98] and [Sjö99]. All the contents are contributed by the author of this thesis, except for the standard frequency analysis relationships.

Chapter 6

Parameterised Preisach Model

Here we present a parameterised version of the Preisach model which enables a modelling of an HTS tape under certain conditions. The Preisach or Everett functions, $w(\mathrm{L},\Gamma)$ or $W(l,\gamma)$, can generally be identified from first order transition curves [May91], but this is tedious and in some cases not applicable, so some alternative methods are suggested here. The parameterisation allows us to identify the model from electric measurements on the HTS tape. A number of identification methods from different kinds of measurements have been developed.

The Preisach model is here applied to a certain scenario, so the quantities that were earlier called input $u(t)$ and output $y(t)$ now take physical meaning: the input signal in this application is a current $i(t)$ ($u(t)$) (notation in the former chapters are in parenthesis), which is often a sinusoid with amplitude I_0 (U_0). The output from the Preisach model is then a flux $\Phi(t)$ ($y(t)$), which means that the differentiated output corresponds to the measured voltage $v(t)$ ($v(t)$). The classical Preisach Model then looks as follows:

$$\Phi(t) = \iint_{\mathrm{L}\leq\Gamma} w(\mathrm{L},\Gamma)\mathbf{R}_{\mathrm{L}\Gamma}[i(t)]d\Gamma d\mathrm{L}\,, \tag{6.1}$$

$$v(t) = \frac{d\Phi(t)}{dt}\,, \tag{6.2}$$

which of course also may be computed with an Everett function as presented in Section 4.3.

First in this chapter is considered the possibility of using the Preisach model on superconductors followed by a model parametrisation in order to prepare for an identification process. Different identification methods are then presented in the consecutive sections: from time-series, from losses, from higher harmonics. The two last sections consider the inverse model M^{-1} : $\Phi(t) \rightarrow i(t)$ and the saturation of the hysteresis in the HTS as the critical current is approached.

The notational convention in this chapter is the following: a quantity q retrieved from measurement is denoted $\hat{\hat{q}}$ and an estimate of this quantity in a parametric model is written $\hat{q}$.

6.1 Model identification of HT Superconductors

6.1.1 Necessary and Sufficient Conditions (Consequences of Critical State Model)

It was stated in Section 2.8 how the critical state model is a good first approximation of a type-II superconductor in certain cases. We consider here HTSs that are supposed to be within the

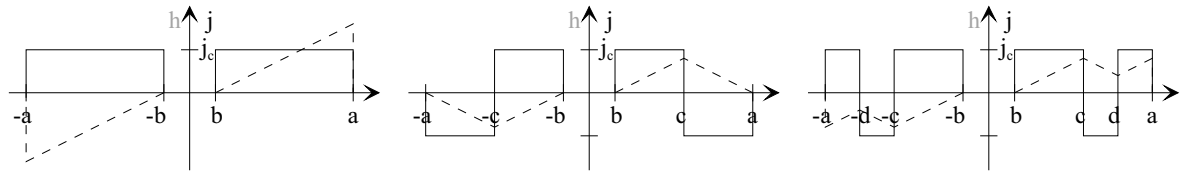

(a) (b) (c)

Figure 6.1: Current and magnetic field distributions for an infinite superconducting slab of width $2a$ for the critical state model. (a) Current distribution for a transport current increased to $I = 2(a-b)\cdot j_c$ from zero current. (b) The flux is pinned inside the superconductor and stays the same until it is forced to change. A front of (negative) current starts penetrating from the edge when the transport current is decreased. (c) An alternating current with decreasing amplitude produces persistent currents of opposite signs in the superconductor. The critical state model possesses the wiping-out and congruency properties of the Preisach model.

limits of these limits. Next, we investigate the properties of the hysteresis exhibited by a material that applies to the critical state model. In order to do so, we examine the evolution of flux and current density of an infinite superconducting slab of width $2a$ with a constant critical current density j_c [A/m] across the slab width when an alternating current runs through it in self-field. First, the current is increased to a value of $I = 2(a-b)\cdot j_c$ by which the current penetrates the HTS from the edges and gives a distribution according to Fig. 6.1(a). The magnetic flux in the superconductor is pinned and so stays there even if the current (and therefore the flux) is decreased again. This means that the innermost position corresponds to a certain maximal current level, which is 'remembered' by the superconductor. The decreased current implies that a current with opposite direction starts to penetrate from the edges, see Fig. 6.1(b). (Note that the total current is zero for the special case in the figure.) If the current increases again from this situation, the last current level (the local minima) is 'remembered' by the pinned flux at position c in Fig. 6.1(c). We see how the local extrema are registered in the 'flux-memory' of the superconductor when the current amplitude is reduced. Hence, there can exist several such persisting currents of opposite directions, if the current's amplitude decreases with alternating signs. This discrete memory of the extrema is characteristic to rate-independent hysteresis.

Let us now look at two different continued evolutions for the transport current and so also for the superconductor memory. Suppose firstly that the current continues to increase. The point d in Fig. 6.1(c) will then maintain its inward movement until it reaches c. At this point, the flux and current distributions are again as in Fig. 6.1(a), i.e. as if the negative persistent current had never existed. The history point c has in this way been wiped out from the history of local extrema of the current. From the above discussion, it is clear that the persisting currents exhibit the wiping out property of the Preisach model [May96]. Secondly, the flux Φ caused by the averaged flux density $B = \int \mu_0 h(x)\,dx$ produces a closed minor loop, if instead the current in Fig. 6.1(c) is reversed until a new negative current front reaches point d and then is increased over again in order to reach the same distribution as in Fig. 6.1(c). Now, the change of the flux $\Delta\Phi$ due to a certain change in current Δi is independent of the persistent currents interior to point d. It is thus understood that back-and-forth variations in the introduced (or induced) current between two values are independent of the layers of persisting currents inner to the maximum of these two values. Therefore, it is clear that the output forms congruent minor loops and the congruency property of the Preisach model holds [May96]. To conclude is that the critical state model possesses the necessary and sufficient properties to be described with the Preisach model. Experimental testing of these propertied has been found to be in good compliance with experimental data [FLK94, MS00].

At present, the tool to investigate these interior persistent currents for superconductors of arbitrary shape is to apply the $E-J$ model in numerical simulations, see Section 2.9. However, this is very time consuming, especially if only the global variables, such as current and voltage, are of interest. The Preisach model can in such circumstances be used with advantage by finding the Preisach function $w(\mathrm{L},\Gamma)$ or the Everett function $W(l,\gamma)$ from experimental data, because the simulations time is decreased considerably. These functions can be found from first-order transition curves [May96] (magnetic measurements), but also from electric measurement as will be shown in Sections 6.3, 6.4 and 6.5. Particularly, once the Everett function is found, the application of the Preisach model allows to find output and losses for an arbitrary input signal.

An important note is that the behaviour of the critical state model can *exactly* be described by the Preisach model. However, the former is in certain cases a first approximation of the behaviour of a superconductor, which means that a full compliance to the critical state model cannot be expected. As a consequence, care must be taken to measured higher harmonics and harmonics predicted from the model, see Section 6.5.5

6.1.2 Weighting Function for Sharp Transition Current Density

The critical state model for a superconductor of arbitrary shape has a sharp transition for the current density, which takes the values $\pm J_c$ only. As a consequence, an absolute change in input current $\Delta i = i_2 - i_1$ implies the same flux difference $\Delta\Phi = \Phi_2 - \Phi_1$, independent of the current amplitude, as long as Δi is small enough in order not to influence points where the current has opposite sign, e.g. the point d should not reach c as the current increases in Fig. 6.1(c). The Everett function for such a case can be investigated by considering the difference of outputs as in (4.24):

$$\Delta\Phi = \Phi_2 - \Phi_1 = W(i_1, i_2) = W(i_1 + c, i_2 + c)\,. \tag{6.3}$$

The last equality must be true for any constant c because the flux change $\Delta\Phi$ depends only on the current difference $i_2 - i_1$. The preceding equation implies that the Everett function $W(\mathrm{L},\Gamma)$ must be constant on any line $\Gamma - \mathrm{L} = C$, C =constant, in the Preisach plane. This means that the Everett function (and therefore the Preisach function) depends only on the differences of their arguments [May98]:

$$W(\mathrm{L},\Gamma) = W(\Gamma - \mathrm{L}) \quad \Leftrightarrow \quad w(\mathrm{L},\Gamma) = w(\Gamma - \mathrm{L}) \tag{6.4}$$

Hence, these functions are one-dimensional. The consequence is that it is no longer necessary to investigate losses for all combinations of input differences in order to identify the Preisach function using (4.31):

$$w(\mathrm{L},\Gamma) = -\frac{1}{\Gamma - \mathrm{L}}\,\frac{\partial^2}{\partial \mathrm{L}\partial\Gamma}\,Q_c(\mathrm{L},\Gamma)\,. \tag{6.5}$$

It suffices to know the losses from a symmetric input current ($i^- = -i^+$) to identify the model for all L and Γ.

6.1.3 Models with Norris' Losses

A general method of calculating the losses in a wire from first principles was presented by Norris [Nor70]. It states that when the input current changes form i^- to i^+ the energy loss in half a cycle per unit length is

$$\frac{Q_c(i^-, i^+)}{2} = \int_{i^-}^{i^+} i\, d\Phi \tag{6.6}$$

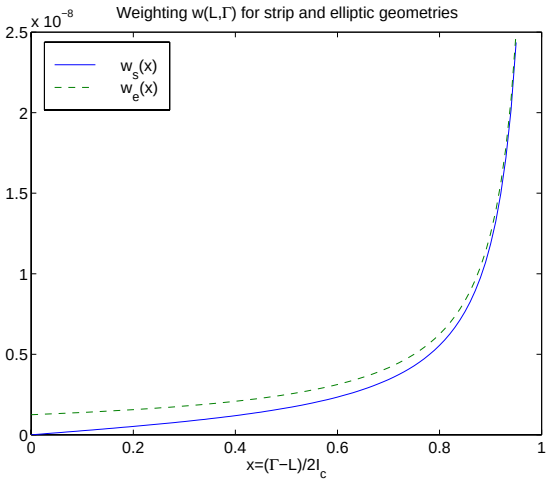

Figure 6.2: Exact weighting functions for the cases of strip and elliptical cross section geometry superconductors. Solid and dotted lines correspond to (6.10) and (6.11), respectively

where i is the current in the wire and Φ is the induced flux. Thus, it is sufficient to know the relationship between the flux and the current to calculate the dissipated energy per cycle. Norris calculated these losses for transport currents in superconductors with strip (index s) and elliptical (index e) cross-sections [Nor70]. When the current varies between i^- and i^+ the cyclic energy losses are, respectively,

$$Q_{c(s)}(i^-, i^+) = \frac{\mu_0 {I_c}^2}{\pi}((1-f)\ln(1-f) + (1+f)\ln(1+f) - f^2) \tag{6.7}$$

$$Q_{c(e)}(i^-, i^+) = \frac{\mu_0 {I_c}^2}{\pi}((1-f)\ln(1-f) + (2-f)\frac{f}{2}) \tag{6.8}$$

$$\text{where} \quad f = \frac{i^+ - i^-}{2I_c} \tag{6.9}$$

where μ_0 is the permeability in free space. The corresponding Preisach functions $w(\mathrm{L}, \Gamma)$ for these two cases are obtained by applying the inverse formula (6.5) [DSD98, SDD00]:

$$w_s(\mathrm{L}, \Gamma) = \frac{\mu_0}{4\pi I_c}\frac{x}{1-x^2}, \tag{6.10}$$

$$w_e(\mathrm{L}, \Gamma) = \frac{\mu_0}{8\pi I_c}\frac{1}{1-x}, \tag{6.11}$$

$$\text{where} \quad x = \frac{\Gamma - \mathrm{L}}{2I_c} \tag{6.12}$$

Fig. 6.2 presents these one-dimensional weighting functions. The models can equally be described by the Everett functions

$$W_s(\mathrm{L}, \Gamma) = \frac{\mu_0 I_c}{2\pi}[(1-x)\ln(1-x) - (1+x)\ln(1+x) + 2x], \tag{6.13}$$

$$W_e(\mathrm{L}, \Gamma) = \frac{\mu_0 I_c}{2\pi}[(1-x)\ln(1-x) + x], \tag{6.14}$$

The above weighting functions $w(\mathrm{L}, \Gamma)$ and $W(\mathrm{L}, \Gamma)$ enable simulations of these two special cases for arbitrary transport currents giving correct flux, voltage and energy losses.

6.2 Parameterisation

We mentioned in Section 4.3 that it is better to use the Everett function $W(\mathrm{L},\Gamma)$ instead of the Preisach function $w(\mathrm{L},\Gamma)$ for implementation reasons. Furthermore, the Everett function can easily include the modelling of a part that is reactive only, as will be clarified in Section 6.4. Therefore, we will mainly be considering $W(\mathrm{L},\Gamma)$.

The exact Everett functions for the cases of strip and elliptic cross-section superconductors given in (6.13) and (6.14) can also be expressed as Maclaurin-series of the variable $x = \frac{\Gamma-\mathrm{L}}{2I_c}$:

$$W_s(\mathrm{L},\Gamma) = \frac{\mu_0 I_c}{\pi} \sum_{p=1}^{\infty} \frac{x^{2p+1}}{(2p+1)2p} \tag{6.15}$$

$$W_e(\mathrm{L},\Gamma) = \frac{\mu_0 I_c}{2\pi} \sum_{p=1}^{\infty} \frac{x^{p+1}}{(p+1)p}\,. \tag{6.16}$$

It should be clear from the above derivation that the variable x (6.12) is a normalised difference of the input variables L and Γ of the Everett function. As the input to the applied Preisach model (6.1) is a current $i(t)$, this variable x is a normalised difference of currents. It is then clear that an input current below the critical current I_c

$$|i(t)| < I_c\,, \tag{6.17}$$

(i.e. full flux and current penetration is not achieved) implies a modulus of x inferior to one

$$|x| = \frac{|\Gamma-\mathrm{L}|}{2I_c} \le \frac{|\Gamma|+|\mathrm{L}|}{2I_c} \le \frac{|i(t)|+|i(t)|}{2I_c} \le 1\,, \tag{6.18}$$

and so a truncation of the series gives small errors, especially far away from $x = 1$. Our approach to parameterise the weighting function then becomes

$$W(\mathrm{L},\Gamma,\theta) = I_c \sum_{p=1}^{P} a_p \left(\frac{\Gamma-\mathrm{L}}{2I_c}\right)^p\,, \tag{6.19}$$

where θ denotes the parameters $[a_1, a_2, \ldots, a_P]$.

It is also possible to select a parameterisation that uses every second term in (6.19), which reflects the sum in (6.15). We have, however, chosen to include all the terms since a parameterisation by every second term has not revealed any advantages in our investigations. Another issue is the number of parameters P that can be chosen freely. A large number assures that the true system can well be fitted in the model set. On the other hand, there might then be some parameters close to zero with minimal influence on the output. We use a method considering the confidence interval of the parameters to select a good P, see Section 6.4. See also Appendix B for estimations with the least square method.

For completion, we express the parameterised Everett function (6.19) in a parameterised Preisach function by applying (4.21), which then takes the form

$$w(\mathrm{L},\Gamma,\theta) = \frac{a_1}{4I_c}\delta\left(\frac{\Gamma-\mathrm{L}}{2I_c}\right) + \frac{1}{4I_c}\sum_{p=2}^{P} a_p\, p(p-1)\left(\frac{\Gamma-\mathrm{L}}{2I_c}\right)^{p-2}\,, \tag{6.20}$$

where $\delta(x)$ is the Dirac function.

6.2.1 Model limits

The parameterised Everett function (6.19) is derived by assuming a subcritical input current (6.17) partly to avoid an infinite response of the weighting function. Now, having the parameterised version, that is no longer necessary, since $W(\mathrm{L},\Gamma,\theta)$ does not take infinite values for bounded L and Γ. Hence, the model does not beak down for currents superior to I_c, which is a desired behaviour. The hysteresis saturation that appear above the critical current is dealt with in Section 6.7. For the time being, we concentrate on a restricted model when saturation has not been reached.

Our approach is to estimate the parameters from different kinds of measurements. The identification from loss measurements has turned out to give the most satisfactory results. Noteworthy is that this estimation method also gives correct outputs: flux $\Phi(t)$ and voltage $v(t)$ (including reactive part). The reason is that the critical state model implies a weighting function that depends on the difference $(\Gamma - \mathrm{L})$, as described in Section 6.1.2.

6.3 Identification from Time-Series

There are several ways to estimate the parameters of the Preisach model with the parameterised Everett function (6.19). Time series of input current and output voltage enable a first estimate of the weighting function that can be used to retrieve the parameters [DSD98, Sjö98]. It is demonstrated in this section that such an estimate has low significance in the higher order parameters (a_p, $p \geq 2$) due to the strong influence of the linear (direct) term that represents the reactive voltage.

An advantage with the parametrisation of the Everett function (6.19) is its linearity in the parameters θ, which means that it can be written as a linear regression

$$W(\mathrm{L},\Gamma,\theta) = \varphi^T(\mathrm{L},\Gamma)\,\theta \tag{6.21}$$

with the regression vector

$$\varphi(\mathrm{L},\Gamma) = \left[\left(\frac{\Gamma-\mathrm{L}}{2I_c}\right), \left(\frac{\Gamma-\mathrm{L}}{2I_c}\right)^2, \ldots, \left(\frac{\Gamma-\mathrm{L}}{2I_c}\right)^P\right]^T. \tag{6.22}$$

The linear regression enables identification of the parameters with the Least Square Error Estimation (LSE) technique, if $W(\mathrm{L},\Gamma)$ can be identified from measurements. A raw estimate of the Everett function can be retrieved by letting a number of sinusoids of different amplitude be used as input current $i(t)$, and then estimate the Everett function from the output flux $\Phi(t)$ or its differentiated version, the voltage $v(t)$. The consecutive measurements use a single sinusoid with a fixed amplitude. The measurement output, the voltage $v(t)$, consists in this way of only odd harmonics. This coincides well with the fact that the Preisach model produces only odd harmonics, which was clarified in Chapter 5. Therefore, the measurement data are firstly filtered from noise by extracting only the odd harmonics by the method described in Section 5.6. The resulting data $v_{odd}(t)$ can then be used to give raw estimates of the weighting functions $w(\mathrm{L},\Gamma)$ and $W(l,\gamma)$. First the voltage must be integrated in order to give the flux $\Phi(t)$, which corresponds to the output of the Preisach model.

$$\Phi(t_2) - \Phi(t_1) = \int_{t_1}^{t_2} v(t)dt \tag{6.23}$$

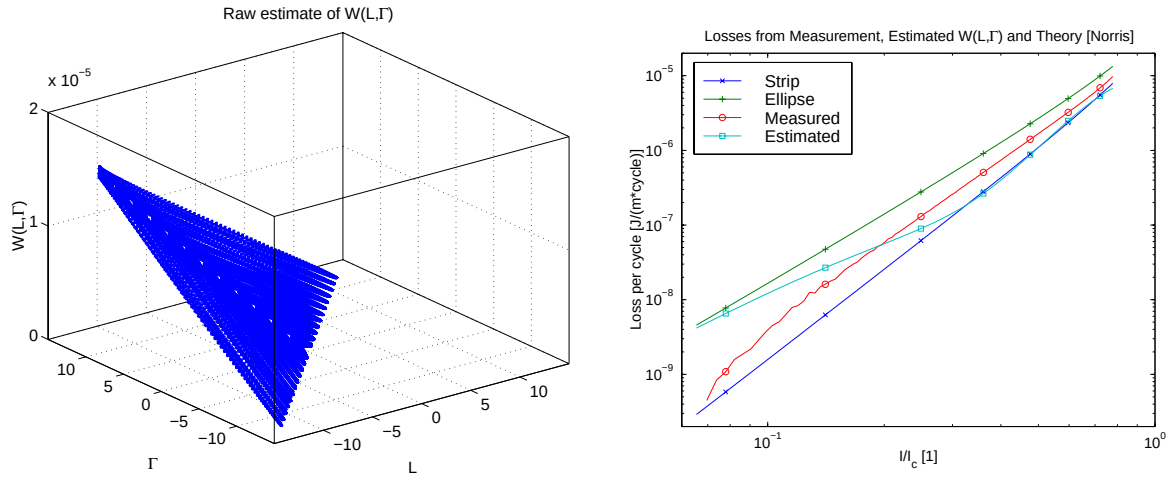

(a) (b)

Figure 6.3: Identification from Time-Series. (a) Raw estimate of the Everett function $W(l,\gamma)$. The linear part of this estimate is dominant. (b) The simulated losses per cycle using the estimated Everett function $W(\mathrm{L},\Gamma,\hat{\theta})$ from time-series does not coincide with measured losses.

The Everett function can then be computed directly by applying formula (4.24), which yields

$$\hat{\hat{W}}(-I_0, i(t)) = \Phi(t) - \Phi(t_{-I_0}) = \int_{t_{-I_0}}^{t} v(\tau)d\tau\,, \quad \frac{di(t)}{dt} > 0 \tag{6.24}$$

and

$$\hat{\hat{W}}(i(t), I_0) = \Phi(t_{I_0}) - \Phi(t) = -\int_{t_{I_0}}^{t} v(\tau)d\tau\,, \quad \frac{di(t)}{dt} < 0\,, \tag{6.25}$$

with an amplitude below the critical current $I_0 < I_c$. Fig. 6.3(a) depicts the result of such an estimation applied to high temperature superconductors [DSD98], where several measurements of different amplitudes I_0 were used to cover many values of the Preisach-plane. The Preisach function $w(\mathrm{L},\Gamma)$ can be computed directly by differentiation (4.21). However, differentiation of a signal containing noise gives an unreliable result, and it is advantageous to use $W(l,\gamma)$ instead of $w(\mathrm{L},\Gamma)$ for time-series, since it is less influenced by the noise, as mentioned in Section 4.3.3

The LSE technique means that the estimated parameters $\hat{\theta}$ are the arguments that minimise the sum of square errors between measured data $\hat{\hat{W}}(\mathrm{L},\Gamma)$ and modelled data $\hat{W}(\mathrm{L},\Gamma,\theta)$ and are calculated as

$$\hat{\theta} = \arg\min_{\theta} \sum_{\mathrm{L},\Gamma} \alpha(\mathrm{L},\Gamma)\,(\hat{\hat{W}}(\mathrm{L},\Gamma) - \varphi^T(\mathrm{L},\Gamma)\,\theta)^2 \tag{6.26}$$

where we also included a possibility to put a weight $\alpha(\mathrm{L},\Gamma)$ to each measured point, see Appendix B. It is seen in Fig. 6.3(a) that $\hat{\hat{W}}(\mathrm{L},\Gamma)$ is fairly linear in $x = \frac{\Gamma-\mathrm{L}}{2I_c}$. Hence, we suspect that higher order parameters are difficult to identify from the time-series data. This can be formalised by considering the parameter variance and carrying out standard statistical tests or by inspecting confidence intervals, c.f. Appendix B. When the confidence interval for a parameter contains zero, we could consider to remove that parameter, since it has no significance for the

Parameter	Estimated value	95% Confidence Interval		
$\hat{a}_1$	$1.176 \cdot 10^{-6}$	$1.160 \cdot 10^{-6}$	$\rightarrow$	$1.193 \cdot 10^{-6}$
$\hat{a}_2$	$0.136 \cdot 10^{-6}$	$-0.136 \cdot 10^{-6}$	$\rightarrow$	$0.408 \cdot 10^{-6}$
$\hat{a}_3$	$-0.487 \cdot 10^{-6}$	$-2.093 \cdot 10^{-6}$	$\rightarrow$	$1.119 \cdot 10^{-6}$
$\hat{a}_4$	$0.825 \cdot 10^{-6}$	$-3.438 \cdot 10^{-6}$	$\rightarrow$	$5.088 \cdot 10^{-6}$
$\hat{a}_5$	$-0.249 \cdot 10^{-6}$	$-5.444 \cdot 10^{-6}$	$\rightarrow$	$4.945 \cdot 10^{-6}$
$\hat{a}_6$	$-0.179 \cdot 10^{-6}$	$-2.542 \cdot 10^{-6}$	$\rightarrow$	$2.184 \cdot 10^{-6}$

Table 6.1: Estimated parameters from time-series measurements and their confidence intervals. The parameters $\hat{a}_p$ identified from time-series measurements have bad statistical significance for $p > 1$. The table presents the estimated values and the calculated 95 % confidence intervals. When the latter includes zero, the parameter has no significance for the model.

Specimen	I	II	III
Critical current I_c [A]	17.86	18.75	24.29
Power-law exponent n	14.17	16.21	22.82
No. filaments	19	1	19
Width w [mm]	2.78	2.75	3.01
Thickness h [mm]	0.30	0.32	0.24
Sheath	Ag	Ag	Ag (4% Au)
Length l_t [m]	0.050	0.050	0.050

Table 6.2: Bi-2223 specimen specification for Identification from Losses.

model. The 95% confidence interval for each of $\hat{a}_p$ for the same specimen as in Fig. 6.3(a) is presented in Table 6.1, showing that all $\hat{a}_p$ for $p > 1$ include zero with a large margin. The estimation of parameters from time-series measurements is therefore insufficient to identify a good parametrised Preisach model, but can be used to retrieve a value of $\hat{a}_1$. We also see in Fig. 6.3(b) that the simulated losses with the estimated weighting function $W(\mathrm{L}, \Gamma, \hat{\theta})$ does not correspond to measured losses.

As conclusion we can say that in the superconducting case above, a large part of the measured voltage is purely inductive and contains no hysteresis which makes the method less useful. This is reflected in the straight slope of the Everett function in Fig. 6.3(a) and corresponds to the Everett function $W_{0,2s-1}(\mathrm{L}, \Gamma) = c_1(\Gamma - \mathrm{L})$ in (5.38).

6.4 Identification from Losses

In this section we present results from measurements on three different Bi-2223 tapes, whose physical parameters are described in Table 6.2. We determine the parameters from loss measurements. Such an estimation makes sense since one of the purposes of the model is to predict hysteretic losses.

6.4.1 Losses

The losses measured with the lock-in technique (3.9) can be used to identify the parameterised Preisach model. First we use the parameterisation in (6.19) to calculate the losses with the

expression for inputs symmetric around zero (4.35). This yields the following formula:

$$Q_c(I_0,\theta) = 2{I_c}^2 \sum_{p=1}^{P} a_p \frac{p-1}{p+1} \left(\frac{I_0}{I_c}\right)^{p+1} . \tag{6.27}$$

Note that the first parameter a_1 has no contribution to the losses, and so it is clear that a_1 cannot be identified from loss measurements. We remark that the parameterised expression for the losses (6.27) is linear in the parameters so that the parameters θ can easily be estimated as the LSE estimate [Lju87]:

$$\hat{\theta} = \arg\min_{\theta} \sum_{I_0} \alpha(I_0)\, \varepsilon^2(I_0,\theta)\,, \tag{6.28}$$

$$\varepsilon(I_0,\theta) = \hat{\hat{Q}}_c(I_0) - Q_c(I_0,\theta)\,, \tag{6.29}$$

where we also include a possibility to weigh each measured point with $\alpha(I_0)$ in the optimisation routine.

The quality of the identification results depends on the number of parameters P and on the chosen estimation weighting $\alpha(I_0)$, where a bad choice can produce bizarre results such as negative simulated losses. It is important with a good correspondence between modelled and measured losses in regions where losses are large, i.e. for large I_0. The error $\varepsilon(I_0,\theta)$ grows quickly with input current amplitude I_0, meaning that larger I_0 naturally get more weight in the estimation procedure (6.28). To achieve a better model for small input currents, the estimation weighting $\alpha(I_0)$ can be chosen to $(I_c/I_0)^2$ or $(I_c/I_0)^3$, where the former approximately corresponds to a weighting with the noise-to-signal ratio (NSR). [Note the contradiction to [DSD98].] The number of parameters P can be decided by conventional methods, e.g. by mean square error with penalty for model complexity or by confidence intervals of estimated parameters [Lju87]. We have chosen to formalise the selection of P by considering the Mean Square Error (MSE) in combination with standard statistical tests on parameter variances, i.e. parameter confidence intervals. The MSE decreases always with increasing number of parameters P [Lju87], so by starting with a small P and successively increasing it until one or several parameter estimates include zero in their confidence intervals [SDD98] is simple and satisfactory method. See also Appendix B.

For the first specimen we used uniform weighting $\alpha(I_0) = 1$ giving $P = 7$. The simulated losses using the estimated Everett function $W(\mathrm{L},\Gamma,\theta)$ have a good agreement with the measured losses, see Fig. 6.4(a). Fig. 6.4(b) and 6.4(c) depict the simulated and measured losses for the other two specimens, each with a P of 9 and 8. For these specimens the weighting $\alpha(I_0)$ was chosen to $(I_c/I_0)^2$ and $(I_c/I_0)^3$, respectively, since these gave the best agreement with the measured losses. Table 6.3 shows the parameter values for the three specimens. We note the differences in their values, which are due to their different constitutions (number of filaments, geometry and I_c) and therefore result in different losses.

6.4.2 Reactive part

We have just concluded that the parameters in the parameterised Preisach model can be identified from loss measurements with one exception, a_1, since it has no contribution to the losses. In fact, it has no contribution to hysteresis, but we show here how it contributes to the reactive part of the output voltage and it can, therefore, also be identified from lock-in measurements.

The technique to estimate the parameter a_1 is to consider the voltage contribution at a phase $\pi/2$ after the input current $i(t)$, which is computed from measurements with (3.10). An

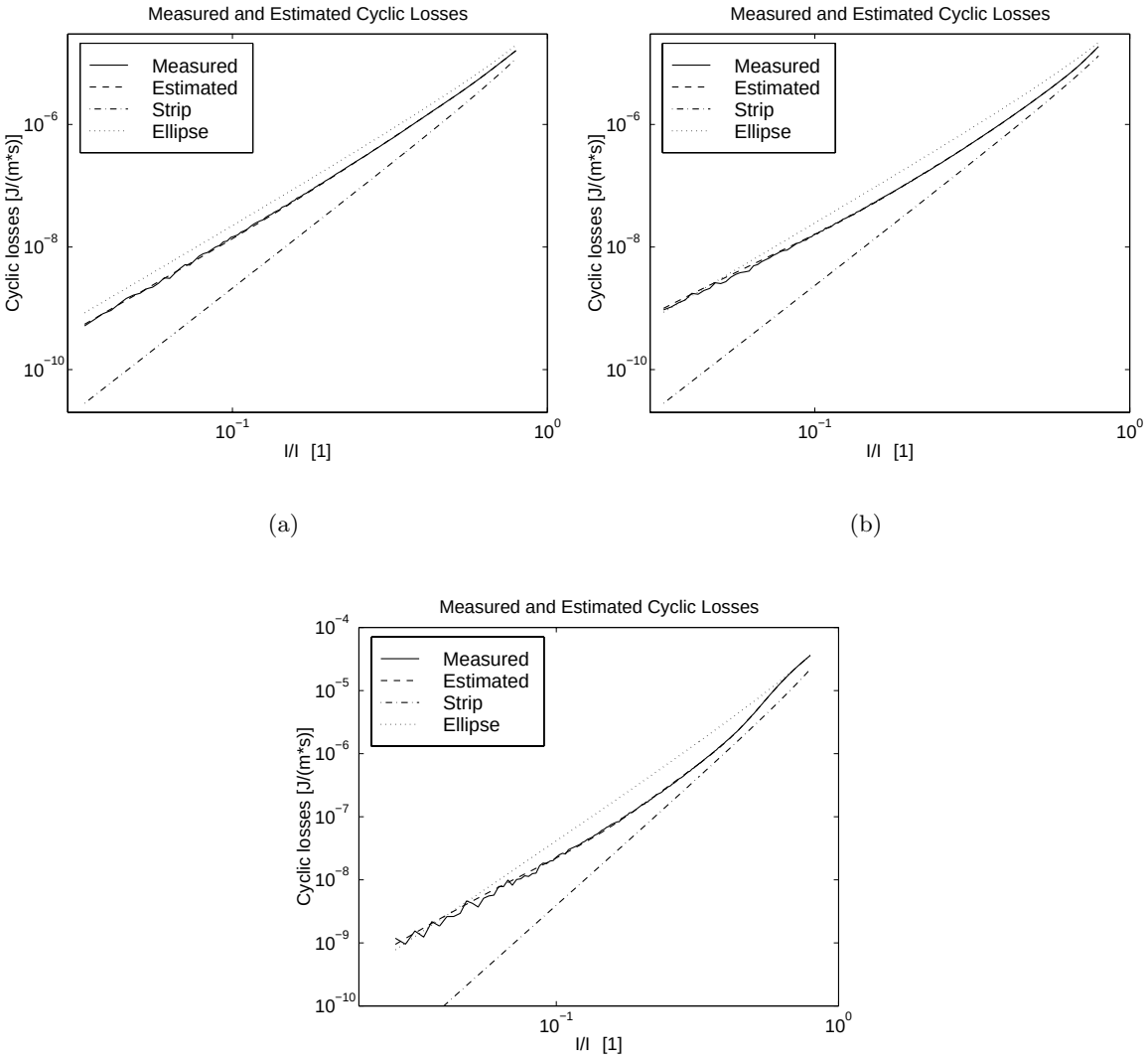

Figure 6.4: Measured (solid) and estimated (dashed) losses per cycle of (a) specimen I, (b) specimen II and (c) specimen III.

expression for the same quantity using the Preisach model is retrieved by taking the derivative of the model output $d\Phi(t)/dt$ when the increasing input current is equal to zero, since that corresponds to where the reactive voltage v_r has its maximum, see Fig. 6.5(a). That corresponds to the time derivative of $W(-I_0, i(t))$:

$$v_r(I_0) = \left.\frac{d\Phi(t)}{dt}\right|_{i(t)=0} = \left.\frac{d}{dt}W(-I_0, i(t))\right|_{i(t)=0} \tag{6.30}$$

When (6.30) is applied to the parameterised Everett function (6.19), the reactive voltage takes

Specimen	I	II	III
$\alpha(I_0)$	1	$(I_c/I_0)^2$	$(I_c/I_0)^3$
P	7	9	8
$\hat{a}_1$	$9.69 \cdot 10^{-7}$	$9.46 \cdot 10^{-7}$	$9.25 \cdot 10^{-7}$
$\hat{a}_2$	$7.11 \cdot 10^{-8}$	$1.78 \cdot 10^{-7}$	$8.91 \cdot 10^{-8}$
$\hat{a}_3$	$-1.32 \cdot 10^{-7}$	$-1.58 \cdot 10^{-6}$	$-8.40 \cdot 10^{-7}$
$\hat{a}_4$	$9.41 \cdot 10^{-7}$	$1.07 \cdot 10^{-5}$	$6.52 \cdot 10^{-6}$
$\hat{a}_5$	$-2.18 \cdot 10^{-6}$	$-4.15 \cdot 10^{-5}$	$-2.45 \cdot 10^{-5}$
$\hat{a}_6$	$2.40 \cdot 10^{-6}$	$9.64 \cdot 10^{-5}$	$4.77 \cdot 10^{-5}$
$\hat{a}_7$	$-9.75 \cdot 10^{-7}$	$-1.31 \cdot 10^{-4}$	$-4.47 \cdot 10^{-5}$
$\hat{a}_8$	–	$9.57 \cdot 10^{-5}$	$1.60 \cdot 10^{-5}$
$\hat{a}_9$	–	$-2.89 \cdot 10^{-5}$	–

Table 6.3: Parameter Values for Specimen

the following expression

$$v_r(I_0,\theta) = \frac{d}{dt} I_c \sum_{p=1}^{P} a_p \left(\frac{I_0 \sin(\omega_0 t) - (-I_0)}{2I_c} \right)^p \Bigg|_{t=0} \tag{6.31}$$

$$= \frac{\omega_0 I_0}{2} \sum_{p=1}^{P} a_p \, p \left(\frac{I_0}{2I_c} \right)^{p-1} , \tag{6.32}$$

and we understand that all the parameters contribute to the reactive amplitude. In principle, we could estimate all the parameters from (6.32), but since a correct hysteretic dissipation has high priority, we insert the parameters identified from losses $\hat{\theta}_Q = [\hat{a}_2, \ldots, \hat{a}_P]$ and retrieve

$$v_r(I_0, [a_1, \hat{\theta}_Q]) = \frac{\omega_0 I_0}{2} a_1 + \frac{\omega_0 I_0}{2} \sum_{p=2}^{P} \hat{a}_p \, p \left(\frac{I_0}{2I_c} \right)^{p-1} \tag{6.33}$$

The formula (6.33) allows us to use the LSE technique to identify the parameter a_1:

$$\hat{a}_1 = \arg\min_{a_1} \sum_{I_0} \alpha(I_0) \left(\hat{\hat{v}}_r(I_0) - v_r(I_0, [a_1, \hat{\theta}_Q]) \right)^2 , \tag{6.34}$$

where $\hat{\hat{v}}_r$ is the reactive part measured according to (3.10). The values of $\hat{a}_1$ for each investigated specimen are given in Table 6.3 The estimated reactive amplitude, using the described method, coincides very well with measured $\hat{\hat{v}}_r(I_0)$, as can be seen in Fig. 6.5(b). The relative error is commonly below 1.5 %. Note that the graph of the reactive amplitude has a slightly nonlinear shape. However, the voltage-currant relationship in Fig. 6.5(b) is almost linear, which is due to the dominant contribution by a_1. The above calculus shows that this parameter describes a linear inductance per unit length,

$$L/l_t \approx a_1/2 \, , \tag{6.35}$$

for the specimen when a_1 dominates the reactive voltage. The inductances obtained in this paper are those measured in the experiments, but we remind the reader that these values are not directly proportional to the specimen length and that they must be computed for each separate geometry. For instance, a tape with thickness h, width w and length l_t has the inductance

$$L = 0.2 \cdot 10^{-6} \, l_t \left[\ln(2 \, l_t \, / (h + w)) + 0.5 - r \right] \tag{6.36}$$

where r ($\lesssim 0.0025$) depends on the ratio h/w [Gro73].

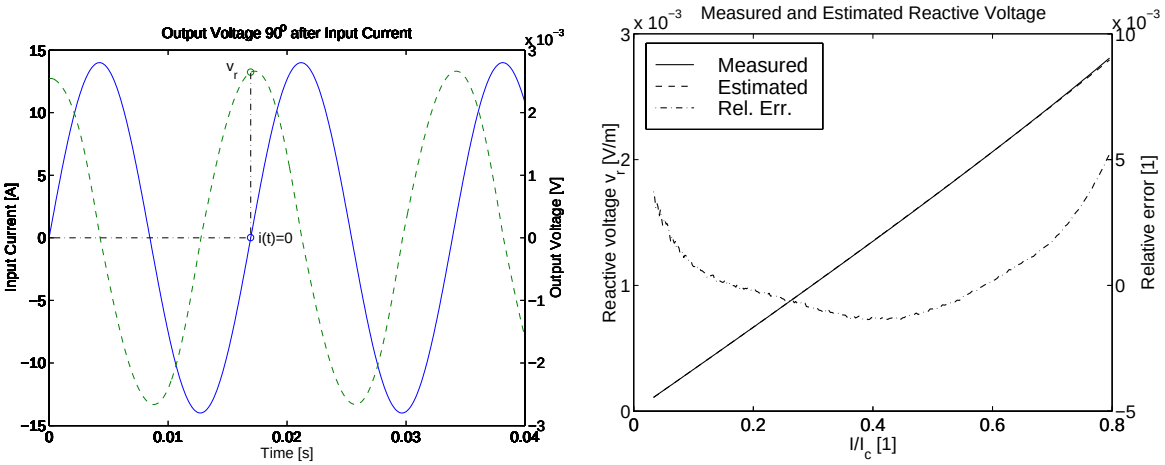

(a) (b)

Figure 6.5: (a) The reactive part of the output voltage (dashed) is at a phase delay of $\pi/2$ after the input current (solid). The amplitude of the reactive part is hence when the increasing current is zero. (b) The estimated reactive amplitude ($\pi/2$ after input current) (dashed) fits very well with measured data (solid) when the parameter a_1 has been used to adjust the output, here for specimen II. Note that the graph is slightly nonlinear c.f. (6.32). The relative error (dash-dotted, right scale) is below 1 % for this parameterisation.

We conclude from the above discussion that a_1 can be used to conform the modelled output to have a correct reactive part. However, the clear sighted reader notices that the linear contribution by a_1 could be modelled separately by

$$\Phi_{a_1}(t) = \frac{L}{l_t}\, i(t) = \frac{a_1}{2}\, i(t)\,. \tag{6.37}$$

The advantage of having this part within the Everett function becomes clear when an inverse model shall be computed as in Section 6.6.

6.4.3 An arbitrary transport current

An advantage with the suggested model is that it predicts flux, voltage and dissipated losses for an arbitrary input current. The specimens, for which models have been identified, have also been measured with an 'arbitrary' transport current, defined in Section 3.2 and again depicted in Fig. 6.6(a). When simulating the voltage using the identified model, we find a good agreement between measured and simulated voltages for all the specimens, see the results for specimen I in Fig. 6.6(a). The figure also shows the voltage due to a pure inductance (i.e. $a_p = 0$, $p \geq 2$) which does not model the output satisfactorily. Note that the 'wiggly' appearance of the curves is due to the fact that the measured current flowing through the specimen is not perfectly following the defined current.

An arbitrary input signal makes the loss measurement for HTS tapes impossible. However, the suggested parameterised Preisach model can predict the losses once the parameters have been identified. The losses between each sample instant $Q_s = P_m/f_s$ (P_m = mean dissipated effect between the samples, f_s = sample frequency) for the three considered HTS specimen are predicted when the 'arbitrary' transport current in Fig. 6.6(a) is applied. These losses are depicted in Fig. 6.6(b) on a relative scale ($Q_s/{I_c}^2$) to be comparative. Note also that the 'arbitrary' current is scaled in such way that its maximum amplitude is $0.8 \cdot I_c$ for each specimen.

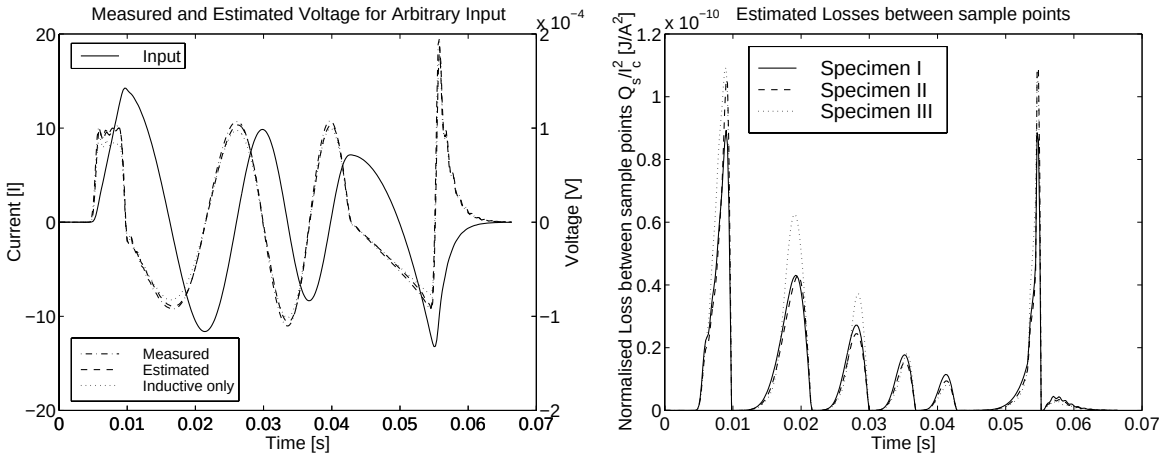

(a) (b)

Figure 6.6: (a) Measured (dash-dotted) and simulated (dashed) output voltage over the length $l_t = 0.05$ m for an 'arbitrary' input current (solid) for specimen I. The dotted curve depicts the voltage induced in a pure inductance (i.e. $a_p = 0$, $p \geq 2$). (b) Predicted losses in the three specimens when the 'arbitrary' input current is applied.

6.5 Identification from Higher Harmonics

6.5.1 Separation of resistive and hysteretic losses

It is well known that nonlinear phenomena produce higher harmonic frequencies (see Chapter 5), which can be measured in experiments (see Section 3.7) and which are not present for linear elements. The idea here is to identify the hysteretic part from higher harmonics and so separate losses from linear and hysteretic elements. First, we consider a model consisting of a hysteretic coil in series with a linear resistor as in Fig. 6.7(a). The total losses per cycle $Q_c^{(tot)}$ are retrieved by measuring the voltage produced over the two elements with the given sinusoidal input current $i(t) = I_0 \cos(\omega_0 t)$:

$$Q_c{}^{(tot)}(I_0) = \frac{\pi I_0 V_1}{\omega_0} \cos(\varphi_1)\,, \tag{6.38}$$

where V_1 is the peak amplitude of the 1st harmonic voltage, φ_1 the phase difference between the 1st harmonic voltage and the input current, and finally ω_0 is the frequency of the input. The hysteretic losses can be computed from (6.27) after the parameters θ have been identified from higher harmonics, and so the resistive losses can be retrieved by subtraction:

$$Q_c{}^{(r)} = Q_c{}^{(tot)} - Q_c{}^{(h)}\,. \tag{6.39}$$

6.5.2 Simulation of Hysteretic Coil and Resistor

Simulations has been carried out according to the model in Fig. 6.7(a) with the following values: $R = 5 \cdot 10^{-7}\Omega$, $I_c = 20$, $\omega_0 = 100\pi$ rad/s, sample time = 0.1 ms, number of samples = 10000, $I_0 = 2 \rightarrow 30$A with step of 2A. The parameter vector θ is given in Table 6.4. A current is led through the hysteretic coil and the resistor, both producing a voltage. The voltage is further corrupted by an additive white Gaussian noise:

$$v(t) = v_h(t) + v_r(t) + n(t)\,. \tag{6.40}$$

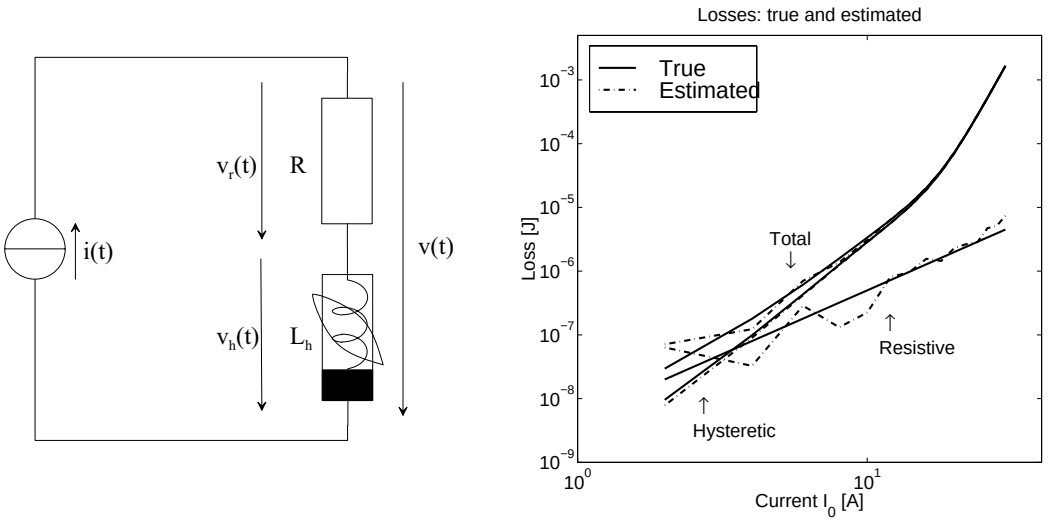

(a) (b)

Figure 6.7: (a) Model consisting of a linear resistor R and a hysteretic coil. The latter is defined by the parameterised Everett function (6.19). (b) True (given by simulation set-up) and estimated losses: total, hysteretic and resistive.

Parameters	Given	Estimated
a_1	$1.184 \cdot 10^{-6}$	–
a_2	$3.660 \cdot 10^{-8}$	$2.620 \cdot 10^{-8}$
a_3	$-6.174 \cdot 10^{-8}$	$-3.201 \cdot 10^{-8}$
a_4	$5.762 \cdot 10^{-7}$	$5.367 \cdot 10^{-7}$
a_5	$-9.545 \cdot 10^{-7}$	$-9.300 \cdot 10^{-7}$
a_6	$5.581 \cdot 10^{-7}$	$5.521 \cdot 10^{-7}$

Table 6.4: Given and estimated parameter values of the hysteretic coil. The first parameter a_1 cannot be estimated from higher harmonics.

The noise is selected such that the signal-to-noise ratio (SNR) is 3 dB at the frequency of the third harmonic for an input current with $I_0 = I_c$, giving a SNR of 28 dB at the principal frequency and -3.7 dB at the fifth harmonic. The amplitude and phase of each harmonic were retrieved by applying the discrete Fourier transform.

6.5.3 Parameter Estimation

A series of simulations with different input amplitudes I_0 gives an over-determined system when applied to the relationship between frequency distribution and parameter values (5.57)–(5.64) in Theorem 5.3 and 5.4. the parameters can thereby be estimated with the LSE method. A direct application of the mentioned equations renders complex estimates of the parameters, $a_p = a_p^{(r)} + j \cdot a_p^{(i)}$. This can be avoided by considering real and imaginary parts separately. However, all parameters do not contribute to $\Phi_{Re}^{(p)}(\omega)$ for all harmonics, so $\Phi_{Im}^{(p)}(\omega)$ must be used to estimate some of the parameters, see Table 5.1. We also understand from that table that the first parameter a_1 cannot be estimated from higher harmonics. The best results from a minimised MSE and parameter variance point of view are obtained by combining real and

imaginary parts in the estimation procedure:

$$\begin{bmatrix}\mathrm{Re}\{V(\omega)\}\\ \mathrm{Im}\{V(\omega)\}\end{bmatrix} = \sum_{p=1}^{P} a_p \begin{bmatrix}\mathrm{Re}\{j\omega\,\Phi^{(p)}(\omega)\}\\ \mathrm{Im}\{j\omega\,\Phi^{(p)}(\omega)\}\end{bmatrix} \tag{6.41}$$

Estimates can in general be improved by increasing the SNR or by including more data, e.g. more simulations of different current amplitudes I_0. Another way to include more data is to consider both third and fifth harmonic voltages. However, it was found that using only the third harmonic gives slightly smaller mean square error for both voltages and losses in most cases. A reason for this can be that the fifth harmonic always has much smaller SNR than the third, also when the noise level is reduced.

The number of parameters P has as in earlier sections been decided by minimising MSE with acceptable confidence intervals of the estimated parameters, see Section 6.4. See also Appendix B. An example of parameter estimates by using real and imaginary parts of the third harmonic according to (6.41) are given in Table 6.4.

6.5.4 Losses

The hysteretic losses computed with (6.27) were found to have a low sensitivity to small errors in the parameter values. Therefore, they are well estimated from identification from the third harmonic voltage, see Fig. 6.7(b). The hysteretic losses must be smaller than the total losses (6.38), which can be applied as a constraint to see the feasibility of the estimation. Estimations of total losses are not so reliable in the simulations, which then influences the resistive losses, see Fig. 6.7(b).

6.5.5 Application to Superconductors

The critical state model suggested by Bean is a first approximation of the electromagnetic behaviour of a type-II superconductor for subcritical currents, as described in Section 2.8. That approximation is particularly good when the superconductor can be described by the $E-J$ model with a large power-law exponent n, since the $E-J$ model equals the critical state model when $n=\infty$, c.f. Section 2.9 and 4.2.3. The power-law exponent can be approximately achieved by DC electric measurements as described in Section 3.1 in order to have a notice of the applicability of the critical state model. It was further demonstrated in Section 6.1 that the critical state model possesses the necessary and sufficient conditions to be described by the Preisach model. Hence, a superconductor that complies with the critical state model as a first approximation can be described by the Preisach model. We note further that an HTS is embedded in a metal sheath, which is due to production methods. Currents may thus also pass through this metal sheath. For multifilamentary superconductors, current may also pass the sheath between the filaments. These currents in the sheath cause resistive losses, either as coupling losses or eddy-current losses, which argues for the model of a hysteretic coil and a resistor (6.40) in Fig. 6.7(a).

A parameterised Preisach model has so been identified from higher harmonics picked up in lock-in measurements on HTS (Bi-2223) tapes by using the technique (6.41). The measured HTSs had power-law exponents between 14 and 25, which can be considered good enough to be represented by the critical state model as first approximation. Whereas the identification procedure works extremely well, the results did not correspond to expectations: the losses produced by the identified Preisach model did not correspond to those measured, which is quite annoying. The explication lies in the fact that higher harmonics are much more sensitive

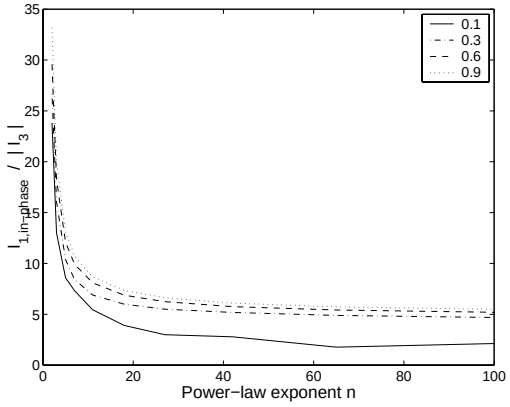

Figure 6.8: Ratio between first harmonic in-phase and third harmonic magnitude of the current produced when applying an electric field across a flat superconductor as a function of the $E-J$ model power-law exponent n. The graphs are given for different maximal normalised current $I_0/I_c = 0.1, 0.3, 0.6, 0.9$.

to the degree of nonlinearity than signals at the fundamental frequency: even if the power-law exponent n is large enough for the superconductor to be represented by the critical state model and hence the Preisach model, the exponent is not large enough to give correct higher harmonics [Yan98]. This fact is demonstrated in a series of $E-J$ model simulations applying the integration method presented in [Bra96a]: a flat superconductor of size (2.2×0.16) mm with a critical current density of $J_c = 100$ kA using different power-law exponents n and current amplitudes is considered. The simulation method does not allow a transport current to be defined, but a sinusoidal voltage can be applied at the ends. The harmonics lies therefore in the current and not in the voltage as for the measurements with the lock-in method in Section 3.3. The ratio between the first harmonic in-phase component and the modulus of the third harmonic of the current is depicted as a function of the power-law exponent n in Fig. 6.8. The different graphs are presented according to their normalised current I_0/I_c, even if it is the voltage that is sinusoidal and therefore may be considered as the reference. In the end, this discrepancy between model and reality means that the identification procedure (6.41) cannot be applied to measurements on superconductors directly, but the higher harmonics can be used to separate losses in the superconductor [MYBH00], as also mentioned in Section 3.7. The so retrieved hysteretic losses can be used to identify a Preisach model according to the identification from losses in Section 6.4.

A question that may arise now is whether the Preisach model can indeed be used to model the hysteretic behaviour of a superconductor. Well, it will not be a perfect model as long as the power-law exponent is finite as observed in this section. However coming back to that the critical state model is often a good first approximation, the Preisach model is equally a good first approximation, even if some care must be taken concerning the higher harmonics it produces.

6.6 Inverse Parametric Model

6.6.1 Current as Function of Voltage

So far we have considered the case when a current source has forced a current through the superconductor and so have produced a voltage drop over it, which is due to the change in flux. In many applications the contrary is done: a voltage is applied to force a current through it. It is therefore desirable to have a model that describes this case as well. The parameterised Preisach model described in this chapter relates the current in the superconductor and the flux

it produces. So in order to describe the inverse model, we must first describe the flux produced by the applied voltage:

$$\Phi(t) = \int_0^t v(\tau)d\tau\,. \tag{6.42}$$

This voltage is only the part that produces a varying flux.

6.6.2 Inverse Everett Function for Non-Saturated Model

We learnt is Section 4.4 that the inverse model is easily obtained if the Everett function only depends on the difference of its arguments $W(\Gamma - \mathrm{L})$. This means that the inverse parameterised model is described by the inverse Everett function. However, in the same section it was understood that such an inverse Everett function cannot be found unless the 'forward' Everett function is indeed described by the difference of its arguments. Hence, it is understood that the inverse Everett function cannot be obtained for an arbitrary Everett function.

Below the critical current, i.e. below any saturation, the inverse Everett function does indeed exists and it can be computed: the inverse of the polynomial (6.19) must be found, which is nothing else but the solution of a polynomial equation of degree P. It is commonly known that a polynomial of degree P has just as many solutions, so the question is which one to choose. The parameterised Everett function (6.19) must be monotone, continuous and odd for an inverse to exist, see Section 4.4. It is therefore clear that $W(\mathrm{L}, \Gamma, \theta)$ must describe a bijective function. Thus, the polynomial equation solution to be use in this case must be real-valued but also *positive* because the parameterised Everett function is in fact only defined for positive values of the argument $x = (\Gamma - \mathrm{L})/2 > 0$, and it is defined as $W(x) := -W(-x)$ for negative arguments $x < 0$, c.f. (A.14). Due to the bijectivity of the function, there exists exactly one such solution, and so the inverse Everett function of the parameterised Preisach model is described by this solution:

$$W_{inv}(\mathrm{L}', \Gamma', \theta) := W^{-1}(\Gamma' - \mathrm{L}', \theta) = 2I_c \underset{x \in \mathrm{Re}^+}{\mathrm{sol}} \left(\sum_{p=1}^{P} a_p\, x^p - \left(\frac{\Gamma' - \mathrm{L}'}{I_c} \right) \right) \tag{6.43}$$

where $sol_x(\cdot)$ means the solution with respect to x for which the argument is zero, and L' and Γ' are the values for down- and up-switching of the relay operators for the input of the inverse model. The inverse Everett function above describes in a direct manner the relationship between the current through the superconductor $i(t)$ and the flux $\Phi(t)$ produced by the applied voltage, c.f. (4.24):

$$i(t_1) - i(t_2) = W_{inv}(\Phi(t_2), \Phi(t_1)) \tag{6.44}$$

6.6.3 Linear Inductance

The advantage of having the linear inductance in the Everett function becomes clear here. The current given by an applied voltage (6.42) can be computed directly by using the Everett function (6.43). If the linear part would be modelled by a separate linear inductance as in (6.37), the following equation would have to be solved for the current $i(t)$ at each time instant:

$$i(t) = \underset{i(t)}{\mathrm{sol}} \left(\frac{a_1\, i(t)}{2} + \Phi_h[i(t)] - \int_{t_0}^{t} v(\tau)d\tau \right) \tag{6.45}$$

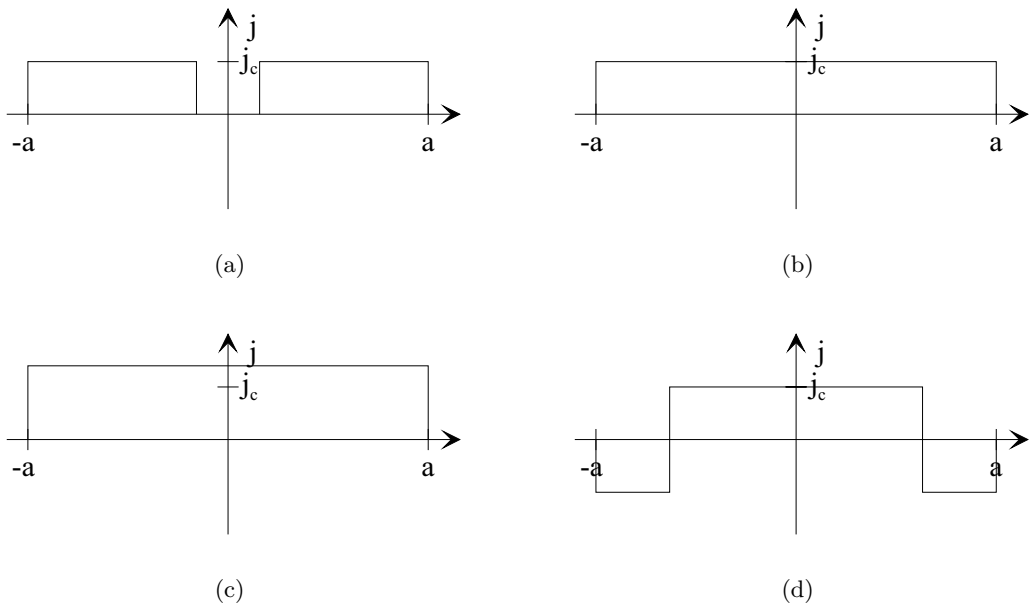

Figure 6.9: Evolution of the current distribution j for a superconducting slab of width $2a$, which complies to the critical state model. (a) A current front enters from the surfaces with a current density equal to the critical current density j_c. (b) The current density is equal to j_c in all the slab at full penetration. (c) If a current larger than the critical current $I_c = 2aj_c$ is forced through the superconductor, the current density increases equally everywhere in the superconductor. (d) The current density decreases again back to j_c everywhere (as in (b)) when the current is decreased to I_c, and then a negative current front starts to penetrate the superconductor from the surfaces.

where $\Phi_h[i(t)]$ is the hysteretic flux modelled with an Everett function as in (6.43) but with a sum starting at $p = 2$. This is obviously much more complicated than using the inverse model described by (6.43) starting at $p = 1$.

6.7 Model with Saturation

One of the prerequisites of the model considered in this chapter so far has been that the input current shall be below the critical current, $I < I_c$. So what happens if the current is increased above this value? Well, first of all, the model in the previous sections is not defined for larger currents than for which it was identified, so non-significant values will be obtained if the input limit is exceeded. It is, however, possible to extend the model to take supercritical currents into account. In order to find such a model, we investigate first how the critical state model behaves for such currents.

6.7.1 Saturation in Critical State Model

We examine again an infinite superconducting slab of width $2a$, through which we force a current. A current distribution front enters the superconductor when the current is increased, just as has been observed before, see Fig. 6.9(a). This is the case until the critical current is attained, i.e. the current density front has fully penetrated to the centre of the slab, by which the superconductor has a current distribution equal to j_c everywhere, as can be observed in Fig. 6.9(b). Now, if the current is further increased above the critical current $I > I_c$, the current density increases *equally* over all the slab width as in Fig. 6.9(c). A decreased current from

this state implies again that the current density is equally reduced everywhere until the critical current is reached. The critical current distribution has then returned to be as in Fig. 6.9(b). From here on the superconductor works as the critical state model presented before: the current density stays at j_c until it is forced to change due to the current front that is entering from the edges of the superconductor, see Fig. 6.9(d). The corresponding behaviour is of course to be found when the superconductor is fully penetrated with a negative current and the current decreases below $-I_c$. This behaviour of the current density fits very well with what is observed in $E-J$ model simulations too.

The illustrated behaviour of the current distribution in the superconductor makes it clear that it has a reversible behaviour above the critical current. Furthermore, the memory effect of persistent currents exists only for current amplitudes below the critical current. It is thus understood that the superconductor reaches a saturation as the current amplitude surpasses the critical current. In the reversible part above I_c, the flux vortices in the superconductor start to move because the Lorenz force exceeds the pinning force. One talks about flux creep or flux flow depending on the speed of their movement. The moving flux produces an electric field in the superconductor, which corresponds to a nonlinear resistivity. Inductive measurements (see Section 3.6) have also shown that there is no loss contribution (possible eddy currents in the sheath apart) due to changes in flux above the critical current. The nonlinear behaviour for supercritical currents can therefore be described by a nonlinear resistivity. However, the reversible part of the flux above I_c has still a linear part described by the linear inductance L_0.

6.7.2 General Smooth Saturation

The saturation of a hysteresis modelled by the Preisach model has a Preisach function $w_s(\mathrm{L},\Gamma)$ that is zero above some saturation level of the input, c.f. (4.27). A possible way to enforce the saturation to an arbitrary Preisach function $w(\mathrm{L},\Gamma)$ is to multiply it with a limiting function $l(\cdot)$. This function then forces the Preisach function to be zero for currents I larger than a saturation current I_s, which is often equal or close to I_c for the application to superconductors:

$$w_s(\mathrm{L},\Gamma) = w(\mathrm{L},\Gamma)\cdot l(s\cdot(\mathrm{L}+I_s))\cdot l((-s)\cdot(\Gamma-I_s)) \tag{6.46}$$

The saturation speed parameter s can be used to produce a more or less fast saturation for some smooth limiting functions, i.e. a large speed parameter implies an abrupt change from one to zero of the limiting function, whereas an s close to zero means that the transition is widespread.

The simplest of such limiting functions is the step function (5.33):

$$l_s(x) = s(x) = \begin{cases} 1\,, & x \geq 0 \\ 0\,, & x < 0\,. \end{cases} \tag{6.47}$$

This is a non-smooth limiting function, i.e. it produces an abrupt saturation, which means that the saturation speed parameter s has no influence. Other limiting functions that possess a smooth transition to the saturation are for instance the logarithmic sigmoid,

$$l_\sigma(x) = (1+\mathrm{e}^{-x})^{-1} \tag{6.48}$$

and the integrated B-spline function of arbitrary order n (arbitrary smoothness),

$$l_{\beta^n}(x) = \int_{-\infty}^{x} \beta^n(y)\,dy = \int_{-\infty}^{x} \frac{1}{n!}\sum_{k=0}^{n+1}\binom{n+1}{k}(-1)^k\left(y-k+\frac{n+1}{2}\right)_+^n dy\,. \tag{6.49}$$

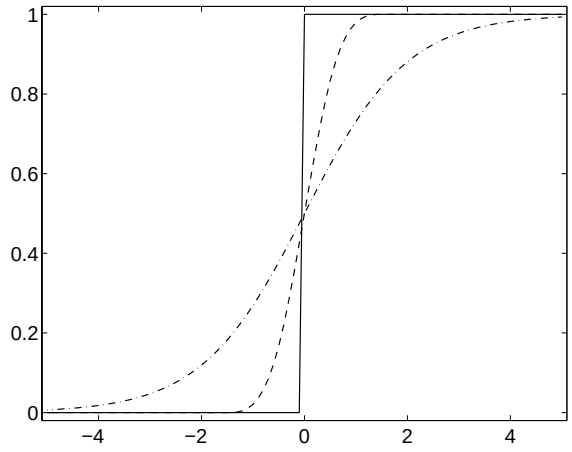

Figure 6.10: Limiting functions: step function (solid), logarithmic sigmoid (dash-dotted) and β^2-spline sigmoid (dashed). Here $s = 1$.

The notation $(\cdot)_+^n$ means the one-sided power function, that is, $(x)_+^n = x^n \cdot s(x)$. (See Fig. 6.10 for a graphical representation of these limiting functions.) The integral in (6.49) can be computed as an infinite sum of shifted splines of order $n+1$, which is due to the fact that the $n+1$ order spline is a convolution of β^0 and β^n. In practice, is suffices often to sum over a limited number of shifted splines:

$$l_{\beta^n}(x) = \sum_{k=0}^{\infty} \beta^{n+1}(x - k - 0.5) \approx \sum_{k=0}^{10} \beta^{n+1}(x - k - 0.5)\,. \tag{6.50}$$

Alternatively, low order B-splines can be computed and expressed explicitly in polynomials as this second order B-spline:

$$l_{\beta^2}(x) = \begin{cases} 0\,, & x < \frac{-3}{2} \\ \frac{(3/2+x)^3}{6}\,, & \frac{-3}{2} \le x < \frac{-1}{2} \\ \frac{1}{2} + \frac{3x}{4} - \frac{x^3}{3}\,, & \frac{-1}{2} \le x < \frac{1}{2} \\ 1 - \frac{(3/2+x)^3}{6}\,, & \frac{1}{2} \le x < \frac{3}{2} \\ 1\,, & x \ge \frac{3}{2} \end{cases} \tag{6.51}$$

It would be desired to express the Everett function analytically for the saturated Preisach model (6.46) with either of these limiting functions. The advantage of doing so is of course that a simulation becomes much faster. It turns out that this is extremely difficult. In fact, there exists no explicit function for the Everett function for neither the logarithmic nor the B-spline sigmoid as limiting function. The step-function is the only one where the Everett function can be found. This may be surprising, especially for the B-spline, which is a combination of polynomials. It is then not difficult to understand that there is no explicit expression for the cyclic losses (4.30) for the saturated Preisach model with these limiting functions. All integrations for the saturated Preisach model must therefore be carried out numerically.

6.7.3 Inverse and Saturation with Prandtl Model

Reminding us the discussion about inverses in Section 4.4 we note that an inverse hysteresis operator of the saturated Preisach model exists with a Preisach memory, as long as the the Preisach function $w_s(\mathrm{L}, \Gamma)$ is odd and non-zero, c.f. Section 4.4.3. This inverse then only exists

Specimen data	
Critical current I_c [A]	16.85
Power-law exponent n	17.41
No. filaments	19
Width w [mm]	2.28
Thickness h [mm]	0.30
Sheath	Ag
Length l_t [m]	0.050

(a)

Estimated parameters	
I_s	16.8575
s	$5.8209 \cdot 10^{-1}$
$\hat{a}_2$	$-9.4478 \cdot 10^{-8}$
$\hat{a}_3$	$2.5608 \cdot 10^{-6}$
$\hat{a}_4$	$-2.0025 \cdot 10^{-5}$
$\hat{a}_5$	$8.9229 \cdot 10^{-5}$
$\hat{a}_6$	$-2.4741 \cdot 10^{-4}$
$\hat{a}_7$	$4.4688 \cdot 10^{-4}$
$\hat{a}_8$	$-5.2704 \cdot 10^{-4}$
$\hat{a}_9$	$3.9227 \cdot 10^{-4}$
$\hat{a}_{10}$	$-1.6956 \cdot 10^{-4}$
$\hat{a}_{11}$	$3.5009 \cdot 10^{-5}$
$\hat{a}_{12}$	$-1.6988 \cdot 10^{-6}$

(b)

Table 6.5: Saturated parameterised Preisach model. (a) Specification of specimen used for identification. (b) Estimated parameter values. The weighting $\alpha(I_0) = 1$ was used for the optimisation process.

below the total saturation. However, the saturated Preisach model described by (6.46) is no longer a function of the difference $(\Gamma - \mathrm{L})$. This means that there exist no Everett function for this inverse of the saturated Preisach model. The exception to this rule is the inverse of the saturated Preisach model that is limited by a step function. An Everett function below the saturation can indeed be found for the inverse of that model, but this is not different from the cases of a restricted model.

This exception leads us to consider a model that uses an Everett function of the form $W(\mathrm{L}, \Gamma) = W(\Gamma - \mathrm{L})$ up to a point beyond the critical current where a saturation has already started, i.e. part of the saturation would be modelled by such an Everett function and then an abrupt saturation would occur above the critical current: $I_s > I_c$. An inverse model would then be utterly easy to obtain as demonstrated in Section 4.4.4 and 6.6. An identification from loss measurements is also straightforward with an parameterised model (6.19) because it uses a linear LSE technique, as been shown in this chapter.

Now, does such a model $W(\mathrm{L}, \Gamma) = W(\Gamma - \mathrm{L})$, which is identified from losses up to and beyond saturation, give correct results? It turns out that a simulation of an identified model produces transition lines in the flux-current (input-output) diagram that cross one another. This is a non-physical behaviour, and this model is therefore not acceptable. This signifies that that the assumption of the sharp transition of critical current density in the superconductor is not satisfied when the saturation is approached.

6.7.4 Identification of Saturated Preisach model from Loss Measurements

Next, it is considered how a saturated Preisach model (6.46) may be identified from loss measurements. The data for the superconductor specimen used in these measurements are specified in Table 6.5(a). We exploit here the inductive measurement method presented in Section 3.6 in order to observe the saturation in the superconductor. It implies that only the hysteretic losses are registered as long as the frequency of the input current is low enough to avoid eddy-current losses in the silver matrix. We use therefore a frequency of $f_0 = 59$ Hz. A saturation of losses

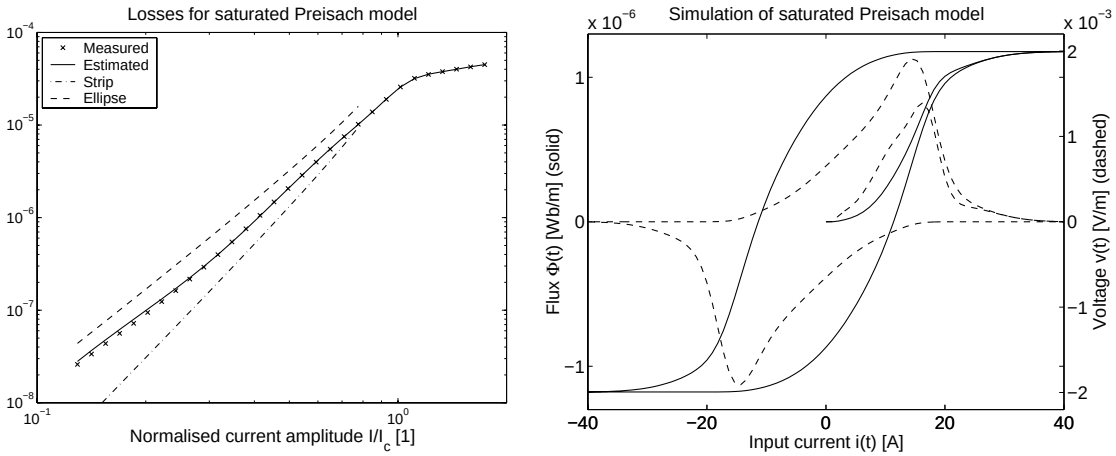

(a) (b)

Figure 6.11: (a) Losses measured with inductive method and estimated with the identified saturated Preisach model (6.46). (b) Simulation of the saturated Preisach model with the estimated parameters. The transition lines do not cross one another, which suggests physically correct model.

is then clearly observed when current amplitude pass the critical current, see Fig. 6.11(a).

The saturated Preisach model applied for this identification process is the parameterised model (6.20) ($n \geq 2$) where the limiting is achieved by the logarithmic sigmoid (6.48):

$$w_s(\mathrm{L}, \Gamma, \theta_s) = w(\mathrm{L}, \Gamma, \theta_Q) \cdot l_\sigma(-s(\Gamma - I_s)) \cdot l_\sigma(s(\mathrm{L} + I_s)) \,. \tag{6.52}$$

In addition to the normal parameters, the saturation limit I_s and its speed s are parameters to be estimated from losses: $\theta_s = [I_s, s, a_2, \cdots, a_P] = [I_s, s, \theta_Q]$. The parameter a_1 is not considered because it does not contribute to the losses; a value of a_1 can be retrieved by applying the estimation method using the reactive part, see Section 6.4.2. This saturation model allows to compute the cyclic hysteresis losses according to (4.30):

$$Q_c{}^{(s)}(I_0, \theta_s) = \iint\limits_{T(-I_0, I_0)} w_s(\mathrm{L}, \Gamma, \theta_s)(\Gamma - \mathrm{L}) d\Gamma d\mathrm{L} \,, \tag{6.53}$$

which makes it possible to estimate the parameters θ_s by minimising the square error to the measured losses $\hat{\hat{Q}}_c(I_0)$ by employing a nonlinear LSE optimisation routine:

$$\hat{\theta}_s = \arg\min_{\theta_s} \sum_{I_0} \alpha(I_0) \left(\hat{\hat{Q}}_c(I_0) - Q_c{}^{(s)}(I_0, \theta_s) \right)^2 \,. \tag{6.54}$$

The identification of the number of parameters P can as before be established with a combination of MSE and parameter variances.

The saturated Preisach model has been identified by applying this method, where a good agreement with measured losses was obtained, see Fig. 6.11(a). The estimated parameters $\hat{\theta}_s$ that gives those results are given in Table 6.5(b). A simulation of the output flux and voltage for a sinusoidal current starting at zero with the identified model is presented in Fig. 6.11(b), where the smooth saturation is clearly noticed. Furthermore, the transition curves do not cross in this simulation, contrary to what has been observed for the saturation with the Prandtl model. This suggests that the saturated model (6.52) better represents a correct model from a physical point of view.

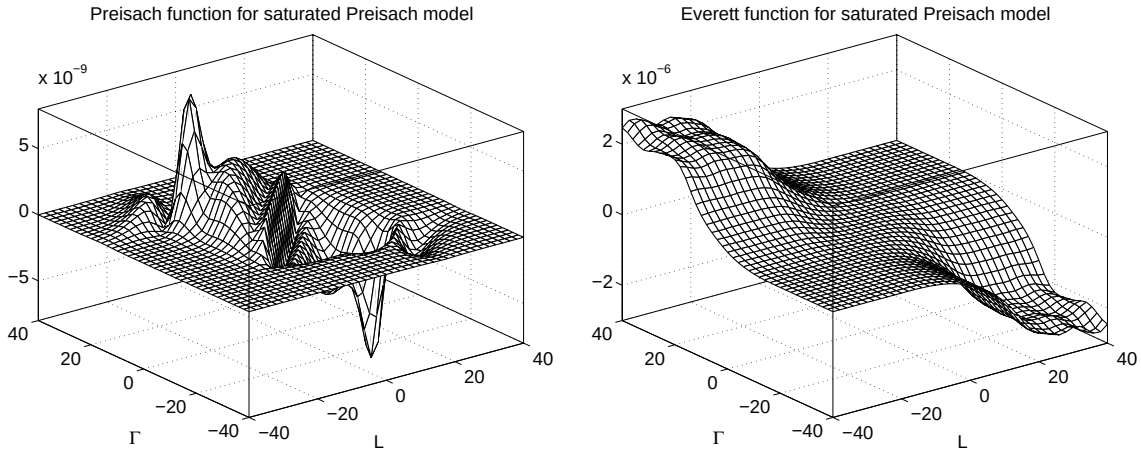

(a) (b)

Figure 6.12: (a) Preisach function of the identified saturated Preisach model. (a) Everett function of the identified saturated Preisach model.

Procedure of Parameter Estimation

The estimation process (6.54) must employ an iterative nonlinear LSE optimisation technique [CBG99] because the parameters cannot be written as a linear regression, which was possible for the identification processes presented earlier in this chapter. It is therefore not as straightforward to find a good solution as before. Some extra testing and adjustments of identification parameters are most certainly required in order to obtain a satisfactory result. Moreover, the computation of losses must be carried out in numerical integrations. These may first of all be inaccurate if a too coarse method is utilised; second, an accurate method is commonly very time-consuming. It is suggested to avoid a too large number of data (different current amplitudes) in order to make estimation times reasonable.

The iterative nonlinear LSE algorithm starts at a initial value of the parameters and then looks for a better solution along a search direction[1]. The new solution becomes the initial solution for the next iteration, and the process is interrupted when the tolerance of error or tolerance of the parameter vector is achieved. Hence, it is important to choose appropriate tolerances[2]. At some extent, the weighting and tolerance can be interchanged: if the tolerance is set small enough, such that the smallest errors (i.e. at smallest amplitude I_0) are larger than the tolerance, then the weighting has less influence. The weighing has, however, an influence on the result and must be selected appropriately[3] to give good results. Another important aspect is that the two parameters s and I_s are much larger than the others. A re-normalisation of the parameters $a_1, \ldots, a_P$ where made in order to avoid numerical problems in the computation of the search direction. The initial estimate that is used to start the iteration was found by using an identification from losses with no saturation ($I_0 < 0.8I_c$). Hence, no limiting function was applied. The linear LSE technique in (6.28) can thereby be applied. The initial values of saturation parameters where set to $I_s(0) = I_c$ and $s(0) = 0.5$, respectively.

A number of improvements for the identification procedure can be considered. First, the amplitude range does not include a total saturation for the identification made with the data in Fig. 6.11(a), which could lead to poor estimation results of the saturation. Hence, larger

[1] A Levenberg-Marquardt algorithm was used to compute the search direction.
[2] The tolerances used here were $10 \cdot 10^{-10}$ for both error and parameter vector.
[3] A weighting of $\alpha(I_0) = 1$ was used in the estimation procedure.

current amplitudes could be taken into account in order to cover a larger part of the saturation and exploit these data in the parameter estimation. However, thermal aspects may influence measurements with currents that are much larger than the critical current. But any thermal aspects are not comprised in this hysteresis model and such measurements should hence be avoided. Second, the amplitude range does not include very small amplitudes values either, which may be the reason to the strange (wavy) behaviour of the Preisach function close to the origin, see Fig. 6.12(a) However, this strange behaviour of the Preisach model is not reflected in the Everett function, which is due to the smoothing when integrating the Preisach function, see Fig. 6.12(b). The identified saturation model should therefore reproduce a satisfactory result. (The Everett function in the figure has an uneven shape for large values of Γ and small values of L where it should in fact be flat. This is due to problems in the numerical integration process.)

6.8 Chapter Summary

The Preisach model of hysteresis was in this chapter applied to the case of high temperature superconductors, where it relates the hysteretic behaviour of the magnetic flux $\Phi(t)$ as a function of transport current $i(t)$. It was demonstrated that the critical state model complies to the necessary and sufficient conditions to be described by the Preisach model and that a sharp transition current density implies an Everett function of the kind $W(\mathrm{L}, \Gamma) = W(\Gamma - \mathrm{L})$. Models that comply to the losses predicted by Norris were then derived easily.

A parameterised model was then proposed, where its parameterisation is based on the Maclaurin series of Everett functions for the models with Norris' losses. After that, it was shown how the model can be identified from different kinds of measurements. It turned out that the estimation of the parameters is not very reliable from time-series measurements because the linear inductance has a too large influence. Loss measurements are better to utilise in order to identify the model, which was made obvious by estimating the parameters for three different superconducting specimens. The linear inductance was also identified by considering the reactive part of the registered voltage. The excellent agreement with measurements were then validated in a comparison between the voltage due to an 'arbitrary' transport current. These models allow also to compute the momentary losses, which are not possible to measure.

Thereafter, it was shown in an invented example how an identification of the Preisach model from higher harmonics permits to separate hysteretic and resistive losses. The hysteretic losses in such an identification are very robust to small deviations in parameter values. The method is, however, not directly applicable to existent superconductors because the higher harmonics change drastically when the transition of the current distribution is not perfectly sharp.

The inverse of the parametric Preisach model was also dealt with, which is the straightforward solution to a polynomial equation. It was pointed out how the inverse is found much easier when the linear inductance is described in the Everett function than in a separate equation.

The hysteresis in a superconductor reaches a saturation when the specimen is fully penetrated, which was explained with the critical state model. A general smooth saturated Preisach model was then established by introducing different kinds of limiting functions. Such a function in combination with the the parameterised Preisach model was then used to identify a saturated hysteresis model from loss measurements with very good results, even if the identification procedure is a bit more complicated. The inverse of a saturated model was also discussed.

The contents of this chapter were founded on the properties of the critical state model, which comply to the necessary and sufficient conditions to be described by the Preisach model [May96]. The parameterisation and its consequences: its identification from different kinds of measure-

ments, its inverse and its saturation (Section 6.2 and onwards) is a unique work provided by the author of this thesis.

Chapter 7

Generalised Equivalent Circuit for Superconductors

A model describing the hysteretic part of a high temperature superconductor for currents up beyond the critical current has been treated in the previous chapters of this thesis, where the superconductor was always considered to be in a superconducting state. We continue here the modelling aspect of a superconductor by dealing with a representation that takes into account also the resistive part as well as a transition to a normal state of the superconductor. A *generalised equivalent circuit* is proposed in this chapter. This model is very wide-ranging in the sense that it may represent a superconductor in many different applications depending on parameter values. A few examples of applications of the circuit are presented.

7.1 Motivation

In many cases, the global behaviour of a superconductor is what interests engineers who are employing superconductivity in different applications. For them, a detailed model, such as FEM-simulations with the $E - J$ model, which produces extremely accurate values of electric and magnetic field as well as current density inside the superconductor, is too cumbersome. Furthermore, the results given by such a model often need extensive simulation time, which is not very appealing. Instead a simple model that produces only global quantities, such as current and voltage (c.f. current density and electric field), would be advantageous if it is accurate enough and speeds up computations compared to FEM simulations. A simple and applicable model must also be general in the sense that it should be adjustable to different material characteristics and to diverse simulation scenarios which may also take into account supercritical values and transitions between superconducting and normal states. The resulting model, as is or reduced, may be a valuable tool for engineers and researchers working with applied superconductivity.

7.2 Electric Circuit

A model that complies to the requirements in the previous section is the *generalised equivalent circuit for a superconductor* that is suggested here. The measurement methods presented in Chapter 3 showed that any voltage can be decomposed in one part that originates in the material's resistivity and another that is due to time-changes in flux according to Maxwell's equations

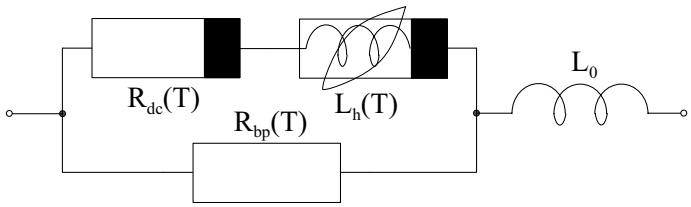

Figure 7.1: Generalised equivalent circuit for a superconductor.

(3.13):

$$v_{tot} = E \cdot l_t + \frac{d\Phi}{dt} = v_r + v_l \,. \tag{7.1}$$

This separation of voltages is indeed recorded in electrical measurements on superconductors (c.f. Section 3.5 and 3.6), which will be discussed more in detail in Section 7.5.1 The equivalent circuit is therefore divided into elements that represent the resistive behaviour and into others that corresponds to its inductive conduct, see Fig. 7.1.

The behaviour of the superconducting material is separated into a *nonlinear resistance* $R_{dc}(T)$ and a *nonlinear inductance* $L_h(T)$, which each deal with the corresponding voltages in (7.1). The former has the index *dc* because it is the behaviour of the superconductor when a direct current flows through the superconductor. The nonlinear inductance is not an inductance in the circuit-theoretic sense [HN86] because it expresses not only the time-dependent relationship between current and flux (implying a voltage), but it may also contain some hysteretic memory, and it so includes a *hysteretic behaviour* with corresponding losses. Hence, its symbol has been complemented with a hysteresis loop. Both of these elements are also temperature dependent.

The resistance $R_{bp}(T)$, in parallel with the two elements characterising the superconductor, represents a by-pass material. The circuit is therefore *natural* in the sense that it describes a superconductor in parallel with an another material, which often occurs in reality. The by-pass material can for instance be a sheath of a superconductive tape or a by-pass of a bulk material. The resistivity in such a by-pass material changes with the temperature and hence also in this equivalent resistance.

The *linear part of the inductance* L_0 that appears in all electric circuits is placed in series with the parallel circuit. This inductance depends only on the shape of the conductor and the current distribution therein. So in fact, it is not completely linear because the current distribution in the superconductor changes with time and current amplitude, c.f. Section 6.7. However, it is left as a normal inductance, since the nonlinearity is minor in many cases.

7.2.1 Models for the Nonlinear Resistance

There are many different approaches to represent a nonlinear resistance. One of the simplest ways is to model it as a piece-wise linear resistance. Other possibilities are piece-wise nonlinear equations that each deal with the behaviour in a certain current, voltage and/or temperature ranges. It is, for instance, common to use the voltage-current power-law (3.1) for small and medium currents, by which the exponent n may take different values for these two current intervals. The critical current and the exponent would also change with the temperature. For large currents and/or large temperatures, the model would turn to a linear but temperature-

dependent resistance. Here we represent such a change for the temperature:

$$R_{dc}(T) = \begin{cases} \frac{V_0}{I_c(T)} \cdot \left| \frac{I}{I_c(T)} \right|^{n(T)-1}, & T < T_c \\ R_{ns}(T), & T \geq T_c \end{cases} \tag{7.2}$$

7.2.2 Models for the Nonlinear Inductance

An inductance with hysteretic behaviour can be modelled in many different ways. This kind of modelling was investigated from a a circuit-theoretic point of view in [CS70, CB72], but the hysteresis models described in Chapter 4 can also be applied for this purpose. For this reason, such models will not be discussed further here.

7.3 Temperature Dependence

The superconductor is temperature dependent, so some kind of temperature modelling must be present in a generalised equivalent circuit. It has already been mentioned in the previous section how the temperature enters the resistance of the superconductor. The temperature dependence is particularly strong when the critical temperature T_c is approached. Furthermore, it is well known that the resistivity of normal conductors are temperature dependent as well, which can be looked up in standard tables. Hence, it is understood that the by-pass resistance must contain a temperature dependency. On the contrary, an inductance depends only on the current distribution and the geometry of the conductor, so L_0 does not change considerably with temperature and is thus modelled as a constant inductance.

Now, the evolution of the temperature is defined by diffusion in the materials and how much power is produced in them. The temperatures can so be modelled in parallel to the electrical equations by applying the Fourier equation (i.e. heat diffusion equation) to each material,

$$c(T)\frac{\partial T}{\partial t} - \frac{\partial}{\partial x}\left(\kappa(T)\frac{\partial T}{\partial x}\right) = P\,, \tag{7.3}$$

and appropriate boundary conditions, which consists of the heat transfer to the cooling environment. The specific heat $c(T)$, the thermal conductivity $\kappa(T)$ and the cooling coefficient to the cooling material $\alpha(T)$ all depend on the temperature. Their relationships to the temperature are not trivial to obtain, so piece-wise linear functions can be used as first approximations. The heat source P is the effect that is released in the material due to its resistivity and the current flowing. The resistivity depends normally on both the temperature and the instantaneous value of the current, which should also enter the diffusion equation (7.3).

In order to simplify the modelling, the temperature can be computed only at the centre of each material and then use this value in supposing that it is uniform throughout each material, when computing the temperature dependence of the different elements. Moreover, the diffusion is only considered in one direction perpendicular to the conductor-plane, i.e the direction where the heat flow is the largest, see Fig. 7.2.

A thin superconductor is very often built on a substrate, which itself is heat conducting. A similar situation is also common for bulk superconductors. Hence, the heat diffusion consists in this situation of two materials, which both are in contact with the cooling media, see Fig. 7.2(a). Some other superconductors are processed in tubes of metals. This is typical for superconducting tapes of Bi-2223 type. Now, for the case when the superconductor is surrounded by a by-pass material in this way, one can make the assumption that the thickness of the surrounding by-pass is equal all around. In this way, the temperature in the by-pass is equal on both sides,

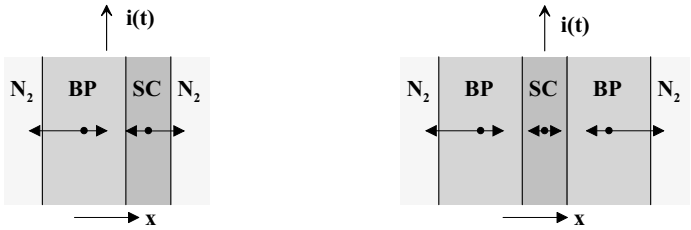

(a) (b)

Figure 7.2: Temperature diffusion is only computed in one direction and for one point per material in order to simplify the model. (a) Superconductor in parallel to a by-pass material (e.g. superconductor on substrate). (b) Superconductor is surrounded by a by-pass material (e.g. superconducting tape or cable).

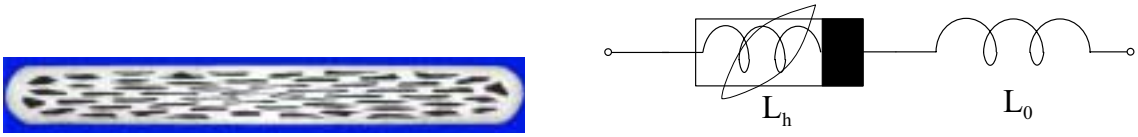

(a) (b)

Figure 7.3: Superconducting tape with subcritical currents and fields can be modelled by a hysteretic and linear inductance, e.g. with the Preisach model. Such a scenario implies that the temperature stays constant and no diffusion equation is necessary. (a) Cut of a multifilamentary superconducting tape. (b) Reduced equivalent circuit.

see Fig. 7.2(b), so that a symmetry in the central point can be enforced. The model of the temperature evolution is thus further simplified.

7.4 Reduced Models

The suggested equivalent circuit model for superconductors is very general and covers many different applications. However for certain applications, some elements of the model can be removed or simplified in order to have a model that is not overly complex. The appropriate simplifications in such a reduced model depend very much on area of model application. A couple of scenarios are portrayed in the following.

7.4.1 Superconducting Tape with Subcritical Current

A superconducting tape of Bi-2223 type immersed in liquid nitrogen remains at constant temperature as long as it is not exposed to excessive currents and/or magnetic field. Therefore, a model of a Bi-2223 tape can be reduced, first of all, from a temperature dependence if the current and magnetic field are kept subcritical, but also the by-pass resistance is not necessary because it is much larger than the nonlinear resistance. A reduced equivalent circuit for the superconducting tape is shown in Fig. 7.3. As has been explained in Chapter 6, this situation has successfully been modelled by L_h and L_0 concerning voltage, flux and losses by applying the Preisach model, where temperature dependence is not necessary.

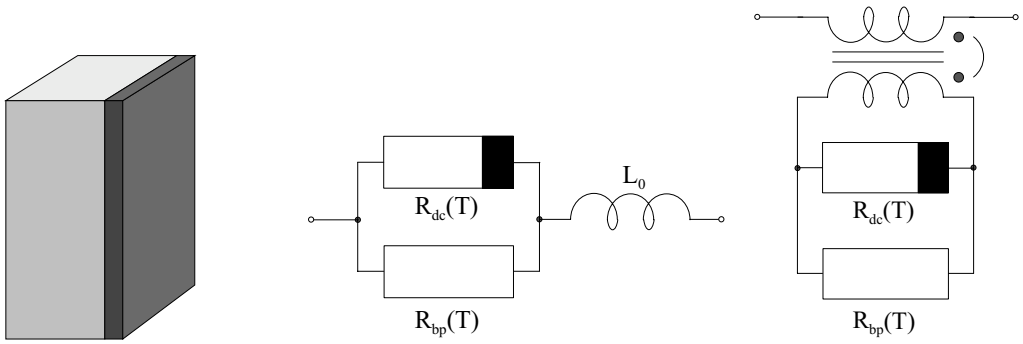

(a) (b) (c)

Figure 7.4: A superconducting bulk material parallel to a by-pass (a) is often used in a superconducting fault current limiter (FCL). A reduced equivalent circuit of a resistive FCL is found in (b). An inductive FCL can be represented by the reduced model on the secondary side of a transformer as in (c).

7.4.2 Superconducting Fault Current Limiter

The voltage-current characteristics of a superconductor can be utilised to construct a so-called fault current limiter (FCL). It is a device that can be introduced in a power system in series with other equipment that needs to be protected against too large currents. Such currents are not uncommon when there is a fault in the system. The superconductor has in principle no voltage drop over it when the current is below the critical current, but as soon as the current surpasses this limit, the resistance in the superconductor increases rapidly. The increased resistance is normally not enough to limit a fault current, but due to the heating of the superconductor, there is a rapid transition from superconducting to normal state. This behaviour improves the current limiting ability.

The superconductor is often processed to be in parallel to a by-pass material when an FCL in produced, see Fig. 7.4. These materials are then configured in different manners in order to build the two major types of superconducting FCLs: resistive and inductive. The former uses the escalated resistance directly in series with the element to be protected, whereas the latter increases the impedance of the system by first transforming the current to an appropriate value and then limit the current in the secondary winding of the transformer. The hysteretic behaviour in the superconductor is not relevant for the application of an FCL, so an equivalent circuit of these types can be as presented in Fig. 7.4.

A simple outline of the parameters required to apply these models is as follows. A superconductor and by-pass of length l is considered, where the cross-sections of the two materials are supposed to be S_{sc} and S_{bp}, respectively. One can further assume a nonlinear resistivity of the superconductor that depends on its temperature T_{sc} and the current-density in the superconductor. This may for instance be a piece-wise nonlinear function as described in Section 7.2.1, which is identified from measurements. The nonlinear resistor R_{dc} normally looks something like the graph in Fig 7.5. For simplicity we suppose an equal current distribution in the materials so that the resistivity depends on the current (not the current density) flowing in the superconductor, $\rho_{sc}(I_{sc}, T_{sc})$. Equally, a resistivity of the by-pass is assumed to be temperature dependent, $\rho_{bp}(T_{bp})$ with an equal current distribution. Ohm's and Kirchhoff's laws then give a

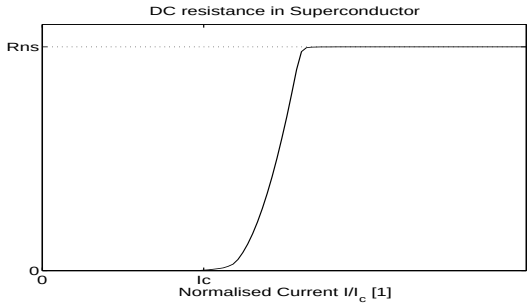

Figure 7.5: Nonlinear DC-resistance in a superconductor (solid).

model as follows:

$$U = \frac{l \cdot \rho_{sc}(I_{sc}, T_{sc})}{S_{sc}} \cdot I_{sc} \tag{7.4}$$

$$U = \frac{l \cdot \rho_{bp}(T_{bp})}{S_{bp}} \cdot I_{bp} \tag{7.5}$$

$$I = I_{sc} + I_{bp}\,, \tag{7.6}$$

where U is the voltage over the parallel linear and nonlinear resistors in the equivalent circuits. The inductance L_0 can be estimated according to conventional methods.

Superconducting FCLs have been simulated with temperature dependent models similar to those presented above [Rei98]. The resistive type FCL using a comparable model to the equivalent circuit in Fig. 7.4(b) was exploited in [SCD99], whereas the inductive type in Fig. 7.4(c) is very similar to the model presented in [PBRP95].

7.5 Full models

We have now looked at some reduced models of the full general equivalent circuit for the superconductors. Those models are appropriate in the described situations. So when should the full model be employed? The answer is a scenario where all aspects of the superconductor represented in the different circuit elements have an impact on the results. Now, the hysteretic behaviour is exhibited for subcritical currents, whereas the nonlinear resistance is mainly observable above the critical current. The temperature dependence enters the equations only when the heating of the superconductor is considerable due to internal losses or imposed external temperature difference. A combination of all these aspects is, for instance, when the current is mainly subcritical but supercritical excursions occur. The hysteretic behaviour is then the normal situation, but the nonlinear resistance with heating as a consequence occurs for the currents above the critical current. Next, two such scenarios will be considered.

7.5.1 Superconducting Tape with Supercritical Current Excursions

We start by investigating the case of a superconducting tape (Fig. 7.3(a)) through which a current with an amplitude up to and beyond the critical current flows. Due to these supercritical excursions, the full generalised equivalent circuit model in Fig. 7.1 is utilised of the reasons mentioned above.

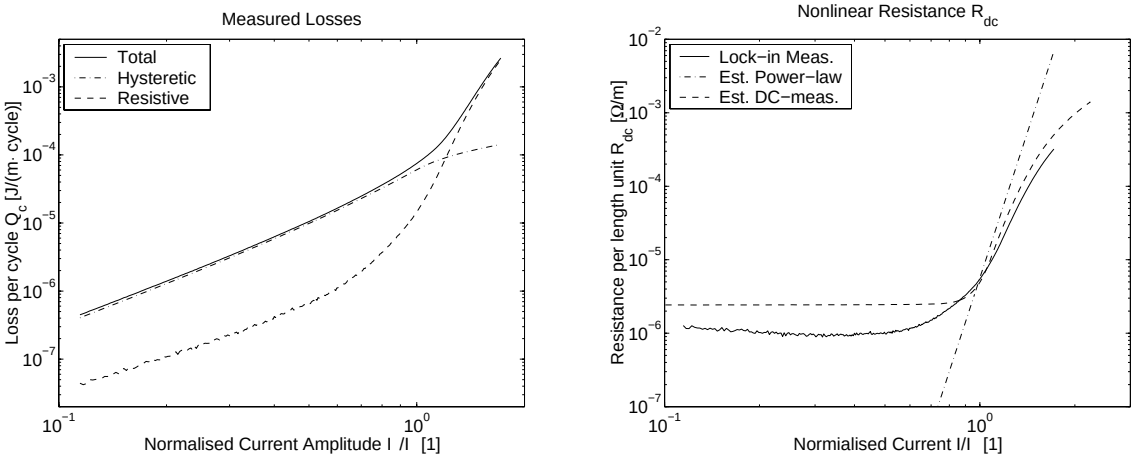

(a) (b)

Figure 7.6: (a) Measured losses with the resistive-inductive and inductive method using the lock-in technique. The resistive losses are obtained by subtracting the hysteretic from the total losses. (b) Estimated nonlinear resistance per unit length R_{dc} from loss and DC measurements as well as the global power-law estimation.

Linear and Hysteretic Inductance

Starting with the linear inductance L_0, this inductance is directly identifiable because the main part of the measured voltage at small current amplitudes are directly caused by this inductance. The quadrature voltage w.r.t. the phase of the current also gives this value for all current amplitudes. Alternatively, a value can also be calculated by using conventional methods and or tables, see for instance (6.36) and [Gro73]. We have also seen in Section 3.6 that the hysteretic losses ${Q_c}^{(h)}$ can be measured by applying the inductive measurement method. Now, under the assumption that the temperature does not change considerably below the critical current[1], the saturated parameterised Preisach model can be employed to describe the hysteretic inductance L_h. This hysteretic model can be identified from loss measurement as pointed out in Section 6.4 and 6.7.

Nonlinear DC Resistance

Turning to the resistances, the resistive losses can be obtained from measurements by deducting the hysteretic losses from the total losses. This is valid as long as the frequency is small enough to avoid eddy-currents, as demonstrated in Section 3.5 and 3.6, see Fig. 7.6(a). Furthermore, the temperature should not change during these measurements in order to know the losses at the certain temperature of the measurements. However, the losses retrieved in this way are the total resistive losses, but we would like to separate these total losses into losses resulting from the nonlinear and linear resistance. In order to identify any resistance from these measurements, it is necessary that the by-pass resistance is dominant for the current amplitudes in the measurements. If so, one can identify R_{dc} from the resistive losses. The value of the nonlinear resistance

[1] A possible temperature dependence of the parameterised Preisach model can be introduced by letting the critical current depend on the temperature, $I_c(T)$. This option has, however, not been investigated in detail, so a clear answer whether this is possible cannot be given at present.

is then deduced from its relationship with the losses, which gives

$$R_{dc}(I_0) = \frac{\omega_0 \cdot {Q_c}^{(r)}(I_0)}{\pi {I_0}^2} \qquad [\Omega/m] \tag{7.7}$$

with the simplification that the effective current is $I_{eff} = I_0/\sqrt{2}$. Under the assumption that R_{bp} is large, the nonlinear resistance is also recorded in DC measurements. The nonlinear resistance normalised per unit length is retrieved by Ohm's law in this case:

$$R_{dc}(I) = \frac{V_{dc}}{I \cdot l_t} \qquad [\Omega/m]\,. \tag{7.8}$$

The data from DC-measurements are also fitted to the global power-law between voltage and current (3.1), so that their relationship is parameterised in the critical current I_c and the exponent n. Taking this fitted global power-law to describe a nonlinear resistance, one obtains the following expression:

$$R_{dc}(I) = \frac{V_0 \cdot I^{n-1}}{{I_c}^n} \qquad [\Omega/m]\,, \tag{7.9}$$

where $V_0 = 1.0\mu$V/cm is the conventional definition of the critical current. Interestingly, it is then possible to express the cyclic losses due to a sinusoidal transport current $i(t) = I_0 \cos(\omega_0 t)$ through the specimen by the following explicit formula:

$${Q_c}^{(r)}(I_0) = \int_0^T u(t)i(t)\,dt = \frac{2\sqrt{\pi} V_0 {I_0}^{n+1}}{\omega_0 {I_c}^n} \cdot \frac{\Gamma(n/2+1)}{\Gamma(n/2+3/2)} \tag{7.10}$$

Sadly enough, the resistance described by the global power-law does not correspond very well to what is measured in the superconductor. This is seen in Fig. 7.6(b), which depicts a comparison of the nonlinear resistances retrieved from lock-in measurements (7.7) with those obtained by the voltage-current relationship in DC-measurements directly (7.8) and via the global power-law (7.9). This comparison shows that all three approaches give similar results around the critical current I_c, but the global power-law does not represent a good description for the rest of the current range. The other two methods are very similar bearing in mind the difficulties there are to determine these small voltages in the measurements. The discrepancy on the upper part of the current axis is more annoying. These could possibly be explained by a heating of the specimen in DC measurements, but also by the use of the simplification of $I_{eff} = I_0/\sqrt{2}$ in identifying R_{dc} from loss-measurements. However, we conclude that the nonlinear DC resistance in series with the hysteretic inductance is found to correspond very well to measurements and is therefore considered as a good model of the superconducting material for the global parameters voltage and current. Now, in order to know the nonlinear resistance's dependence of the temperature, it is necessary to perform several measurements at different temperatures and include that characteristic in the model.

By-pass Resistance

An approximate value of the by-pass resistance can be obtained by consulting Physics tables for standard values, since it is made up of a conventional material. The material's temperature dependence is equally given by such tables, so the by-pass resistance is therefore identifiable with standard tables. The temperatures in all elements evolve, of course, according to the diffusion equation (7.3).

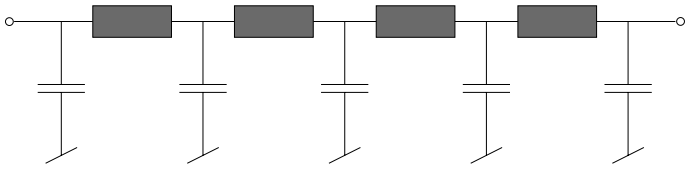

Figure 7.7: Model of superconducting cable with symmetric 3-phase voltages and currents consisting of four so-called π-elements. The grey box consists normally of a resistance and an inductance, but here it is the generalised equivalent circuit for the superconductor.

7.5.2 Superconducting Cable

Next, we turn again to an example in the world of power systems. A superconducting cable is considered from a global perspective, i.e. the voltage, current and possibly losses in the cable should be taken into account in some kind of system study. Supposedly, the cable is not protected for fault-currents that may be supercritical, i.e. the fault currents may surpass the critical current of the cable so that a nonlinear resistance will produce extra heat in the cable. The full general equivalent circuit model in Fig. 7.1 must then be utilised in order to cover all aspects of the superconducting cable's characteristics for the study in question.

Now, it is well known that conventional cables possess a large capacitance relative to ground and to the other phases. It is therefore common to model long cables by a simple capacitance in system studies with symmetric 3-phase voltages and currents. When the cable is shorter or, as here, it has a nonlinear behaviour, a resistance and a inductance are placed between capacitances. Together these constitute so-called π-elements of the cable model. The capacitive load depends only on the geometry of the cable, so the capacitances can be given values as for conventional cable models. In the case of a superconducting cable, the resistance and inductance are due to the superconducting material, so these must be replaced by the generalised equivalent circuit model in Fig. 7.7.

The parameters of the superconductor equivalent circuit can be chosen as follows. First of all, the hysteretic inductance can be disregarded when the value of the linear inductance is selected. The latter should be given a value that correspond to a conventional cable because the inductance depends solely on geometry and current distribution in the cable, and the difference in current distribution to a conventional cable is minor from a global viewing point. The nonlinear DC resistance and the by-pass resistance can be modelled in a similar way as was done for the fault current limiter. Two materials, superconducting and 'normally' conducting, are in parallel so that the voltage drop and the current distribution between the two can be expressed as in (7.4)–(7.6) with different values for the surfaces and lengths. The evolution of the temperature in the cable is also different because the by-pass material surrounds the superconductor, whose modelling was dealt with in Section 7.3.

7.6 Chapter Summary

This chapter has dealt with a generalised equivalent circuit model suggested by the author of this thesis. It describes the behaviour of a superconducting device viewed from an external user, for which the global variables voltage and currents are of interest. The simplicity of the model makes it fast and easy to apply. The suggested equivalent circuit unifies into one generalised model the many different global models of superconductors that can be found in the literature.

This fairly straightforward electric circuit is based on consequences of Maxwell's equations as well as measurements on superconductors and its application devices. The superconducting

material is described by a nonlinear resistance in series with a hysteretic inductance, and a by-pass material is expressed by a resistance in parallel to the two former elements. These elements depend all on their internal temperature, whose evolution is modelled in a heat diffusion equation. Lastly, a conventional inductance is placed in series with the other elements. The separation of the properties of the superconducting material in a nonlinear resistance and a hysteretic inductance has been validated by comparing the nonlinear resistance retrieved from loss measurements (difference between total and hysteretic losses) and DC measurements.

It has been shown how the model can be applied to small scale applications, such as superconducting tapes, and to large scale applications, such as superconducting fault current limiters and cables, where suitable assumptions about resistivity, hysteresis and temperature dependence were made. Depending on the investigated scenario, the model may be used in its complete or in a reduced form.

The suggested equivalent circuit model has so shown to be a good incentive to generalise global models of superconductor devices. However, this research is still very undeveloped and there rest many aspects to be investigated further. Those are for instance to validate the model in all the presented scenarios by comparing the results with measurements, and to identify more scenarios where the model is applicable in its full or reduced form.

Chapter 8

Conclusions

This thesis has presented the basic features of **superconductivity** (i.e. perfect conductivity, perfect diamagnetism and flux quantum), and especially pointed out the pinning of flux tubes as the fundamental reason to *hysteresis* in type-II superconductors, of which high temperature superconductors (HTSs) are extreme cases. It has also been mentioned that motion of these flux tubes produces a *resistive* voltage. Classical micro- and macroscopic models of superconductors have shortly been exposed, in particular the critical state model and its power-law approximation ($E - J$ model). It has been demonstrated how different kinds of electric measurements may be used to characterise a superconducting specimen concerning its magnetic field dependent critical current $I_c(B)$, the power-law exponent $n(B)$ and alternating current losses. The losses may be separated in resistive, hysteretic and eddy-current losses by applying different measurement configurations and investigating *higher harmonics*, which is due to the hysteretic behaviour. A parametric description has been suggested by the author, which expresses the magnetic field dependence of $I_c(B)$ and $n(B)$.

The concept of **hysteresis** has been contemplated, leading to that it is difficult to adopt an exact definition. However, it has been noticed that hysteresis is a nonlinear behaviour due to a persistent memory effect that causes delays and looping with branching after input extrema, which leads to losses. A number of hysteresis models have been presented, with concentration on the classical *Preisach model*. It is a superposition of relay operators weighted by the two-dimensional Preisach function $w(\mathrm{L}, \Gamma)$ or equally represented by the Everett function $W(\mathrm{L}, \Gamma)$.

It has been proven in this thesis that the Preisach model produce *only* **odd harmonics** (i.e. output is half-wave symmetric) for a monotonic half-wave symmetric input without direct term if and only if the symmetry relation $w(\mathrm{L}, \Gamma) = w(-\Gamma, -\mathrm{L})$ applies (Proposition 5.1, p. 58), and when the input includes a direct term, only odd harmonics appear if and only if $w(\mathrm{L}, \Gamma) = w(\mathrm{L} - \Gamma)$ (Proposition 5.2, p. 59). The latter result can be used to identify from measurements that a hysteresis can be described with the simpler 1-dimensional Preisach function $w(\mathrm{L}, \Gamma) = w(\mathrm{L} - \Gamma)$. Furthermore, the frequency contents of the output from the Preisach model have been investigated for a general polynomial Everett function, which includes a large class of functions through MacLaurin-series. It has been proven that *all odd* harmonics are then present in the output signal, except in very special cases (Theorem 5.1, p. 62). This is equally true when the Everett function is a polynomial of the difference $\Gamma - \mathrm{L}$ (Theorem 5.2 and 5.3, p. 64 and 65 resp.). It has also been shown how the frequency contents of the differentiated output can be retrieved with common Fourier analysis (Theorem 5.4, p. 67). An output signal from a hysteresis can thus be *filtered* by extracting all odd harmonics above a certain noise-level. A perfect reconstruction is however not possible without all frequency information.

The critical state model of superconductors possesses the *necessary and sufficient proper-*

ties to be represented by the Preisach model, which hence can represent the hysteresis in all type-II superconductors as long as the flux motion is minimal. Moreover, the sharp transition of current density in the critical state model implies that a 1-dimensional Preisach function $w(\mathrm{L}, \Gamma) = w(\mathrm{L} - \Gamma)$ is applicable, which simplifies the modelling. A **parameterised Preisach model** has been introduced here, which gives a large flexibility in the modelling of superconductors. A limited number of identified parameters so gives an analytical expression of the Preisach function instead of having an immense look-up table, which allows for a faster and more accurate modelling. It has been demonstrated how the parameters can be *identified* from different kinds of measurements. *Time-series measurements* contain a large inductive part, so that higher order parameters have little significance. Excellent results were obtained with lock-in *loss measurements*, where the *reactive part* can also be identified and included in the model. Identification from *higher harmonics* is also possible, through which a separation of resistive and hysteretic losses is obtained. The latter method is, however, not directly applicable to superconductors because the critical state model applies only as a first approximation: the discrepancy in measured and computed data emerges clearly in the higher harmonics. The results of the identifications have been *validated* on three HTS specimen by comparing the measured and predicted voltage due to an 'arbitrary' transport current, which has shown an excellent conformity. An additional advantage of the model is that the losses can be computed for the arbitrary signal, something that cannot be obtained directly in measurements. What is more, it has been shown that the 1-dimensional structure of the Everett function allows for an easy *inversion* of the model so that the current is expressed by an applied voltage. The direct inclusion of the reactive part in the parameterised Preisach model simplifies further the inversion, by which an iterative search for a solution is avoided. It has been established in the thesis that a *saturation of hysteresis* can be modelled by introducing smooth limiting functions in the Preisach models, which may be applied to model the saturation of hysteresis that is observed in measurements at the critical current when flux motion is commenced. It is demonstrated in the thesis that an identification of the parameterised Preisach model with saturation is possible from loss measurements.

An extended model that takes into account the consequences of flux motion has been proposed. This **generalised equivalent circuit** describes the global electric behaviour of the superconductor seen by an external viewer. It is based on the measurement methods discussed in the thesis, which *separates the resistive and inductive behaviour*. The superconducting material is modelled by a hysteretic nonlinear inductance (e.g. the Preisach model) and a nonlinear resistance. There is almost always a 'normal' material in parallel to the superconductor, whose behaviour is expressed by a linear resistor. These three elements may possibly be temperature dependent. Finally, a linear inductance is placed in series. It has been demonstrated in several examples that the equivalent circuit is applicable in many different situation, either in reduced or full description.

We finish with a **comparison** of the parameterised Preisach model with the critical state model and the $E-J$ model, which all three can describe the hysteretic effect in a superconductor. The critical state model can in principle be applied to any material, but complicated geometries makes it difficult to use, and it cannot take flux motion into account. It allows for loss computations, but it might be complicated in general cases, and a voltage source cannot be applied. The $E - J$ model is very general when it comes to materials, flux motion and computation of losses, and it gives the best correspondence with measurements. However, it requires simulations with finite element methods with a superconductor module or an own-developed software for the integration description, which both are time consuming. A voltage or current may be applied depending on the employed equations to be solved. The parameterised Preisach model can be applied to all materials using identification from measurements, and it is fast. The flux motion can be considered by a saturation and the extension with the equivalent circuit. Losses are directly computed and a voltage may be applied using the inverse model.

Appendix A

Preisach Symmetry Description

In this appendix the Preisach Symmetry Description is derived. It has large similarities with the description for a numerical implementation method presented in [May91]. However, it allows a simulation to start with any memory function, whether it be saturated, unsaturated or anything in between. This means that it can also deal with signal surpassing existing memory vertices in the memory function. Furthermore, under the natural assumption of symmetry (4.25),

$$W(l,\gamma) = W(-\gamma,-l) \quad \text{and} \quad w(\mathrm{L},\Gamma) = w(-\Gamma,-\mathrm{L})\,, \tag{A.1}$$

an implementation code can be written very concise when the memory function contains vertices in both upper and lower part of the memory 'staircase', see Fig. A.1(a) (c.f. (A.5)). The implementation description in [May91] only uses the upper bends of the 'staircase', which means that the symmetry description uses more memory but less code.

A.1 Numerical Implementation

The Preisach model can be numerically implemented directly by applying the integral (4.18),

$$y(t) = \frac{1}{2}\iint\limits_{S^+(t)} w(\mathrm{L},\Gamma)d\Gamma d\mathrm{L} - \frac{1}{2}\iint\limits_{S^-(t)} w(\mathrm{L},\Gamma)d\Gamma d\mathrm{L}\,, \tag{A.2}$$

or by using the Everett function $W(l,\gamma)$ in (4.20), c.f. [May91]:

$$W(l,\gamma) := \iint\limits_{T(l,\gamma)} w(\mathrm{L},\Gamma)d\Gamma d\mathrm{L}\,. \tag{A.3}$$

The fact that there is no fundamental difference between an increasing ($du/dt > 0$) or a decreasing input signal ($du/dt < 0$) is used here; it just corresponds to a change of indices. This is used to simplify the model description for a possible implementation. This technique works for both the output signal $y(t)$ and the energetic losses $Q(t)$. A fully demagnetised state where the material has no memory is treated as such, with no approximations when symmetry (A.1) applies. The following simplification of notation is applied:

$$u(t_i) = u_i\,, \qquad y(t_i) = y_i\,. \tag{A.4}$$

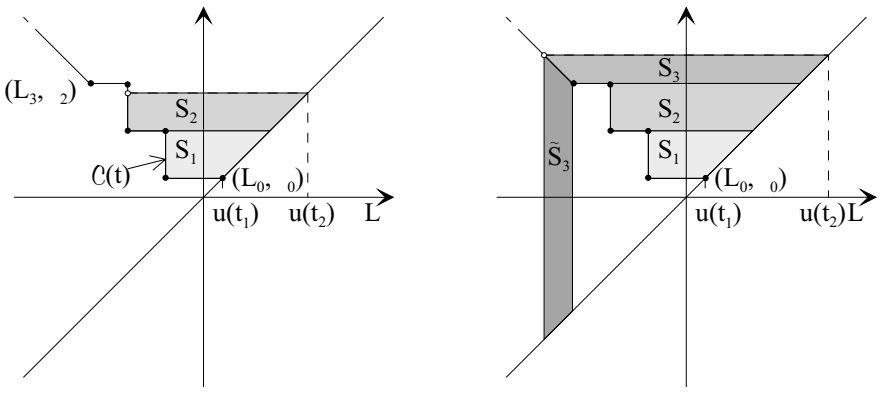

(a) (b)

Figure A.1: The numerical implementation of the Preisach model involves integration of a number of surfaces, Q_k. (a) In the case where there exists a hysteresis memory, these surfaces are differences of triangles, so that the Everett function $W(l,\gamma)$ can be used. (b) When the input signal reaches outside of the memory function $\mathcal{C}(t)$, the integration must be between the lines L=-Γ and L=Γ, i.e. S_3 in the figure. The function $W(l,\gamma)$ can only be used in this case if it is assumed that the integrals over S_3 and $\tilde{S}_3$ are equal, i.e. symmetry applies.

A.2 The Output

First, assume a situation as in Fig. A.1(a) or A.1(b) where the memory function consists of the vertices

$$\mathcal{C}(t) = \{(\mathrm{L}_3,\Gamma_2),(\mathrm{L}_2,\Gamma_2),(\mathrm{L}_2,\Gamma_1),(\mathrm{L}_1,\Gamma_1),(\mathrm{L}_1,\Gamma_0),(\mathrm{L}_0,\Gamma_0)\}. \tag{A.5}$$

The difference of the output at arbitrary times $t_2 > t_1$ is then a sum of integrals over the surfaces S_1 and S_2, or generally:

$$\Delta y_2 = y_2 - y_1 = \sum_{k=1}^{n(t)} \iint_{S_k(t)} w(\mathrm{L},\Gamma)\,d\Gamma\,d\mathrm{L}\,. \tag{A.6}$$

Henceforth, the dependence of time for $n(t)$ and $S_k(t)$ will not be expressed explicitly. The surface S_k is equal to the difference of two triangular surfaces so that the integrals in (A.6) can be calculated as differences of integrals over triangular surfaces. But the values of these integrals were defined to be the Everett function $W(l,\gamma)$, and the expression (A.6) can be simplified to be a sum of differences:

$$\begin{aligned}\Delta y_2 = \sum_{k=1}^{n-1} \Bigg(&\iint_{T(\mathrm{L}_k,\Gamma_k)} w(\mathrm{L},\Gamma)\,d\Gamma\,d\mathrm{L} - \iint_{T(\mathrm{L}_k,\Gamma_{k-1})} w(\mathrm{L},\Gamma)\,d\Gamma\,d\mathrm{L} \Bigg) \\ &+ \iint_{T(\mathrm{L}_n,u_2)} w(\mathrm{L},\Gamma)\,d\Gamma\,d\mathrm{L} - \iint_{T(\mathrm{L}_n,\Gamma_{n-1})} w(\mathrm{L},\Gamma)\,d\Gamma\,d\mathrm{L} \qquad \text{(A.7)} \\ = \sum_{k=1}^{n-1} &\big(W(\mathrm{L}_k,\Gamma_k) - W(\mathrm{L}_k,\Gamma_{k-1})\big) + W(\mathrm{L}_n,u_2) - W(\mathrm{L}_n,\Gamma_{n-1})\,. \qquad \text{(A.8)}\end{aligned}$$

The model is assumed to have a history described by the memory function $\mathcal{C}(t)$ as in (A.5) to come to this result. If the input is increased beyond the last vertex of the memory function, yet

not being saturated, it is here assumed that the material had not yet been 'magnetised', i.e. it has no memory. This means that the last term in (A.6) is an integral over a surface limited by the lines L=Γ and L=-Γ, i.e. S_3 in Fig. A.1(b):

$$\iint_{S_n} w(\mathrm{L},\Gamma)d\Gamma d\mathrm{L} = \int_{\Gamma_n}^{u_2}\int_{-\Gamma}^{\Gamma} w(\mathrm{L},\Gamma)d\mathrm{L}d\Gamma\,. \tag{A.9}$$

This term cannot be expressed with $W(l,\gamma)$ as is, but with the assumption of symmetry (A.1), the two integrals

$$\int_{\Gamma_n}^{u_2}\int_{-\Gamma}^{\Gamma} w(\mathrm{L},\Gamma)d\mathrm{L}d\Gamma \quad \text{and} \quad \int_{u_2}^{\mathrm{L}_n}\int_{\mathrm{L}}^{-\mathrm{L}} w(\mathrm{L},\Gamma)d\Gamma d\mathrm{L}\,, \tag{A.10}$$

i.e. the integrals over the two surfaces S_3 and $\tilde{S}_3$ in Fig. A.1(b), are equal, which means that the sought integral is

$$\iint_{S_n} w(\mathrm{L},\Gamma)d\Gamma d\mathrm{L} = \frac{1}{2}\big(W(-u_2,u_2) - W(\mathrm{L}_n,\Gamma_{n-1})\big)\,. \tag{A.11}$$

This completes the description how to calculate the difference of two outputs for an increasing input signal, and the total formula is given by

$$\begin{aligned}\Delta y_2 &= G(u_1,u_2,\mathcal{C}(t))\\ &= \sum_{k=1}^{n-1}\big(W(\mathrm{L}_k,\Gamma_k) - W(\mathrm{L}_k,\Gamma_{k-1})\big)\\ &\qquad + \begin{cases}\frac{1}{2}\big(W(-u_2,u_2) - W(\mathrm{L}_n,\Gamma_{n-1})\big)\,, & u_2 \text{ beyond last vertex } (\mathrm{L}_n,\Gamma_{n-1})\\ W(\mathrm{L}_n,u_2) - W(\mathrm{L}_n,\Gamma_{n-1})\,, & \text{otherwise}\,,\end{cases}\end{aligned} \tag{A.12}$$

where last vertex refers to the last memory point in $\mathcal{C}(t)$, i.e. the point, beyond which there is no memory, as for (L_3,Γ_2) in fig. A.1.

So far the case when the input is increasing, $du/dt > 0$, has only been considered. With the same reasoning as above, the difference of two outputs with decreasing input, $du/dt < 0$, is

$$\begin{aligned}y_2 - y_1 &= -\sum_{k=1}^{n-1}\big(W(\mathrm{L}_k,\Gamma_k) - W(\mathrm{L}_{k-1},\Gamma_k)\big)\\ &\qquad - \begin{cases}\frac{1}{2}\big(W(u_2,-u_2) - W(\mathrm{L}_{n-1},\Gamma_n)\big)\,, & u_2 \text{ beyond last vertex } (\mathrm{L}_n,\Gamma_{n-1})\\ W(u_2,\Gamma_n) - W(\mathrm{L}_{n-1},\Gamma_n)\,, & \text{otherwise}\,.\end{cases}\end{aligned} \tag{A.13}$$

The similarities between (A.12) and (A.13) are obvious, which can be used to simplify an implementation. First, we need some new relationships to be defined. The lower right part of the Preisach-plane ($\Gamma < \mathrm{L}$) is not used by the Preisach model so far. Therefore it is allowed to define $W(l,\gamma)$ in that region to be the negative function value mirrored in $\mathrm{L} = \Gamma$:

$$W(l,\gamma) := -W(\gamma,l)\,. \tag{A.14}$$

(This implies that $w(\mathrm{L},\Gamma) = -w(\Gamma,\mathrm{L})$.) Further, an alternative memory function $\mathcal{C}'(t)$ is defined to be equal to $\mathcal{C}(t)$, except that the coordinates (L_k,Γ_k) change places. For the example in (A.5) this means

$$\mathcal{C}'(t) = \{(\Gamma_2,\mathrm{L}_3),(\Gamma_2,\mathrm{L}_2),(\Gamma_1,\mathrm{L}_2),(\Gamma_1,\mathrm{L}_1),(\Gamma_0,\mathrm{L}_1),(\Gamma_0,\mathrm{L}_0)\}\,. \tag{A.15}$$

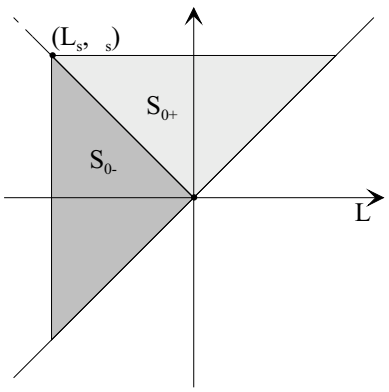

Figure A.2: The starting value y_0 can be chosen to any instant. The fully demagnetised state implies $y_0 = 0$, whereas positive and negative saturation corresponds integration over the surfaces S_{0+} and S_{0-}, respectively.

A general expression for the difference of two outputs then takes the following form:

$$\Delta y_2 = \begin{cases} G(u_1, u_2, \mathcal{C}(t))\,, & du/dt > 0 \\ 0\,, & du/dt = 0 \\ G(u_1, u_2, \mathcal{C}'(t))\,, & du/dt < 0\,. \end{cases} \tag{A.16}$$

The output from the numerical Preisach model is a number of sampled data $y_k = y(t_k)$ whose time instants coincide with the ones of the sampled input $u_k = u(t_k)$. The difference of the output from one time instant to another is calculated according to (A.12) and (A.16), so that the actual output is a sum of these differences

$$y_k = y_0 + \sum_{p=1}^{k} \Delta y_p\,. \tag{A.17}$$

where y_0 is the initial value of the output.

A.2.1 Initial Values

The initial values of output y_0 and input u_0 can be selected to any desired instant, such as demagnetised or saturated state. For the demagnetised state $y_0 = u_0 = 0$, but for the saturated state, y_0 must be calculated. It is then equal to the integral over S_{0+} or S_{0-} in Fig. A.2 for positive and negative saturation, respectively:

$$y_0 = \begin{cases} \int_0^{\Gamma_s} \int_{-\Gamma}^{\Gamma} w(\mathrm{L}, \Gamma) d\mathrm{L} d\Gamma = \frac{1}{2} W(\mathrm{L}_s, \Gamma_s)\,, & \text{pos. sat.} \\ -\int_{\mathrm{L}_s}^{0} \int_{\mathrm{L}}^{-\mathrm{L}} w(\mathrm{L}, \Gamma) d\Gamma d\mathrm{L} = -\frac{1}{2} W(\mathrm{L}_s, \Gamma_s)\,, & \text{neg. sat.} \\ 0\,, & \text{demagn.} \end{cases} \tag{A.18}$$

The expression above makes use of the assumptions that $\mathrm{L}_s = -\Gamma_s$ and that the symmetry (A.1) applies.

A.3 The Differentiated Output

A simple and straightforward estimate of the differentiated output $v(t) = \frac{dy}{dt}$ in this simulation context becomes

$$v_i = \frac{\Delta y_i}{\Delta T} = \Delta y_i \cdot f_s \tag{A.19}$$

if the sampling frequency f_s is large enough. The problem with this implementation is that it produces a timing error: the computed derivative is not in time t but rather in $t + \Delta T/2$. In order to get better results, the values at the sample instant can be computed by means of interpolation:

$$\hat{v}_i = \frac{v_i + v_{i+1}}{2} = \frac{\Delta y_i + \Delta y_{i+1}}{2\Delta T} = \frac{y_i - y_{i-1} + y_{i+1} - y_i}{2\Delta T} = \frac{y_{i+1} - y_{i-1}}{2\Delta T} \tag{A.20}$$

The information about the output signal at time t (y_i) is not used for the differentiation with this method.

A second method is to apply the differentiation directly on the Everett function. First we consider the case when the input derivative is positive $du/dt > 0$. The differentiation is then carried out on the G-function (A.12):

$$v_i = v(t) = \frac{dy(t)}{dt} = \frac{d}{dt}\big(y_{i-1} + G(u_{i-1}, u(t), \mathcal{C}(t))\big) \tag{A.21}$$

$$= \frac{d}{dt}\left(\sum_{k=1}^{n-1}\big(W(\mathrm{L}_k, \Gamma_k) - W(\mathrm{L}_k, \Gamma_{k-1})\big) + \begin{cases} \frac{1}{2}\big(W(-u(t), u(t)) - W(\mathrm{L}_n, \Gamma_{n-1})\big)\,, & u(t) \text{ beyond last vertex } (\mathrm{L}_n, \Gamma_{n-1}) \\ W(\mathrm{L}_n, u(t)) - W(\mathrm{L}_n, \Gamma_{n-1})\,, & \text{otherwise} \end{cases}\right) \tag{A.22}$$

$$= \begin{cases} \frac{1}{2}\left(\frac{\partial W}{\partial \Gamma}(-u(t), u(t)) - \frac{\partial W}{\partial \mathrm{L}}(-u(t), u(t))\right) \cdot \frac{du}{dt}\,, & u(t) \text{ beyond last vertex } (\mathrm{L}_n, \Gamma_{n-1}) \\ \frac{\partial W}{\partial \Gamma}(\mathrm{L}_n, u(t)) \cdot \frac{du}{dt}\,, & \text{otherwise.} \end{cases} \tag{A.23}$$

The problem with this derivation is that when the input passes a vertex of the memory function, i.e. when it is on the limit between two fields in Fig. A.1(b), it is not clear at which point the derivatives $dW/d\mathrm{L}$ and $dW/d\Gamma$ are to be evaluated. A natural alternative is to choose the derivative as the mean of the limits from below and from above. For the case when the input passes to another vertex ($(\mathrm{L}_1, \Gamma_1) \to (\mathrm{L}_2, \Gamma_1)$ in Fig. A.1(b)), the derivative becomes

$$v_i = \frac{1}{2}\left(\lim_{\Delta t \to 0^-} \frac{y(t + \Delta t) - y(t)}{\Delta t} + \lim_{\Delta t \to 0^+} \frac{y(t + \Delta t) - y(t)}{\Delta t}\right) \tag{A.24}$$

$$= \frac{1}{2}\left(\lim_{\Gamma \to \Gamma_1^-} \frac{W(\mathrm{L}_1, \Gamma) - W(\mathrm{L}_1, \Gamma_1)}{\Gamma - \Gamma_1} + \lim_{\Gamma \to \Gamma_1^+} \frac{W(\mathrm{L}_2, \Gamma) - W(\mathrm{L}_2, \Gamma_1)}{\Gamma - \Gamma_1}\right) \cdot \frac{du}{dt} \tag{A.25}$$

$$= \frac{1}{2}\left(\frac{\partial W}{\partial \Gamma}(\mathrm{L}_1, \Gamma_1) + \frac{\partial W}{\partial \Gamma}(\mathrm{L}_2, \Gamma_1)\right) \cdot \frac{du}{dt}\,, \tag{A.26}$$

which is the same as taking the mean of the derivatives in the two point. Commonly, the Everett function is a smooth functions, so the derivative could also be evaluated in a point in between the two vertices, where the middle point would be a natural choice:

$$v_i = \left(\frac{\partial W}{\partial \Gamma}((\mathrm{L}_1 + \mathrm{L}_2)/2, \Gamma_1)\right) \cdot \frac{du}{dt}\,. \tag{A.27}$$

The better choice is however to take the mean of the derivatives in the two points as in (A.26). This is especially clear when considering the case when the input passes the last vertex ($(\mathrm{L}_2, \Gamma_2) \to (\mathrm{L}_3, \Gamma_2)$ in Fig. A.1(b)), where the derivative is

$$v_i = \frac{1}{2}\left(\lim_{\Delta t \to 0^-} \frac{y(t+\Delta t) - y(t)}{\Delta t} + \lim_{\Delta t \to 0^+} \frac{y(t+\Delta t) - y(t)}{\Delta t}\right) \tag{A.28}$$

$$= \frac{1}{2}\left(\frac{\partial W}{\partial \Gamma}(\mathrm{L}_2, \Gamma_2) + \frac{1}{2}\left(\frac{\partial W}{\partial \Gamma}(\mathrm{L}_3, \Gamma_2) - \frac{\partial W}{\partial \mathrm{L}}(\mathrm{L}_3, \Gamma_2)\right)\right) \cdot \frac{du}{dt}\,. \tag{A.29}$$

This completes how to calculate the derivative of the output for an increasing input signal, and so the total formula is given by

$$\begin{aligned} v_i &= H(u_i, \frac{du_i}{dt}, \mathcal{C}(t)) \\ &= \frac{du_i}{dt} \cdot \begin{cases} \frac{1}{2}\left(\frac{\partial W}{\partial \Gamma}(\mathrm{L}_{n-1}, u_i) + \frac{\partial W}{\partial \Gamma}(\mathrm{L}_n, u_i)\right)\,, & u_i \text{ is on a vertex, } \mathrm{L}_n \neq \mathrm{L}_{n-1} \\ \frac{1}{2}\left(\frac{\partial W}{\partial \Gamma}(\mathrm{L}_{n-1}, u_i) + \frac{1}{2}\left(\frac{\partial W}{\partial \Gamma}(\mathrm{L}_n, u_i) - \frac{\partial W}{\partial \mathrm{L}}(\mathrm{L}_n, u_i)\right)\right)\,, & u_i \text{ on the last vertex} \\ \frac{1}{2}\left(\frac{\partial W}{\partial \Gamma}(-u_i, u_i) - \frac{\partial W}{\partial \mathrm{L}}(-u_i, u_i)\right)\,, & u_i \text{ beyond last vertex} \\ \frac{\partial W}{\partial \Gamma}(\mathrm{L}_n, u_i)\,, & \text{otherwise,} \end{cases} \end{aligned} \tag{A.30}$$

where u_i equals the vertex coordinate Γ_{n-1} in the two first lines, and last vertex is $(\mathrm{L}_n, \Gamma_{n-1})$ in the two middle lines. (It is supposed that the evolution of the memory function is on or has passed the coordinate L_n.) The derivative du_i/dt must be computed separately according to common methods. The analysis of the differentiation for the case when $du/dt < 0$ is carried out analogously. The general expression for the derivative $v = dy/dt$ is therefore

$$v_i = \frac{dy_i}{dt} = \begin{cases} H(u_i, \frac{u_i}{dt}, \mathcal{C}(t))\,, & du/dt > 0 \\ 0\,, & du/dt = 0 \\ H(u_i, \frac{u_i}{dt}, \mathcal{C}'(t))\,, & du/dt < 0 \end{cases} \tag{A.31}$$

A.4 Energy Losses

The energy loss between two input values with a memory function $\mathcal{C}(t)$, such that the integration area is triangular, can be implemented directly by taking half the value of (4.30) giving

$$Q_c(u^-, u^+) = \frac{1}{2} \iint\limits_{T(u^-, u^+)} w(\mathrm{L}, \Gamma)(\Gamma - \mathrm{L}) d\Gamma d\mathrm{L}\,, \tag{A.32}$$

or by applying (4.32):

$$Q_W(u^-, u^+) = \frac{1}{2}(u^+ - u^-)W(u^-, u^+) - \frac{1}{2}\int_{u^-}^{u^+} W(l, u^+) dl - \frac{1}{2}\int_{u^-}^{u^+} W(u^-, \gamma) d\gamma\,. \tag{A.33}$$

In the case when an arbitrary memory function $\mathcal{C}(t)$ [and hence an arbitrary input signal] is to be applied, those methods cannot be used. A way to calculate the losses in the general case is to apply (4.29):

$$Q(u_1, u_2) = \frac{1}{2} \iint\limits_{S} w(\mathrm{L}, \Gamma)(\Gamma - \mathrm{L}) d\Gamma d\mathrm{L}\,. \tag{A.34}$$

By noting that the surface S corresponds to the sum of S_k's in Fig. A.1(a), the calculation of the losses can be numerically implemented by applying

$$Q(u^-, u^+) = \frac{1}{2}\sum_{k=1}^{n(t)} \iint_{S_k(t)} w(\mathrm{L}, \Gamma)(\Gamma - \mathrm{L}) d\Gamma d\mathrm{L}\,. \tag{A.35}$$

This expression contains a number of double integrals which makes it computationally cumbersome.

An alternative is to proceed in a similar way as for the output signal $y(t)$ above. Such an analysis leads to that the losses between two input values u_1 and u_2 with an arbitrary $\mathcal{C}(t)$ as in (A.5) can be calculated by

$$\begin{aligned} Q(u_1, u_2) &= M(u_1, u_2, \mathcal{C}(t)) \\ &= \sum_{k=1}^{n-1} \big(Q_W(\mathrm{L}_k, \Gamma_k) - Q_W(\mathrm{L}_k, \Gamma_{k-1})\big) \\ &\quad + \begin{cases} \frac{1}{2}\big(Q_W(u_2, u_2) - Q_W(\mathrm{L}_n, \Gamma_{n-1})\big)\,, & u_2 \text{ beyond last vertex } (\mathrm{L}_n, \Gamma_{n-1}) \\ Q_W(\mathrm{L}_n, u_2) - Q_W(\mathrm{L}_n, \Gamma_{n-1})\,, & \text{otherwise,} \end{cases} \end{aligned} \tag{A.36}$$

when the input is increasing, $du/dt > 0$ and where $Q_W(\cdot)$ is defined in (A.33). Note that each term of the sum in (A.36) involves only three integrations, since two of the integrals have the same integration variable:

$$\begin{aligned} &Q_W(\mathrm{L}_k, \Gamma_k) - Q_W(\mathrm{L}_k, \Gamma_{k-1}) = \\ &\qquad = \frac{1}{2}(\Gamma_k - \mathrm{L}_k) W(\mathrm{L}_k, \Gamma_k) - \frac{1}{2}(\Gamma_{k-1} - \mathrm{L}_k) W(\mathrm{L}_k, \Gamma_{k-1}) \\ &\qquad\quad - \frac{1}{2}\int_{\mathrm{L}_k}^{\Gamma_k} W(l, \Gamma_k) dl + \frac{1}{2}\int_{\mathrm{L}_k}^{\Gamma_{k-1}} W(l, \Gamma_{k-1}) dl - \frac{1}{2}\int_{\Gamma_{k-1}}^{\Gamma_k} W(\mathrm{L}_k, \gamma) d\gamma\,. \end{aligned} \tag{A.37}$$

Analogously to the analysis for the signal output $y(t)$ a general expression of the losses is found to be

$$Q(u_1, u_2) = \begin{cases} M(u_1, u_2, \mathcal{C}(t))\,, & du/dt > 0 \\ 0\,, & du/dt = 0 \\ M(u_1, u_2, \mathcal{C}'(t))\,, & du/dt < 0 \end{cases} \tag{A.38}$$

Mathematically these proposed description for an implementations may seem complicated, but the formulae (A.16), (A.31) and (A.38) witness that a code can be very concise.

Appendix B

Least Square Estimations

The least square estimation (LSE) technique is a well-known method to optimise some model parameters so that the mean square error (MSE) between the modelled and the measured data becomes as small as possible. The LSE technique is here recapitulated for the case when data can be written as a linear regression, and particularly the case of the parameterised Preisach model identified from time-series data, c.f Section 6.3. Moreover, the statistical tests made to evaluate the significance of each parameter is explained, just as how the number of parameters P has been selected in identification process.

The parameterised Everett function (6.19) can be expressed as a linear regression

$$W(\mathrm{L},\Gamma,\theta) = \varphi^T(\mathrm{L},\Gamma)\,\theta \tag{B.1}$$

with the regression vector

$$\varphi(\mathrm{L},\Gamma) = \Big[\Big(\frac{\Gamma-\mathrm{L}}{2I_c}\Big),\Big(\frac{\Gamma-\mathrm{L}}{2I_c}\Big)^2,\ldots,\Big(\frac{\Gamma-\mathrm{L}}{2I_c}\Big)^P\Big]^T \tag{B.2}$$

and the parameter vector $\theta = [a_1, a_2, \cdots, a_P]^T$. A first estimate of the Everett function $\hat{\hat{W}}(\mathrm{L},\Gamma)$ is retrieved directly from measured data by applying the formulas (6.24)–(6.25) (see Fig. 6.3(a)), and is used to find a modelled Everett function $\hat{W}(\mathrm{L},\Gamma) = W(\mathrm{L},\Gamma,\hat{\theta})$. The LSE technique means that the estimated parameters $\hat{\theta}$ are the arguments that minimise the sum of square errors between measured data and modelled data:

$$\hat{\theta} = \arg\min_{\theta} \sum_{\mathrm{L}\le\Gamma} \alpha(\mathrm{L},\Gamma)\,(\hat{\hat{W}}(\mathrm{L},\Gamma) - \varphi^T(\mathrm{L},\Gamma)\,\theta)^2 \tag{B.3}$$

$$= \Big[\sum_{\mathrm{L}\le\Gamma} \alpha(\mathrm{L},\Gamma)\,\varphi(\mathrm{L},\Gamma)\varphi^T(\mathrm{L},\Gamma)\Big]^{-1}\Big[\sum_{\mathrm{L}\le\Gamma} \alpha(\mathrm{L},\Gamma)\,\varphi(\mathrm{L},\Gamma)\hat{\hat{W}}(\mathrm{L},\Gamma)\Big], \tag{B.4}$$

where a possibility to put a weight $\alpha(\mathrm{L},\Gamma)$ to each of the N measured points is also included [Lju87].

Some parameters may have a very little influence on the model, so they can be considered to be excluded from the regression. This significance of the parameters can be formalised by considering the parameter variance and carrying out standard statistical tests or equally by looking at confidence intervals. To do so, noise $n(\mathrm{L},\Gamma)$ is defined as the part of the measured data that cannot be explained by the parametrised model. It is suppose to be additive with zero

mean and independent of each other for different values,

$$\hat{\hat{W}}(\mathrm{L},\Gamma) = \varphi^T(\mathrm{L},\Gamma)\,\theta_0 + n(\mathrm{L},\Gamma), \quad \forall\,\mathrm{L} \le \Gamma \tag{B.5}$$

$$\mathrm{E}\,n(\mathrm{L},\Gamma) = 0 \tag{B.6}$$

$$\mathrm{E}\,n(\mathrm{L},\Gamma)n(l,\gamma) = \lambda_0\delta_k(\mathrm{L}-l)\delta_k(\Gamma-\gamma) \tag{B.7}$$

where the expectation E is taken for all $\mathrm{L} \le \Gamma$, and $\delta_k(\cdot)$ is the Kronecker-delta function. The variance of the noise is therefore equal to λ_0. The assumptions (B.5) to (B.7) imply that the expectation and the covariance matrix C_θ of $\hat{\theta}$ are as follows

$$\mathrm{E}\,\hat{\theta} = \theta^* \tag{B.8}$$

$$C_\theta = \mathrm{E}\,\hat{\theta}\,\hat{\theta}^T = \lambda_0 \cdot R_\alpha^{-1}\Big[\sum_{\mathrm{L},\Gamma} \alpha^2(\mathrm{L},\Gamma)\,\varphi(\mathrm{L},\Gamma)\varphi^T(\mathrm{L},\Gamma)\Big]R_\alpha^{-1}\,, \tag{B.9}$$

where R_α is short for the following expression:

$$R_\alpha = \Big[\sum_{\mathrm{L}\le\Gamma} \alpha(\mathrm{L},\Gamma)\,\varphi(\mathrm{L},\Gamma)\varphi^T(\mathrm{L},\Gamma)\Big]\,. \tag{B.10}$$

The covariance matrix C_θ is thus determined by the noise variance λ_0, the properties of the regression vector, as well as the weighting $\alpha(\mathrm{L},\Gamma)$. If further a 'true' weighting function $W_0(\mathrm{L},\Gamma)$ can be expressed as a linear regression of dimension P (*not* an infinite dimension as in (6.15) and (6.16)),

$$W_0(\mathrm{L},\Gamma) = \varphi(\mathrm{L},\Gamma)\theta_0\,, \tag{B.11}$$

then the expectation of $\hat{\theta}$ is equal to the 'true' parameters [Lju87],

$$\mathrm{E}\,\hat{\theta} = \theta_0\,. \tag{B.12}$$

The distribution of the estimated parameters is required in order to carry out hypothesis tests or to calculate confidence intervals. If the noise is normally distributed or the central limit theorem holds, then the estimated parameters are also normally distributed because they are linear combinations of the noise,

$$\hat{\theta} \in N(\theta_0, C_\theta)\,, \tag{B.13}$$

under the assumption (B.12). If the noise variance λ_0 is known, we can go directly to tests and confidence intervals. Otherwise, we use the unbiased estimate of the variance

$$\hat{\lambda} = \frac{1}{N-P}\sum_{\mathrm{L}\le\Gamma}(\hat{\hat{W}}(\mathrm{L},\Gamma) - \varphi^T(\mathrm{L},\Gamma)\,\theta)^2\,, \tag{B.14}$$

where N is the total number of data in the summation and P is the dimension of θ (the number of parameters), which has a distribution such that

$$\frac{\hat{\lambda}}{\lambda_0}(N-P) \in \chi^2(N-P) \tag{B.15}$$

is Chi-square distributed with degree $N-P$. It is then easily verified that

$$S = \frac{\hat{a}_p - a_{p0}}{\sqrt{C_{\theta(pp)}}} \in t(N-P) \tag{B.16}$$

has a student-t distribution of degree $(N-P)$, where a_{p0} is the 'true' value of parameter a_p and $C_{\theta(pp)}$ is the p^{th} diagonal element in the covariance matrix C_θ. However, the larger $(N-P)$ becomes, the more S can be estimated by a normal distribution.

By using S we can test the hypothesis that $a_p = 0$ against $a_p \neq 0$,

$$H_0 : a_p = 0 \tag{B.17}$$

$$H_1 : a_p \neq 0 \tag{B.18}$$

and if H_0 is not rejected, then this indicates that the p^{th} parameter can be deleted from the parametrised model [HM80, Pap91]. An equivalent method is to see if the confidence interval contains zero. When that is the case, we could consider to remove this parameter from the model, since it has no significance.

The selection of number of parameters P can be formalised by considering the mean square error

$$\mathrm{MSE} = \frac{1}{N} \sum_{\mathrm{L} \leq \Gamma} (\hat{\hat{W}}(\mathrm{L}, \Gamma) - \varphi^T(\mathrm{L}, \Gamma)\, \theta)^2 \tag{B.19}$$

[or more accurately, the estimate of the variance (B.14)] in combination with the presented standard statistical tests on parameter variances. The MSE decreases with increasing number of parameters [Lju87]. One could then believe that a better model would be obtained by including more parameters, but more parameters would only adjust the model to the measurement noise. Furthermore, the statistical tests tell us that the parameters have little significance if their confidence intervals include zero, meaning that the model would be unnecessary complex. A procedure to choose a good model without including too many parameters is to start with a small P and successively increase it as long as the 95% confidence interval does not include zero for any of the parameters. The obtained model is then a balance between complexity and accuracy, and the estimated P does indeed coincide with the true number of parameters if $P < \infty$ [Lju87].

Bibliography

[Abr57] A.A. Abrikosov. *Zhurnal Eksperimental noi i Teoreticheskoi Fiziki*, 32:1442, 1957. English translation in *Soviet Physics – Journal of experimental and theoretical physics*, 5:1174, 1957.

[AK64] P.W. Anderson and Y.B. Kim. Hard Superconductivity: Theory of the Motion of Abrikosov Flux Lines. *Review of Modern Physics*, 36:39–43, 1964.

[AMBT97] N. Amemiya, K. Miyamoto, N. Banno, and O. Tsukamoto. Numerical Analysis of AC Losses in High T_c Superconductors Based on $E - j$ Characteristics Represented with n-Value. *IEEE Transactions on Applied Superconductivity*, 7(2):2110–2113, June 1997.

[Ame98] N. Amemiya. Numerical modelings of superconducting wires for AC loss calculations. *Physica C*, 310:16–29, 1998.

[And62] P.W. Anderson. Theory of the Flux Creep in Hard Superconductors. *Physical Review Letters*, 9(7):309–311, 1962.

[Ash94] S.P. Ashworth. Measurements of AC losses due to transport currents in bismuth superconductors. *Physica C*, 229:355–360, 1994.

[Bab59] I. Babuška. The nonlinear theory of internal friction. *Aplikace Matematiky*, 4:303–321, 1959. (In Russian).

[BCS57] J. Bardeen, L.N. Cooper, and J.R. Schrieffer. Theory of Superconductivity. *Physical Review*, 108:1175–1204, 1957.

[Bea62] C.P. Bean. Magnetization of Hard Superconductors. *Physical Review Letters*, 8(6):250–253, 1962.

[Bea64] C.P. Bean. Magnetization of High-Field Superconductors. *Review of Modern Physics*, 36:31–39, 1964.

[Ber98] G. Bertotti. *Hysteresis in Magnetism – For Physicists, Material Scientists and Engineers.* Academic Press, New York, USA, 1998.

[BG96] E.H. Brandt and A. Gurevich. Linear AC Response of Thin Superconductors during Flux Creep. *Physical Review Letters*, 76(10):1723–1726, 1996.

[BI93] E.H. Brandt and M. Indenbom. Type-II Superconductor Strip with Current in a Perpendicular Magnetic Field. *Physical Review B*, 48(17):12893–12906, 1993.

[BM86] J.C. Bednorz and K.A. Müller. Possible High-T_c Superconductivity in the Ba-La-Cu-O System. *Zeitschrift für Physik B*, 64(2):189–193, 1986.

[Bou71] R. Bouc. Modèle mathematique d'hystérésis. *Acustica*, 24:16–25, 1971. (In French).

[Bra96a] E.H. Brandt. Superconductors of finite thickness in a perpendicular magnetic field: Strips and slabs. *Physical Review B*, 54(6):4246–4264, 1996.

[Bra96b] E.H. Brandt. Universality of Flux Creep in Superconductors with Arbitrary Shape and Current-Voltage Law. *Physical Review Letters*, 76(21):4030–4033, 1996.

[BS96] M. Brokate and J. Sprekels. *Hysteresis and Phase Transitions*. Springer-Verlag, New York, USA, 1996.

[Cam95] A.M. Campbell. AC Losses in High T_c Superconductors. *IEEE Transactions on Applied Superconductivity*, 5(2):682–687, 1995.

[Car83] W.J. Carr Jr. *AC Loss and Macroscopic Theory of Superconductors*. Gordon and Breach, Science Publishers, Inc., New York, USA, 1983.

[CB72] L.O. Chua and S.C. Bass. A Generalized Hysteresis Model. *IEEE Transactions on Circuit Theory*, CT-19:36–48, 1972.

[CBG99] T. Coleman, M.A. Branch, and A. Grace. *Optimization Toolbox, For Use with Matlab – User's Guide*. The Mathworks, Inc., Natick, MA, USA, 1999.

[CH87] B.D. Coleman and M.L. Hodgon. On a class of constitutive relations for ferromagnetic hysteresis. *Archive Rational Mechanics Analysis*, 99:375–396, 1987.

[Che84] D.K. Cheng. *Field and wave electromagnetics*. Addison-Wesley Publishing Company, Inc., Massachusetts, USA, 1984.

[CS70] L.O. Chua and K.A. Stromsmoe. Lumped-Circuit Models for Nonlinear Inductors Exhibiting Hysteresis Loops. *IEEE Transactions on Circuit Theory*, CT-17:564–574, 1970.

[Del99] E. Della Torre. *Magnetic hysteresis*. Piscataway, IEEE Press, New Jersey, USA, 1999.

[Dju97] D. Djukic. *Modélisation des systèmes non-linéaires: ordre, adaptation des paramètres et hysterèse*. PhD thesis, No. 1739 (1997), Chair of Circuit and Systems, Swiss Federal Institute of Technology Lausanne, Switzerland, 1997. (In French).

[DSD98] D. Djukic, M. Sjöström, and B. Dutoit. Preisach-type hysteresis modelling in Bi-2223 tapes. *Institute of Physics Conference Series No. 158*, 2:1409–1412, 1998.

[DSS99] B. Dutoit, M. Sjöström, and S. Stavrev. Bi(2223) Ag Sheathed Tape I_c and Exponent n Characterization and Modelling under DC Applied Magnetic Field. *IEEE Transactions on Applied Superconductivity*, 9(2):809–812, 1999.

[Duh97] P. Duhem. Die dauernden Aenderungen und die Thermodynamik I. *Z. Phys. Chemie*, 22:543–589, 1897. (In German).

[DWS90] S. Dale, S. Wolf, and T. Schneider. *Energy Applications of High Temperature Superconductivity*, volume 1 and 2. Electric Power Research Institute, Inc., USA, 1990.

[ES54] D.H. Everett and F.W. Smith. A general approach to hysteresis: Part 2. Development of the domain theory. *Trans. Faraday Soc.*, 50:187–197, 1954.

[Eve54] D.H. Everett. A general approach to hysteresis: Part 3. A formal treatment of the independent domain model of hysteresis. *Trans. Faraday Soc.*, 50:1077–1096, 1954.

[Eve55] D.H. Everett. A general approach to hysteresis: Part 4. An alternative formulation of the domain model. *Trans. Faraday Soc.*, 51:1551–1557, 1955.

[EW52] D.H. Everett and W.I. Whitton. A general approach to hysteresis. *Trans. Faraday Soc.*, 48:749–757, 1952.

[FLK94] G. Friedman, L. Liu, and J.S. Kouvel. Experimental Testing of Applicability of the Preisach Hysteresis Model to Superconductors. *Journal of Applied Physics*, 75(10):5683–5687, 1994.

[FMAO94] T. Fukunaga, S. Maruyama, T. Abe, and A. Oota. AC Losses of Ag-Sheathed $(Bi,Pb)_2Sr_2Ca_2Cu_2O_2$ Superconducting Wires. *Physica C*, 235–240:3231–3232, 1994.

[GL50] V.L. Ginzburg and L.D. Landau. On the theory of Superconductivity. *Zhurnal Eksperimental noi i Teoreticheskoi Fiziki*, 20:1064–1082, 1950. (In Russian).

[Gro73] F.W. Grover. *Inductance Calculations*. Dover Publications Inc., New York, USA, 1973.

[HM80] W.W. Hines and D.C. Montgomery. *Probability and Statistics in Engineering and Management Science*. John Siley & Sons, Inc., New York, USA, 2nd edition, 1980.

[HN86] M. Hasler and J. Neirynck. *Nonlinear Circuits*. Artech House Inc., Massachusetts, USA, 1986.

[Hod88] M.L. Hodgon. Application of a theory of ferromagnetic hysteresis. *IEEE Transactions on Magnetics*, MAG-24:218–221, 1988.

[Ish44] A.Y. Ishlinskii. Some applications of statistical methods to describing deformations of bodies. *Izvestija Akademii Nauk SSSR, Otdelenie Techniceskich Nauk*, 9:583–590, 1944. (In Russian).

[JA83] D.C. Jiles and D.L. Atherton. Ferromagnetic hysteresis. *IEEE Transactions on Magnetics*, MAG 19:2183, 1983.

[JA86] D.C. Jiles and D.L. Atherton. Theory of ferromagnetic hysteresis. *Journal of Magnetism and Magnetic Materials*, 61:48–60, 1986.

[Jil92] D.C. Jiles. A self consistent generalized model for the calculation of minor loop excursions in the theory of hysteresis. *IEEE Transactions on Magnetics*, 28(5):2602–2604, 1992.

[Kam11a] H. Kamerlingh Onnes. Further experiments with liquid helium. On the change of the electrical resistance of pure metal at very low temperatures. *Leiden Comm.*, 120b:3–5, April 1911.

[Kam11b] H. Kamerlingh Onnes. Further experiments with liquid helium. On the change of the electrical resistance of pure metal at very low temperatures. *Leiden Comm.*, 122b:13–15, May 1911.

[Kam11c] H. Kamerlingh Onnes. Further experiments with liquid helium. On the change of the electrical resistance of pure metal at very low temperatures. *Leiden Comm.*, 122b:21–25, December 1911.

[KHS62] Y.B. Kim, C.F. Hempstead, and A.R. Strnad. Critical Persistent Currents in Hard Superconductors. *Physical Review Letters*, 9(7):306–309, 1962.

[KHS63a] Y.B. Kim, C.F. Hempstead, and A.R. Strnad. Flux Creep in Hard Superconductors. *Physical Review*, 131(6):2486–2495, 1963.

[KHS63b] Y.B. Kim, C.F. Hempstead, and A.R. Strnad. Magnetization and Critical Supercurrents. *Physical Review*, 129(2):528–535, 1963.

[KP89] M.A. Krasnoselskii and A.V. Pokrovskii. *Systems with Hysteresis*. Springer Verlag, Berlin, Germany, 1989.

[Kre91] P. Krejčí. Hysteresis memory preserving operators. *Applications of Mathematics*, 36(4):305–326, 1991.

[Lju87] L. Ljung. *System Identification – Theory for the User*. Prentice-Hall Inc., New Jersey, USA, 1987.

[LL35] F. London and H. London. The Electromagnetic Equations of the Superconductor. *Proceedings of the Royal Society*, A149:71–88, 1935.

[LPA00] F. Liorzou, B. Phelps, and D. L. Atherton. Macroscopic Models of Magnetization. *IEEE Transactions on Magnetics*, 36(2):418–428, March 2000.

[LPME98] M. Lahtinen, J. Paasi, R. Mikkonen, and J.-T. Eriksson. Computational study of magnetisation losses in HTS composite conductors having different twist-pitch lengths. *Institute of Physics Conference Series No. 158*, 2:1401–1404, 1998.

[Mad05] E. Madelung. Über Magnetisierung durch schnell verlaufende Ströme und die Wirkungsweise des Rutherford-Marconischen Magnetdetektors. *Annalen der Physik*, 17:861–890, 1905. (In German).

[May91] I.D. Mayergoyz. *Mathematical Models of Hysteresis*. Springer Verlag, New York, USA, 1991.

[May96] I.D. Mayergoyz. Nonlinear Diffusion and Superconducting Hysteresis. *IEEE Transactions on Magnetics*, 32(5):4192–4197, 1996.

[May98] I.D. Mayergoyz. *Nonlinear Diffusion of Electromagnetic Fields*. Academic Press, New York, USA, 1998.

[MNZ93] J.W. Macki, P. Nistri, and P. Zecca. Mathematical models for hysteresis. *Society of Industrial and Applied Mathematics Review*, 35(1):94–123, March 1993.

[MO33] W. Meissner and R. Ochsenfeld. Ein neuer Effekt bei Eintritt der Supraleitfähigkeit. *Die Naturwissenschaften*, 21:787–788, November 1933.

[MS00] I.D. Mayergoyz and C. Serpico. Nonlinear diffusion and the Preisach model of hysteresis. *Physica B*, 275:17–23, 2000.

[MYBH00] E. Martínez, Y. Yang, C. Beduz, and Y.B. Huang. Experimental study of loss mechanisms of AgAu/PbBi-2223 tapes with twisted filaments under perpendicular AC magnetic fields at power frequencies. *Physica C*, 331:216–226, 2000.

[Nib99] N. Nibbio. *Nonlinear Electromagnetic Modeling of High Temperature Superconducting Tapes*. PhD thesis, No. 2031 (1999), Chair of Circuit and Systems, Swiss Federal Institute of Technology Lausanne, Switzerland, 1999.

[NO99] M. Noe and B.R. Oswald. Technical and Economical Benefits of Superconducting Fault Current Limiters in Power Systems. *IEEE Transactions on Applied Superconductivity*, 9(2):1347–1350, June 1999.

[Nor70] W.T. Norris. Calculation of Hysteresis Losses in Hard Superconductors Carrying AC: Isolated Conductors and Edges of Thin Sheets. *Journal of Physics D: Applied Physics*, 3:489–507, 1970.

[NSD+00] N. Nibbio, M. Sjöström, B. Dutoit, P. Lombard, and D. Taghezou. Losses in HTS Tapes due to AC External Magnetic Field and AC Transport Current. *Institute of Physics Conference Series No. 167*, 1:875–878, 2000.

[Pap91] A. Papoulis. *Probability, Random Variables and Stochastic Processes*. McGraw-Hill Inc., New York, USA, third edition, 1991.

[PBRP95] W. Paul, Th. Baumann, J. Rhyner, and F. Platter. Tests of 100 kW High-T_c Superconducting Fault Current Limiter. *IEEE Transactions on Applied Superconductivity*, 5(2):1059–1062, June 1995.

[Pip53] A.B. Pippard. *Proceedings of the Royal Society A*, 216:547, 1953.

[PL97] J. Paasi and M. Lahtinen. Computational Comparison of AC Losses in Different Kinds of HTS Composite Conductors. *IEEE Transactions on Applied Superconductivity*, 7(2):322–325, 1997.

[Pra28] L. Prandtl. Ein Gedankenmodell zur kinetischen Theorie der festen Körper. *Zeitschrift angewandte Mathematik und Mechanik*, 8:85–106, 1928. (In German).

[Pre35] F. Preisach. Über die magnetische Nachwirkung. *Zeitschrift für Physik*, 94:277–302, 1935. (In German).

[PSSR01] D. Politano, M. Sjöström, G. Schnyder, and J. Rhyner. Technical and Economical Assessment of HTS Cables. *IEEE Transactions on Applied Superconductivity*, March 2001. In press.

[Rei98] N. Reimann. *Modeling and simulation of high temperature superconducting fault current limiters inserted in a distribution level power system*. PhD thesis, No. 1836 (1998), Dept. of Electrical Engineering, Swiss Federal Institute of Technology Lausanne, Switzerland, 1998.

[Rhy93] J. Rhyner. Magnetic properties and AC-losses of superconductors with power law current-voltage characteristics. *Physica C*, 212:292–300, 1993.

[Rhy98] J. Rhyner. Calculation of AC losses in HTSC wires with arbitrary current voltage characteristics. *Physica C*, 310:42–47, 1998.

[RR78] A.C. Rose-Innes and E.H. Rhoderick. *Introduction to Superconductivity*. Pergamon Press, Oxford, UK, 2nd edition, 1978.

[SCD99] M. Sjöström, R. Cherkaoui, and B. Dutoit. Enhancement of Power System Transient Stability Using Superconducting Fault Current Limiters. *IEEE Transactions on Applied Superconductivity*, 9(2):1328–1330, 1999.

[SD98] M. Sjöstöm and B. Dutoit. Preisach Model Identification from Higher Harmonics. In *1998 International Symposium on Nonlinear Theory and its Applications*, volume 1, pages 275–278, 1998.

[SDD98] M. Sjöström, D. Djukic, and B. Dutoit. Parametrised Preisach Model of Hysteresis in High Temperature Superconductors. Technical Report SSC/1998/007, Systems and Communication Section, EPFL, Lausanne, Switzerland, 1998.

[SDD00] M. Sjöström, D. Djukic, and B. Dutoit. Parameterised Hysteresis Model for High Temperature Superconductors. *IEEE Transactions on Applied Superconductivity*, 10(2):1585–1592, June 2000.

[See98] B. Seeber, editor. *Handbook of Applied Superconductivity*, volume 1 and 2. Institute of Physics Publishing Ltd, Bristol, UK, 1998.

[She94] T.P. Sheahen. *Introduction to High-Temperature Superconductivity.* Plenum Press, New York, USA, 1994.

[SHM91] T. Sugiura, H. Hashizume, and K. Miya. Numerical Electromagnetic Field Analysis of Type-II Superconductor. *International Journal of Applied Electromagnetism in Materials*, 2:183–196, 1991.

[Sjö98] M. Sjöström. Preisach Modelling: Symmetry Implementation and Frequency Analysis. Technical Report SSC/1998/008, Systems and Communication Section, EPFL, Lausanne, Switzerland, 1998.

[Sjö99] M. Sjöström. Frequency Analysis of Classical Preisach Model. *IEEE Transactions on Magnetics*, 35(4):2097–2103, July 1999.

[SP01] M. Sjöström and D. Politano. Technical and Economical Impacts on a Power System by Introducing an HTS FCL. *IEEE Transactions on Applied Superconductivity*, March 2001. In press.

[Ste98] G. Stephens. Anisotropic $J_c - \vartheta$ Measurements at Low Fields on a MoSi Thin Films: Evidence of a Two-Dimensional Regime. *IEEE Transactions on Applied Superconductivity*, 8(1):34–37, 1998.

[SV98] C. Serpico and C. Visone. Magnetic Hysteresis Modeling via Feed-Forward Neural Networks. *IEEE Transactions on Magnetics*, 34(3):623–628, 1998.

[SW48] E.C. Stoner and E.P Wohlfarth. A mechanism of magnetic hysteresis i heterogeneous alloys. *Philosophical Transactions of the Royal Society A*, 240:599–642, May 1948.

[TBK94] H. Theuss, T. Becker, and H. Kronmüller. Influence of geometry on angle-dependent critical current density measurements in thin-film superconductors. *Physica C*, 233:179–184, 1994.

[Tin75] M. Tinkham. *Introduction to Superconductivity.* McGraw-Hill Inc., New York, USA, 1975.

[TT89] M. Tachiki and S. Takahashi. Anisotropy of Critical Current in Layered Oxide Superconductors. *Solid State Communications*, 72(11):1083–1086, 1989.

[UYTM93] M Uesaka, Y. Yoshida, N. Takada, and K. Miya. Experimental and Numerical Analysis of Three-dimensional High-T_c Superconducting Levitation Systems. *International Journal of Applied Electromagnetism in Materials*, 4:13–25, 1993.

[vDT99] T. van Duzer and C.W. Turner. *Principles of Superconductive Devices and Circuits.* Prentice Hall PTR, New Jersey, USA, 2nd edition, 1999.

[VFG91] V.M. Vinokur, M.V. Feigel'man, and V.B. Geshkenbein. Exact Solution for Flux Creep with Logarithmic $U(j)$ Dependence: Self-Organized Critical State in Hight-T_c Superconductors. *Physical Review Letters*, 67(7):915–918, 1991.

[Vin00] E. Vinot. *Modélisation des supraconducteurs HTC – Application au calcul des pertes AC*. PhD thesis, Laboratiore d'Electrotechnique de Grenoble *et* Centre de Recherches sur les Très Basses Températures, Institut National Polytechnique de Grenoble, France, 2000.

[Vis94] A. Visintin. *Differential Models of Hysteresis*. Springer-Verlag, New York, USA, 1994.

[VSM+98] I. Vajda, A. Szalay, L. Mohácsi, J. Lukács, and T. Porjesz. Modelling of Hysteresis of High-T_c Superconductors. *International Journal of Modern Physics B*, 12(29, 30 & 31):2958–2960, 1998.

[VSM+00] C. Visone, C. Serpico, I.D. Mayergoyz, M.W. Huang, and A.A. Adly. Neural-Preisach-type models and their application to the identification of magnetic hysteresis from noisy data. *Physica B*, 275:223–227, 2000.

[Wil83] M. Wilson. *Superconducting Magnets*. Oxford University Press, Oxford, UK, 1983.

[Yan98] Y. Yang. Private communications. Southampton University, UK, 1998.

[YHB+96] Y. Yang, T. Hughes, C. Beduz, D.M. Spiller, R.G. Scurlock, and W.T. Norris. The influence of geometry on self-field AC losses of Ag sheathed PbBi2223 tapes. *Physica C*, 256:378–386, 1996.

Biography

Bengt Erik Mårten SJÖSTRÖM was born on the 5th of April 1967 in Sundsvall, Sweden. He received the Master of Science in applied physics and electrical engineering from Linköping University, Sweden in September 1992, the Licentiate of engineering in signal processing from the Royal Institute of Technology (KTH), Stockholm, Sweden in January 1998, and he has with the present thesis defended the PhD degree in modelling of nonlinear systems at the Swiss Federal Institute of Technology Lausanne (EPFL), Switzerland in April 2001.

He took part of a year of exchange at the Technische Hochschule Darmstadt, Germany, in 1990–1991, and he spent 8 months as a Technical Student at CERN, the European Laboratory for Nuclear Physics in Geneva, Switzerland in 1991–1992. He then spent 1993–1994 in industry working for ABB in Ludvika, Sweden, where he took part in a training programme and worked on high voltage filter protection and synchronised control of high voltage switches. From April 1994 to October 1996, he was appointed Technical Fellow at CERN, where he studied signal processing and parameterised system identification for noise reduction in transfer function measurements of a proton beam. He visited the University of Maryland, USA, in September 1998, where he studied Preisach models of hysteresis under the supervision of Prof. I.D. Mayergoyz.

He has had nine articles published in journals, which treat subjects such as hysteresis models, their application to superconductivity, other phenomenological models for superconductors, as well as different applications of superconductivity in power systems. In five conference publications, he has described the same subjects but also dealt with signal processing techniques for estimation of transfer functions, in particular in noisy measurements of particle beams. He has also written and contributed to six technical reports at CERN, EPFL and within a Swiss project on high temperature superconductors in power systems.

His ever best decision was to marry Julynette in September 1999. He speaks four languages including Swedish, English, German and French. He is very fond of skiing and other outdoor activities, but also amuses himself with different racket sports, running and other sportive activities. Another developed interest is music, preferably a cappella song.